Dynamic Solid State Lighting

by

Matthew Aldrich

B.S., Electrical Engineering
Yale University, 2004

Submitted to the Program in Media Arts and Sciences,
School of Architecture and Planning,
in partial fulfillment of the requirements for the degree of,

Master of Science in Media Arts and Sciences

at the

Massachusetts Institute of Technology

June 2010

Author_____

Program in Media Arts and Sciences
May 7, 2010

Certified by_____

Joseph A. Paradiso
Associate Professor
Program in Media Arts and Sciences
Thesis Supervisor

Accepted by_____

Pattie Maes
Associate Academic Head
Program in Media Arts and Sciences

Dynamic Solid State Lighting

by

Matthew Aldrich

Submitted to the Program in Media Arts and Sciences,
School of Architecture and Planning,
on May 7, 2010, in partial fulfillment of the
requirements for the degree of,
Master of Science in Media Arts and Sciences

Abstract

Energy conservation concerns will mandate near-future environments to regulate themselves to accommodate occupants' objectives and best tend to their comfort while minimizing energy consumption. Accordingly, smart energy management will be a needed and motivating application area of evolving Cyber-Physical Systems, as user state, behavior and context are measured, inferred, and leveraged across a variety of domains, environments, sensors, and actuators to dynamically mitigate energy usage while attaining implicit and explicit user goals. In this work, the focus in on the efficient control of a LED-based lighting network.

This thesis presents a first-of-its-kind pentachromatic LED-based lighting network that is capable of adjusting its spectral output in response to ambient conditions and the user's preferences. The control of the intensity is formulated as a nonlinear optimization problem and the mathematics governing sensed illuminance, color, and corresponding control (feedback and adjustment) are formally defined. The prototype adjustable light source is capable of maintaining an average color rendering index greater than 92 (nearly the quality of daylight) across a broad adjustable range (2800 K - 10,000 K) and offers two modes of control, one of which is an energy efficient mode that reduces the total power consumption by 20%. The lighting network is capable of measuring the illuminance and color temperature at a surface and adjusting its output with an overall update rate of 11 Hz (limited by the MATLAB kernel). The sensor node features an optical suite of sensors with a dynamic range of $10000:1$ lx (rms error: 2 lx). The sensor node measures the color temperature of daylight within $\pm 500\,\mathrm{K}$ (kelvin). Device testing and validation were performed in a series of experiments in which the radiant power was collected using a radiometrically calibrated spectrometer with an expanded uncertainty ($k = 2$) of 14% and validated against a model derived by measuring the individual spectra of the system using custom MATLAB tools. A digital multimeter measured the current in the experiments. The work concludes by estimating the energy savings based on the measured optical and electrical data. In environments with moderate ambient lighting, the networked control reduces power consumption by 44% with an additional 5-10% possible with spectral optimization.

Thesis Supervisor: Joseph A. Paradiso
Title: Associate Professor, Program in Media Arts and Sciences

Dynamic Solid State Lighting

by

Matthew Aldrich

The following people served as readers for this thesis:

Thesis Reader_____

William J. Mitchell
Professor
Program in Media Arts and Sciences

Thesis Reader_____

Ramesh Raskar
Associate Professor
Program in Media Arts and Sciences

Acknowledgments

There are many people and organizations to which I owe thanks and credit. To Joe Paradiso, for the opportunity to join the greatest research group at the Media Lab and second, for his time and guidance on helping me carve out this research area; my readers, Bill Mitchell and Ramesh Raskar, for their support, patience, and flexibility; to Media Lab sponsors Philips-Color Kinetics and Schneider Electric for their pledges of support; to the Color Kinetics staff in Burlington, whose generous donation of lighting equipment facilitated the creation of the first lighting testbed; in particular, Jeff Cassis at CK for his written support of the research and Jim Anderson, Paul Kennedy, John Warwick and Tracey Estabrook at CK; Phil London at Schneider for his written support; thanks to Peter Rombult for working on our grants; the Responsive Environments Group; Alex Reben, Mat Laibowitz, and Gershon Dublon for their help in the machine shop; Nan Wei Gong for Cargonet; to Mike Lapinski, Bo Morgan, and Clemens Satzger for the trips to Peoples'; to Nan Zhao for her work on the CK system; Laurel Pardue for her virtuosic musicianship; Mark Feldmeier for constructing the first half of the building of the future; Spinner; and the ResEnv Country Tyme Band.

I owe a great deal of thanks to Dr. Peter Kindlmann, whose advice and guidance I have always counted on; Jack Rains, Jr. at Renaissance Lighting; for the opportunity to work directly in the design, manufacture, and research of solid state lighting; also, Mike Garbus and Steve Lyons who always provide sound engineering advice; credit goes to Maro Sciacchitano and Josh Tor for their mechanical engineering prowess and the design of the integrating sphere and heatsink; to Lisa Lieberson and Amna Carreiro for supporting the Responsive Environments Group, saying yes to overnight shipping, and for keeping the group running smoothly.

This work is supported by funding from the MIT Media Laboratory.

I want to thank my family and Becky Davis for their love and support over the years.

Contents

List of Figures

List of Tables

Chapter One

Introduction

1.1 Motivation

We have the unique ability to modify and adapt to our surroundings, and for better or worse, shape our environment as we see fit. We live at a time where personal comfort is only a switch, lever, or button press away. When there is not enough light, we flip a switch. When it is too hot or too cold, we immediately adjust the thermostat. As long as the light is on or the room is cold, we are happy and for many of us, the problem ends the moment we are gratified. What reason do we have to consider energy efficiency if our immediate goal is met? We are at the point where the word "green" hardly refers to a color anymore. What we read, watch, eat, and enjoy now comes with some reassurance that we are making the world better for ourselves and for our children. Yet it is not just the choices we make as consumers that reflects our acute sensitivity to the color green. Being "green" means that we modify our behavior; we remember to turn off the lights, or shut down the A/C before leaving the house or office.

But, sometimes we forget. We create technology that attempts to minimize these mistakes. We have programmable HVAC controllers and motion controlled lighting. We introduce new lighting technologies, such as compact florescent lighting (CFL) that are energy efficient, yet contain mercury and produce a low quality of light. Since the adoption of incandescent technology, the benefits of adopting a more energy efficient light source has been undermined by some implicit sacrifice in quality or control.

We have all had some experience in which the outcome of choosing the more energy efficient option fell short of our expectations. As consumers, we have become wary of green technologies. Instead, we prefer the solution that is immediate and attainable within our own financial limits. We are conscious of solutions that contain the word "automatic" and aptly so, the weak automation found in modern lighting and HVAC technologies has left the building manager, the employees, and consumers confused. Why did this turn off? How do I program this? So we ignore these options. We leave the lights on and we turn thermostats to 50 F when we want to cool down quickly. We control the built environment

using mechanisms that are inherently "deaf and mute" [22]. The disparity between "this is what I want" and "this is what I get" has led to inefficient control over utilities and error laden user control. Adding feedback is one way we attempt to balance efficient operation and the user's comfort.

In the academic community, the organization, feedback, control, and deployment of these types of distributed utility systems is a growing area of research, especially in the areas of sensor network utility control. In a broader sense, these intelligent systems are known as cyber-physical systems (CPS) [34, 63]. In this thesis, the author argues that the system presented in this work embodies the very foundations of cyber-physical systems that actively monitor and regulate building utilities. Through the use of sensor networks and advanced control methodologies, the underpinnings of cyber-physical infrastructure are realized: we move beyond reactive control, reduce human-in-loop error, and dynamically adjust and respond to changing physical and environmental conditions.

The goals of this thesis are two-fold. The primary goal is to thoroughly model, build, and test an intelligent lighting network capable of on-the-fly adjustments from both the user and the environment. No assumptions, other than a simple room calibration and a model of the system, are required for run-time controlled optimization of the lighting parameters. The end result is a system capable of tuning its spectral output to not only achieve the correct intensity and color, but also selectively use less energy or maximize the quality of light without user intervention.

In doing so, this work satisfies a second goal. While the efficacy of both active and phosphor based emitters will certainly improve, until we can modulate the band gap or reconfigure the LED phosphors on the fly, we will most likely turn to the control of multiple wavelengths to create precise and high quality light. The methods presented in this thesis certainly apply to the control of a single fixture, but are general enough to apply to the control of an entire network.

The next steps in utility management begin with the integration of these sensor rich cyber-physical systems with hybrid lighting systems, but the approach must remain technology agnostic. The less assumptions made about the operating environment, the better. For if the lighting network is to be truly transparent, then it must handle both the least and greatest perturbation about its equilibrium with as little human intervention as possible.

1.2 Contributions

This thesis presents a first-of-its-kind pentachromatic LED-based lighting network that adjusts its spectral output in response to environmental stimuli and the user's preferences. In this work, the control of the wavelengths is formulated as a nonlinear optimization problem and to the best of the author's knowledge, represents the first known published account of using this approach. This work extends previous research regarding sensor enabled light control, in that solid state lighting is considered to be the primary means of illumination.

Consequently, the lighting network can dynamically optimize the light output for greater efficiency or higher color quality depending on the measured ambient conditions. Whereas previous research considered one linear parameter, intensity, we extend the control methods to highly nonlinear photometric and color criteria that directly govern energy consumption and visual quality. Additionally, we incorporate the ambient color temperature as a feedback parameter and describe the performance of this method. In thoroughly presenting new methods, insights, and approaches regarding the design and control of an intelligent lighting network, a foothold in the area of sensor enabled utility management is established. In summary, this thesis provides the foundation for future research in the areas of efficient lighting control, dynamic utility regulation, persuasive energy, and human computer interaction.

Chapter Two

Dynamic Lighting

In this work, dynamic lighting is considered to be the control and feedback of a light source or group of light sources whose output directly reflects the measured ambient and user supplied operating conditions. In a larger context, the research of dynamic lighting draws from several academic fields of study: applied optics and photonics, feedback and control systems, numerical optimization, electronics design, and human computer interaction. Dynamic lighting is best labeled as a subset of research in the broad field of sensor network enabled utility management and control. In turn, these systems, intended to minimize wasted energy, reduce human-in-loop error, and remain transparent to the user, represent a specific research area of cyber-physical systems (CPS) for intelligent utility management. This emerging field encapsulates any system that incorporates feedback and knowledge models of the environment and user. In general, the goal of these intelligent systems is maximizing the utility afforded by multiple networked subsystems whose augmented performance is derived from measuring or inferring the user's needs and the present state of the operating environment.

2.1 Feedback-Controlled Lighting

Intelligent systems that compensate for varying optical and electrical properties, temperature stability, and the temporal variation of intensity in LEDs are crucial to achieving efficient and long lasting lighting. These systems have been identified as critical research areas by the U.S. Department of Energy [45]. A typical solid-state lamp consists of four main components, each affecting the overall system efficiency. The driver is responsible for controlling the brightness of the LEDs. The LED package affects the efficiency of the LED device. The thermal efficiency refers to the loss of intensity due to thermal heating of the LEDs, board, and electronics. Finally, the fixture optics sets the light loss due to inefficiencies or nonidealality in the reflector or secondary optics.

Increased interest from both academia and industry has led to numerous publications and research concerning efficient and optimal systems to drive LEDs. Van der Broek et al. [76] provide an overview of these topologies. LED intensity is controlled using either linear

current drivers or pulse width modulation (PWM). Green and blue LEDs shift towards longer wavelengths, while red and yellow LEDs shift towards shorter wavelengths at lower junction temperatures. Therefore, PWM is the generally accepted method to control the intensity because current is held constant during the pulse and die temperature stability is improved. Recently, Garcia et al. [23] published results on the overall effect of current and PWM fundamental frequency on the total luminous flux of systems.

As early is 2002, Muthu et al. incorporated optical and temperature feedback into the driver architecture, allowing for compensation of optical, electrical and thermal variations of the system [42, 41]. Subsequent research evaluated the use of neural networks to maintain accurate chromaticity [6] and explored optical feedback using three or more unique LED wavelengths [41, 3]. However, in this work, a very simple (and ineffective) method of controlling the light output is presented for systems comprised of more than three wavelengths. This is achieved by fixing the ratio of intensity at one wavelength to another at the cost of saturated colors and a decreased color gamut. This does not guarantee the best color rendering index for a given white point.

Dynamic and adaptive lighting enabled by environmental sensors offers additional energy savings. Early work by Crisp and Hunt in the 1970s focused on estimating internal illuminance from artificial and external light sources in order to reduce unnecessary lighting and excess energy expenditure [16, 28, 17, 29, 18]. This early work discussed the use of photosensors to monitor the natural daylight in the office place. As early as 1978, Crisp [17] was already considering repurposing the light switch, inspired by the affordances offered by their rudimentary incorporation of daylight harvesting. With the availability of low cost lux sensors (perhaps more importantly, silicon improvements to reign in device variance) and an influx of low cost embedded devices, this simple form of intensity feedback was extended to networks of fixed color incandescent and fluorescent lights. Most relevant is the work by Singhvi et al. [64], in which the group designed and tested closed loop algorithms to maximize energy efficiency while meeting user lighting requirements in an incandescent lighting network. Park et al. [49] developed a lighting system to create high quality stage lighting to satisfy user profiles. Wen et al. [78] researched fuzzy decision making in lighting control networks and Bayesian inference. Machado and Mendes [38] tested automatic light control using neural networks, as did Mozer in a pioneering study from 1992 [40], where light switches and thermostats in his house only provided reinforcement for a neural network that, also utilizing motion sensors, built a user activity model to automatically control utilities.

In industry, Philips Lighting Research has investigated interactive lighting as well, yet the sophistication of these systems is limited by cost and consumer interest. Recently, Philips Lighting (Sluis et al. [66]) produced a lighting demo in which a single device can adjust its output to match the color of a particular object. This device is not designed for white lighting applications or networked control. Instead, its purpose is to enhance the chromaticity of merchandise on display at a retail location. The closest example to the

proposed work is Philip's "Dynamic Lighting" suite of products [51]. Their basic concept revolves around a preprogrammed schedule of color temperature and lighting intensity to mimic a typical daylight cycle on Earth. However, the restrictions are rigid: the system features no feedback, requires programming, and offers only two color temperatures. With these shortcomings, it leaves plenty of open space for advances into this burgeoning field of interactive solid-state lighting control.

2.2 The Promise of Solid State Lighting

Each year, 915 TWh of energy powers incandescent and fluorescent technology in the US. This accounts for 79% of the total lighting energy consumption [45]. By comparing the luminous efficacy (the ratio of luminous flux to the input electric power) of incandescent, fluorescent, and LED technologies, it is clear that white LEDs have great potential to reduce energy consumption and enhance the built environment. The potential savings in energy and reduction of environmental pollution by adopting solid state lighting (SSL) technology is also well studied. Bergh et al. [12] provided early technical discussions of the economic benefits of using LEDs for illumination. In a highly regarded paper concerning the future use of LEDs for illumination, Schubert et al. [61] provided a detailed study of how varying adoption rates of solid state lighting reduced greenhouse gases, crude oil consumption, and increased financial savings. The results of this study, known as the "5.5% and 11% scenarios" state that a 40% and 80% market penetration of solid state lighting technology in the United States would save $22.89 billion to $45.78 billion, depending on the adoption rate. The electrical energy used for lighting is decreased by 25% and 50% respectively. In the US, this translates into yearly savings of 12 million to 24 million barrels of oil and reduction of carbon emissions by 133 Mt to 267 Mt per year. Carbon dioxide emissions have also been studied in [11] which highlights the adoption of solid state lighting an an attractive alternative to carbon capture and sequestration. Subsequent research focused on analyzing the high initial cost of adopting solid state lighting. The US Department of Energy estimates the initial cost of an LED incandescent equivalent to be 560 times that of a traditional incandescent [45]. While the initial cost is quite high, other methods of determining the true cost of the technology exist. The life-cycle cost or "cost of light" is another metric that takes into account the operational lifetimes, labor cost, and energy usage. This is defined as dollars per kilolumen-hours ($/klm-hr). Azevedo, Morgan, and Morgan [11] provide a detailed analysis of both the initial cost and levelized annual cost of solid state lighting. In addition, their estimated economic, energy, and carbon emission savings are consistent with Schubert et al. The analysis concludes that rational consumers will find it cost effective to replace incandescent and fluorescent lighting by 2010, and that solid state lighting will be competitive with conventional lighting before 2015 [11, 21].

The principal focus of current LED research is on improving the maximum efficacy of phosphor based LEDs (white LEDs). At present, near-ultraviolet pumped phosphors

remain the most efficient way to create white light. Yet, these devices, like their active emitter counterparts, have their tradeoffs. In this research, a hybrid active and phosphor based system is employed to create a color-adjustable, high quality white light source.

2.3 White Light using LEDs

Although initial cost impedes market penetration, solid state lighting presents new possibilities in terms of controlling the brightness, the spectral composition, and color rendering properties of white light (the ability of an artificial light source to "render" the true colors of an object) [61, 60, 59]. Although cost is important, the color rendering quality of the light is known to be an important factor [72]. Indeed, the slow adoption of compact fluorescent has, in part, been directly attributed to the fluorescent technology's lower color rendering ability and quality of light [26, 4, 58, 24]. LED-based lighting systems allow for dynamic and automatic modulation of these parameters to enhance the built environment and provide additional energy savings [72, 77, 65]. An artificial white light source is judged by two quantitative metrics, its Correlated Color Temperature or CCT (the temperature in kelvin of an equivalent black body radiator) and its Color Rendering Index (CRI) [79]. Warmer (red) colors have a lower color temperature and cooler (green and blue) colors have a higher color temperature. The CRI is a unitless measurement of how well an artificial illuminant renders the color of an object versus a perfect reference illuminant, where the reference CRI typically has a value of 100. Guo and Houser [25] review the application of CRI for measurement of light sources. Davis and Ohno [20, 47] at the National Institute of Standards and Technology (NIST) in the US are researching an improved color rendering metric.

Boynton reviews the history and current status of research on color spaces derived from human perception [14]. The Commission Internationale de L'Eclairage (CIE) approved several color chromaticity spaces for mathematically representing colorimetric data. The CIE 1931 XYZ color space is a common example (see Wyszecki and Stiles [79], pg. 137). This two dimensional space is based on a set of "color matching functions" that collectively sum to unity. The outermost locus represents saturated primary colors and pure white light falls in the center of the space. The Plankian locus is added for a blackbody reference and the vertical bars represent the correlated color temperature.

The optimal method to create white light using LEDs is still an open question, and while several strategies exist, there are tradeoffs between efficacy and color rendering ability [61]. White light can be created using either multiple current-injected emitters or by non current-injected phosphor wavelength converters. The overall efficacy and color rendering ability are determined by the LEDs selected. The spectral power of the system, defined by the narrowband emission of the LEDs, determines the color rendering ability of the light source. Fewer unique wavelengths result in lower color rendering ability yet the efficacy of the source is often greater.

Common approaches using active emitters include dichromatic (blue and yellow), trichomatic (red, green, blue), and tetrachromatic (red, green, blue and cyan or yellow) sources. These systems have been studied by Narendran et al. [43], Zukauskas et al. [81], Schubert and Kim [60], Stanikunas et al. [67], Lei et al. [35], Zukauskas et al. [82]. In this work the authors report namely on the effects of dominant wavelength, correlated color temperature, and resulting color rendering index. Lei et al., uses a simplistic technique in the evaluation of four wavelengths and Zukauskas et al. [81] applies an exhaustive boundary search to maximize certain optical properties of polychromatic light sources, yet does not provide any information on completion time or provide any empirical results of the study. Ultimately, in each of the papers, the authors provide the theoretical "best" combination of wavelengths and intensities to maximize either the ratio of flux to radiant energy, or to maximize the color rendering index for a given color temperature. It is quite easy to stochastically determine the right mixture of wavelengths using a Gaussian-based model of LED irradiance once the functions to measure the color rendering index and color temperature are programmed.

The problem is that these techniques do not correspond with the ranges of dominant wavelengths provided by the manufactures, nor do they take into account the variance in intensity and dominant wavelength across a particular bin of LEDs; in essence, the conclusions of these papers restrict the applicability of the results to either highly specialized configurations or particular laboratory and operating environments. While performing a sensitivity analysis is one way to at least understand these effects, a better approach is to remain flexible from the the start, specifically, to concentrate on adaptive techniques that require no assumptions of the system. For example, in [35], assumptions of the ratio of amber to red were made in order to resolve the system to three equations and three unknowns. A fixed ratio of these wavelengths to imposes harsh constraints on the range of achieveable CRI. The best ratio is nonlinear in the sense that the dominant wavelengths of all the LEDs, the desired color temperature, and required intensity must be taken into account. One final concern is the length of time required to find the appropriate solution. For example, in this research, Monte Carlo simulations required up to eight hours to terminate. These techniques do not provide the run-time affordances required to control a solid state lighting network. By taking into account the variance of the LEDs and other uncontrollable parameters upfront (i.e., a method of control that requires no assumptions), we free ourselves from heuristic based assumptions about the wavelengths and required intensity of the LEDs.

A different approach uses white LEDs of a fixed color temperature to achieve the illumination goal. These devices do not require careful thought and control like active emitters, however there are other tradeoffs, which in turn, make active emitters a better option for color-adjustable lighting. White LEDs consist of an active emitter, primarily blue or near ultra violet and a down-converting phosphor. The first phosphor used in white LEDs absorbed blue light and emitted yellow light typically between 5500 K and 6500 K [52, 33, 80]. These devices provided adequate efficiency but low CRI. More recently, devices have utilized a blue LED with a yellow and red phosphor. These resulted in warmer white LEDs with

improved CRI. However, the phosphor conversion always leads to an energy loss due to the Stokes shift between absorption and emission. Scattering loss, or reflectance back onto the chip or walls of the package also reduces efficiency. Stevenson [68] provides a recent overview (2009) of Auger recombination (droop) and why LEDs become less efficient with increased current. Present day efficacy and CRI for cool and warm white LEDs (not in a fixture) are 101 lm/W and 70 (5500 K) and 72 lm/W and 90 (3300 K), respectively [45]. Inversely, active emitter designs offer a lower efficacy, closer to 40 lm/W to 50 lm/W (due to quantum efficiency and droop see Krames et al. [33]) but in some cases a higher color rendering index. In this research, we present a state of the art light source capable of color adjustable white points with an average color rendering index greater than 92.

There are practical limits to system performance. Burmen et al. [15] describe four major factors affecting the quality of LEDs: The initial variability of optical and electrical properties, their temperature and electrical dependence, and temporal degradation with corresponding variability. Initial optical and electrical properties such as luminous flux, chromaticity, and forward voltage can vary due to imperfections in the manufacturing process. Manufacturers typically "bin" LEDs to sub-classify the yield based on these three properties. However, higher flux bins add additional system cost. Within a particular bin, wavelength tolerance can adversely effect system performance. Lei et al. [35] reported that red primaries of shorter wavelengths negatively affect CRI and that blue wavelength shifts affect the chromaticity. At the device level, the emission power, peak wavelength, and spectral width of LEDs vary with temperature. The luminous flux of low gap devices (red LEDs) decreases as the junction temperature rises, resulting in chromaticity and CRI shifts as the junction temperature rises. To compensate in trichromatic and tetrachromatic systems, red LEDs are added, reducing efficacy and increasing cost. Finally, the temporal degradation of LEDs, even those within the same bin, can be different. Over time, this causes spatial color and intensity imhomogeneities in LED array light sources [15].

Blue and ultra violet pumped phosphor devices exhibit their own unique set of problems. Increases in junction temperature cause intensity degradation, however this effect is less prominent in the high current region of the diode [15]. Narendran et al. studied the long term heating effects of white LEDs to properly evaluate their useful life and found that heating of junction in white LEDs caused the yellowing of epoxy surrounding the die, resulting in chromaticity shift [43, 44]. Trevisanello et al. [75] also studied degration of white LEDs and determined that excessive heat at the junction led to a decrease in phosphor conversion.

2.4 Dynamic Solid State Lighting

While the optimal control of lighting networks has been researched in the past, it has been done using traditional lighting technologies (e.g., incandescent and fluorescent). The challenges of efficient and optimal control of LED based lighting requires moving away from the strictly linear techniques presented in [64, 78]. Although the goals of the user

may be satisfactorily represented as linear inequality constraints, the greatest challenge imposed by adopting LEDs is accounting for LED variance, temperature dependence, and the difficulties of controlling a network comprised of a large number of variables (i.e., the number of wavelengths to be controlled). The control problem is further complicated by issues of optical sensor variance, occlusion of the sensor, and network update rates (e.g., estimating dark lighting levels, polling sensor nodes, and preprocessing the data). To the user, minimal control is required, as the lighting network must be capable of energy efficient operation without the direct intervention and constant adjustment by the user. In previous research, the use of commercially available sensor nodes imposed limited flexibility and control of these systems. Fixed resolution and no guarantees of timing or update rates were among the greatest problems faced by researchers who favored a top down approach.

Furthermore, as reported in [78], future systems should examine lighting conditions based on tasks or inferred context – in cases where this fails or is inadequate, it is suggested that manual override or a user interface be incorporated into the control. In this research, we leverage multiple domains of expertise to design a custom lighting platform and novel sensor network to bridge the gap between ubiquitous sensing, user interfaces, and run-time control. Clearly, this is an ambitious undertaking, but doing so opens the opportunity to explore ideas and concepts unobtainable by previous research. For example, the system does not require fixed sensor positions, but in fact can dynamically recalibrate. Furthermore, we incorporate color measurements, color control, and closed loop LED control into our design using polychromatic lighting.

In doing so, we embody the underpinnings of an intelligent system conscious of its output and capable of reacting and interacting with dynamic environmental and human phenomena. By developing our tools and hardware from the ground up, we can begin to research the difficult challenges of cyber-physical systems: namely, the transparent integration of ubiquitous sensing and run-time control affordances needed to make these systems truly transparent. This research is the first of many steps. In this embodiment, there is a principal focus on discovering and applying new methods of control and feedback in a lighting network. Accordingly, the proposed techniques are mathematical and the intended purpose is to demonstrate their effectiveness by drawing conclusions from the physical measurements (e.g., energy, response speed, optical parameters). The natural progression is to greater levels of abstraction , where more emphasis is placed on interaction and true run-time control (see Figure 2.1). But first, at the lowest level, are the concepts, methods, and hardware that create the foothold for these more complex systems, and it is these topics that are explored in this thesis.

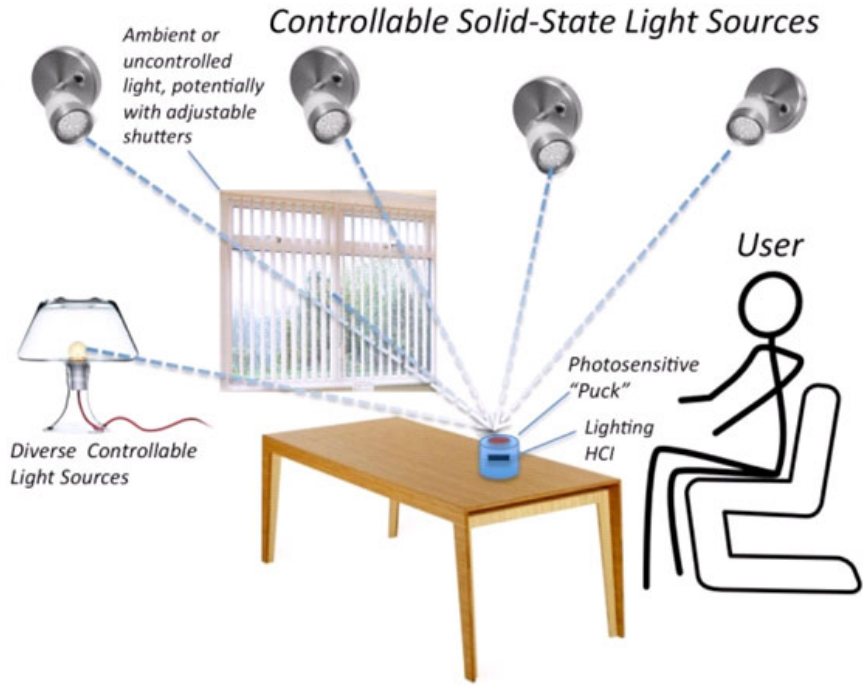

(a)

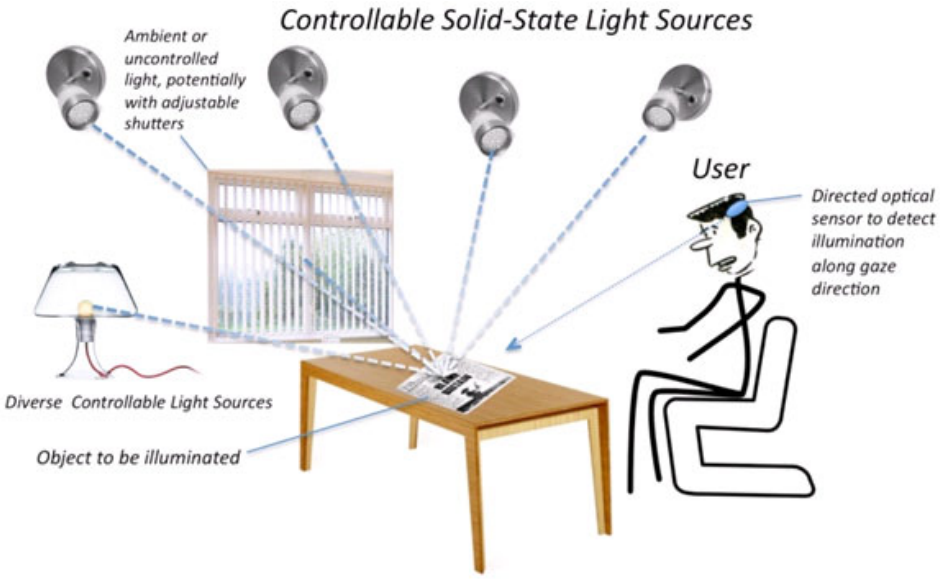

(b)

Figure 2.1: First-phase interactive testbeds to control illumination with diverse light sources exploiting mobile incident sensor/interfaces (a) and wearable first-person sensor/interfaces (b).

Chapter Three

System Modeling

In this chapter, we describe the control problem of estimating the illuminance from multiple light fixtures in the presence of ambient light. We formally define the control problem as an optimization and define the objective function subject to linear inequality constraints. We review existing linear methods of spectral control and propose a new method, direct search, to efficiently control the spectral output of an arbitrary number of wavelengths in a system comprised of an arbitrary number of light fixtures.

3.1 Problem Definition

In this section, a new method to control the spectral output of system comprised of an arbitrary number of light fixtures and wavelengths is presented. Setting the intensity and color of the lighting network is stated as an optimization problem, whereby the feasible set of solutions is determined by an objective function that either maximizes CRI or minimizes the power consumption. The illuminance (E_v) is treated as an linear inequality constraint.

Estimating the Illuminance From a Point Source

First, consider a dark room in which there are n artificial light sources where each light source consists of m wavelengths and j and i are indexing variables of the set $\{j \in \mathbb{Z} : 1 \leq j \leq n\}$ and $\{i \in \mathbb{Z} : 1 \leq i \leq m\}$. If we consider the light source as a spherical point source, then for every ith wavelength in each jth fixture there is a maximum luminous intensity designated, I_{ij}. This is measured as candelas ($\mathrm{lm} \cdot \mathrm{sr}^{-1}$). In the presumed linear system, the intensity of any ith wavelength in fixture j with corresponding maximum intensity I_{ij} is set by column vector x of dimesion $1 \times m$ where $\{x \in \mathbb{R}^m : 0 \leq x \leq 1\}$. Therefore, the total candelas of fixture j is the sum $\sum x_{ij} I_{ij}$ where $1 \leq i \leq m$. Formally defined, the intensity I_v for the entire system of n lights is:

$$\hat{I}_v = \sum_{j=1}^{n} \sum_{i=1}^{m} x_{ij} I_{v,ij}. \tag{3.1}$$

If this luminous intensity is measured by some receiver at a distance d from the light cone, the receiver is said to measure to incident light on a plane perpendicular to the light cone. This intensity is formally known as illuminance (E_v) and is measured in lux ($\mathrm{lm} \cdot \mathrm{m}^{-2}$) (see [79], pp. 265,266). Assuming this light is a point source, we can take advantage of the fact that illuminance decreases at a rate inversely proportional to the square of distance, such that:

$$E_v \propto \frac{I_v}{d^2}, \tag{3.2}$$

where d is the distance between the point source and apex of the solid angle. Using Eq. 3.2, we can calculate the distance between the light source and the receiver. In theory, we are always assured to have sufficient knowledge of the light sources such that I_v for any light source is known and that I_v remains unchanged throughout the operational lifetime of the source. We can then estimate the total $\hat{E}_v$ at the receiver from all the light sources:

$$\hat{E_v} = \sum_{j=1}^{n} k_j \hat{I}_{v,j}, \tag{3.3}$$

where k is a scaling factor found in a calibration step such that $k = E_v/I_v$. A complete way of representing this relationship is:

$$\hat{E_v} = \sum_{j=1}^{n} \sum_{i=1}^{m} k_j x_{ij} \hat{I}_{v,ij}. \tag{3.4}$$

In this case, k_j is measured for every individual light source in the room. Additionally, for a receiver rotated at some angle θ (the oblique angle of incidence) to the plane, the illuminance at the receiver is given as:

$$\hat{E}_{v,\theta} = \frac{I_v}{d^2} \cos(\theta). \tag{3.5}$$

It should be pointed out that prior knowledge of the intensity of the point source is not directly needed to measure the illuminance. The equations above describe the physical laws of how a generic receiver measures illuminance. Such equations are useful when modeling the linear inequality constraints. In the actual operation of the system, the illuminance is measured directly using the sensor node. In turn, these values are used to solve the inequality $\mathbf{Ax} \leq \mathbf{b}$. Therefore, only a calibration step (in which the percentage of lux from each light source and ambient light is measured) is required satisfy the inequality constraint.

In this linear system, for any given setpoint x_{ij} with maximum intensity $\hat{I}_{v,ij}$, there is a corresponding maximum current, $I_{p,ij}$ ($\mathrm{C} \cdot \mathrm{s}^{-1}$) calculated by multiplying the maximum measured current by the setpoint x_i for all $1 \leq i \leq m$, where m is the total number of

wavelengths in the system. The subscript p is used to differentiate the equations from the luminous intensity and current. Using superposition, the total power consumed by a single light fixture is given by:

$$P = V_{in} \sum_{i=1}^{m} x_i I_{p,i}. \tag{3.6}$$

The development of Eqs. 3.1, 3.3 and 3.6 made use of several important assumptions. First, the system was presumed to be linear. This implies that the relationship between setpoint x and measured lux current draw is linear. Empirical results are used to establish this criterion can be found in Chapter 5. At this point we have established the physical relationship between the operational setpoint of a light fixture, the corresponding power consumption, and the perceived illuminance of an optical sensor placed in the room. For the remainder of Chapter 3 we refine Eqs. 3.1 and 3.3, introduce additional lighting parameters T_c and $\mathrm{R_a}$ (i.e., Correlated Color Temperature and the Color Rendering Index), and impose constraints on the values of x.

Room Calibration

In Eq. 3.5, it was assumed that $\hat{E_v}$ was measured without additional light. In order to measure $\hat{E_v}$ (the lux measured by the optical sensor) reliably, several calibration measurements are required for the n fixtures present in the room. First, a dark measurement must be taken. This measurement, denoted E_{dark}, captures the present lighting conditions in the room (e.g., sunlight, incandescent, or fluorescent sources). Second, the scaling factor k_j for $1 \leq j \leq n$ must be measured for all the n light sources in the room. In order to derive the $\hat{E_v}$ contributed by the n fixtures, we simply choose a set point x for each of the n fixtures and subtract E_{dark} for each of the measurements. Once the dark measurements are obtained, the true contribution of each of the n sources can be estimated as long as the optical sensor does not move or the E_{dark} does not change.

Sensing Changes to Operating Environment

In reality, the dark measurements performed by node are not static, but change over time in response to daylight, other light sources being turned on and off, shadows, and occlusion. Additionally, the distance between the receiver and the source may change as well. The sensor node can be moved, lifted, or carried as it measures the lux in the room. The only requirement is that the sensor node remain stationary during calibration. Given this dynamic behavior, it is necessary that the sensor board employ some type of mechanism or intelligence to sense changes to the operating environment.

Color Temperature and Color Rendering Index

If the lighting network in Eq. 3.1 is comprised of LEDs of different wavelengths, then the color rendering index (R_a) and correlated color temperature (T_c) of the system can be controlled as well.

The color rendering index (CRI) is a unitless measurement of how an artificial light source represents that of a perfect illuminant (i.e., daylight) where the reference CRI is typically 100. Any incandescent system, or more generally, any black body radiator, emits temperature-dependent visible energy and has spectral density ($u_{e\lambda}$) given by Planck's formula:

$$u_{e\lambda} = 8\pi hc\lambda^{-5}(e^{hc/kT\lambda} - 1)^{-1}\,(\mathrm{J}\cdot\ \mathrm{m}^{-3}) \tag{3.7}$$

where c is the velocity of light, h is the Planck constant, k is the Boltzmann constant, and T is the temperature in kelvin. Additionally, we can reconstruct the relative spectral energy of daylight using a set of equations derived from the first two eigenvectors of empirically measured daylight (achieved using Principal Component Analysis, see Wyszecki and Stiles [79] pp. 143-147). These models represent ideal sources of radiant energy and serve as the reference illuminant in the calculation of R_a (we quantitatively compare an ideal source and the source we wish to characterize).

The temperature, measured in kelvin is used to classify the color of an artificial light source. Warmer (red) colors have a lower color temperature and cooler (green and blue) colors have higher color temperature. By manipulating the intensity of the system's individual wavelengths R_a and T_c can be tuned perfectly for the given application. The direct calculation of the quantities is a complicated procedure and is not treated formally here. However the formulas, uniform color spaces, and other colorimetric calculations are found in [79]. For this discussion, we treat the calculation of these parameters as a black box, whose result depends on the intensity of the wavelengths.

Revisiting the problem detailed in Sec. 3.1, we introduce two new parameters to control, R_a and T_c. A single fixture consisting of m wavelengths, whose individual wavelengths are denoted λ_i where $\{i \in \mathbb{Z} : 1 \leq i \leq m\}$ also has a CRI that is function of the m wavelengths weighted by setpoint, x_i. That is,

$$R_a = f(x_1 I_{v,1}, x_2 I_{v,2} \ldots, x_m I_{v,m})\,, \tag{3.8}$$

and has a corresponding color temperature denoted as

$$T_c = f(x_1 I_{v,1}, x_2 I_{v,2} \ldots, x_m I_{v,m}). \tag{3.9}$$

It should also be noted that white light (of a fixed T_c) can be created using just two wavelengths and that the greater number of wavelengths in a system, the higher the CRI. This is intuitive; as more energy is spread throughout a larger visible range, a closer approximation of sunlight can be achieved than concentrating a larger amount of energy in

a smaller visible range. Consequently, systems creating white light using only two wavelengths have a lower CRI than systems employing many wavelengths. For an arbitrary color temperature T_c, increasing the CRI requires that we spread the radiant energy out over a larger visible range.

In a system comprised of more than three wavelengths, arriving at the optimal setpoint for a given T_c is a difficult problem and has no unique solution. This limitation arises because of how we mathematically model color vision. The basis for all colorimetric computation starts with the assumption that most humans are trichromats (unfortunately some are dichromats, and some even monochromats) and that we perceive color as a weighted sum of three variables over a visible range of $380\,\text{nm} - 780\,\text{nm}$. As an analogy, this can be thought of as an additive red, green, and blue system.

The problem arises when we try to decipher the color of a light source that is no longer a mixture of three wavelengths but of four, five, six, etc. Biologically, this presents no problems to us, yet mathematically, there is no exact solution. How is this dealt with? In the past, researchers fixed the setpoint of the fourth wavelength (typically an amber color) to ratio of another wavelength (typically red) [3, 42, 41]. In this case, a set of linear equations are solved for and the set point of the red, green, blue, and amber is determined (see Sec. 3.2). However, as will be shown in Chapter 5 this method actually leads to lower overall CRI values. The situation arises because the color temperature of a system can be expressed linearly, yet the optimal CRI for that particular color temperature is nonlinear.

Dynamic Efficacy

The optimization of the number of wavelengths used in the system is referred to in this work as dynamic efficacy. It is the method of selecting the optimal number of wavelengths required to satisfy the lighting condition. For a light fixture n, given T_c and E_v, there exists a group of setpoints $\mathbf{x}$ that minimizes the total radiant energy, hence, the electrical energy of the lighting system. Conversely, for the same T_c and E_v, there exists another group of setpoints $\mathbf{x}'$ that maximizes the color rendering index, requiring more radiant energy, hence more electrical energy is needed.

Let us consider a simple example for two light sources A and B to illustrate these points. Light source A is dichromatic and light source B is pentachromatic. This means A is comprised of two dominant wavelengths and B is also comprised of these same two dominant wavelengths and three other wavelengths. Both light sources are set such they have the same color temperature, $T_c(A) = T_c(B)$, and at some distance d have the same illuminance $E_v(A) = E_v(B)$. Which light source has the greater CRI? According to the logic above, light source B will have a greater CRI. But which light source is more efficient? Or to rephrase the question: which light requires the least amount of radiant energy to have the equivalent illuminance?

First, radiant energy measured on a plane some distance d from a point source is known

as irradiance. Irradiance has the symbol E_e and the units ($\mathrm{W} \cdot \mathrm{m}^{-2}$) and it too, for a point source, obeys the inverse square law. It is analogous to the illuminance calculation in Eq. 3.2, except it describes the electromagnetic power incident on a surface.

Illuminance is calculated using irradiance by integrating E_e and $V(\lambda)$, the photopic efficiency function. This efficiency function is a relative measurement and is dimensionless. The results of integrating E_e and $V(\lambda)$ are scaled by K_m, an empirically derived luminous efficacy function ($\mathrm{lm} \cdot \mathrm{m}^{-1}$), which has a peak sensitivity at 555 nm (Wyszecki and Stiles). Formally, this is written as:

$$E_v = K_m \int_{\lambda} E_e V(\lambda) d\lambda. \tag{3.10}$$

The important conclusion here is that different amounts of radiant energy at different wavelengths result in different amounts of visible energy. We can now answer the question posed at the beginning of this section. If the two dominant wavelengths in light source A require less radiant energy to produce the same illuminance as light source B for a given T_c, then light source A is more efficient, that is, it has a higher efficacy.

In the previous example, we considered a system of fixed illuminance and fixed color temperature. Using LEDs as a light source not only enables the illuminance at a point of interest to be adjusted, but also the ability to dynamically optimize the *number* of wavelengths required to satisfy the lighting goals. These lighting goals might be driven by a user's preferences of illuminance, color, energy efficiency, or color rendering index. We now proceed to formally describe these goals.

Formal Problem Definition

Consider n artificial light sources, where each light source consists of m wavelengths, where the ith wavelength is designated λ_i, the jth light source designated L_j and i and j are indexing variables of the set $\{i \in \mathbb{Z} : 1 \leq i \leq m\}$ and $\{j \in \mathbb{Z} : 1 \leq j \leq n\}$. If we consider the light source as a spherical point source, then for every λ_i in L_j there is a maximum illuminance designated E_{ij} incident on a plane at some distance d from the point source. In the presumed linear system, the intensity of any single wavelength λ_i in light source L_j with corresponding maximum intensity $\hat{I}_{v,ij}$, a corresponding T_c, and a corresponding $\mathrm{R_a}$, is set by x where $\{x \in \mathbb{R}^{mn} : 0 \leq x \leq 1\}$.

The optimal setpoint x has the form:

$$\min_{x \in \Omega} f(x)$$

where $f : \Omega \subset \mathbb{R}^{mn} \to \cup\{\infty\}$ and Ω is set of feasible points subject to linear or nonlinear constraints. The function f does not have a closed form and is non-differentiable. Because there is no direct form of f, an optimization algorithm is required that is driven according to the results of f (see Sec. 3.3).

We define f to be an scaled objective function to minimize square error with z representing our minimization goal:

$$\min_{x\in\Omega} f(x) = \begin{cases} \left(\frac{\hat{T}_c - T_c(x)}{\hat{T}_c}\right)^2 + \Delta uv(T_c)^2 + \left(\frac{\sum_{j=1}^{n} V_{in,j} \sum_{i=1}^{m} x_{ij} I_{p,ij}}{\sum_{j=1}^{n} V_{in,j} \sum_{i=1}^{m} I_{p,ij}}\right)^2 & \text{for } z = 0 \\ \left(\frac{\hat{T}_c - T_c(x)}{\hat{T}_c}\right)^2 + \Delta uv(T_c)^2 - \left(\frac{\mathrm{R_a}(x)}{100}\right)^2 & \text{for } z \neq 0 \end{cases} \tag{3.11}$$

subject to linear inequality constraints

$$\sum_{j=1}^{n}\sum_{i=1}^{m} k_j x_{ij} \hat{I}_{v,ij} \geq E_{desired} - E_{dark}, \tag{3.12}$$

$$\sum_{j=1}^{n}\sum_{i=1}^{m} k_j x_{ij} \hat{I}_{v,ij} \leq E_{desired} - E_{dark} + \beta(E_{desired} - E_{dark}), \tag{3.13}$$

where

$$k_j = \frac{E_{v,j} - E_{dark}}{I_{v,j}}. \tag{3.14}$$

As stated earlier, the left hand side of Eq. 3.12 and Eq. 3.13 can be replaced with the illuminance data directly measured by the sensor node and appropriately weighted by its contribution relative to the total measured lux. In completeness, the full formulation, consistent with Sec. 3.1 is given. The term $E_{desired}$ describes the total lux required at the point of measurement. The dual inequality constraints (rather than a single linear equality constraint) are required to reduce the sensitivity to noise, and to allow the objection function f some flexibility as T_c, $\mathrm{R_a}$, and $E_{desired}$ can not be completely decoupled from each other (Principal Component Analysis could be used to show the extent of which these terms are linearly separable).

The optimization problem can be thought of as a piecewise objective function whose goal is either minimizing energy (i.e., maximize efficacy) or maximizing the color rendering index for a specified color temperature, $\hat{T}_c$. The parameter $\Delta uv(T_c)$ is an error measurement of T_c designed to ensure that the white point defined by the feasible points is a high quality one (it is possible to create a set of T_c, as the color temperature can be described in terms of distance to the black body curve in chromaticity space). This piecewise function satisfies the goals of dynamic efficacy. The desired illuminance $E_{desired}$ is controlled by the user (e.g., a slider).

To conclude, the feasible points found using direct search coincide with our assumptions about the spectral distribution of the system; the efficacy of the system is dependent on the intensity and number of wavelengths used to satisfy the lighting conditions.

Size and Scaling of the Search Space

The feasible solution, Ω contains setpoints x where $\{x \in \mathbb{R}^{mn} : 0 \leq x \leq 1\}$, where m is the number of wavelengths and n is number of light fixtures in the system. For example, consider a finite system with six bits of precision, then a single setpoint x could take on over $10,000,000$ different values. Hence, for one light comprised of five wavelengths, the search space becomes 10^{35}. And this is only for a single fixture.

If a typical office has four light fixtures installed overhead, where each lamp contain five wavelengths, then the search grows to 10^{140}. With each additional light fixture to consider, the search space grows exponentially. Controlling a large workspace consisting of $n = 25$ fixtures is practically out of the question, unless we employ an algorithm that efficiently narrows the search in a short amount of time. Still, future systems will benefit from some sort of localization to infer which light fixtures are closest to the optical sensor node measuring the illuminance. To keep the dimensionality of the search space low, multiple nodes must be installed in large deployments.

Yet there are simpler solutions that may also yield reasonably accurate results. The microcontroller (8, 16, or 32 bit) controlling the intensity of each wavelength in a light source has a finite resolution many times smaller than that of the machines performing the global search. Consider a system in which the setpoint x, where $\{x \in \mathbb{Z}^{mn} : 0 \leq x \leq 2^p - 1\}$, and $p = 16$. Again with $m = 5$ and $n = 1$, then there are $(2^{16} - 1)^5 \approx 10^{24}$ solutions. By considering just unsigned 16-bit integers, our search space shrinks by 11 orders of magnitude. Similarly, if $p = 8$, $m = 5$, and $n = 1$, there are now just 10^{12} solutions. This approximation of the search space makes run-time substrates possible at the cost of system resolution.

3.2 Linear Methods of Controlling the Spectral Power Distribution

Traditional methods of color control assume a linear relationship between the setpoint and the output. These techniques often formulate the problem as a linear mixture of red, green, and blue components, whose tristimulus values were measured in a previous calibration step.

In these problems, the exact solution is found by solving the linear equality $\mathbf{Ax} = \mathbf{b}$ for $\mathbf{x}$. However, the system could also be formulated with more equations than unknowns, hence $\mathbf{x}$ is overdetermined and no exact solution exists. In this case, a common technique uses the pseudoinverse to minimize the sum-squared error between $\mathbf{Ax}$ and $\mathbf{b}$, resulting in an exact minimum square error solution if $\mathbf{A}$ is non-singular. As will be shown in Chapter 5, these methods allow the correct color temperature to be found, but often have a low color rendering index.

While these approaches work well to calibrate most optical sensors (e.g., those in scanners, cameras, etc.), they are not necessarily optimal for lighting. They fail because this linear approach does not take into account the nonlinearity of calculating the color rendering

index. In this case, the only real benefit of these methods is the relatively low computational complexity to obtain an answer.

Exact Solutions

Most often, we are interested in the relationship between a setpoint and the resulting color. If the lighting system is comprised of three wavelengths, say red, green, and blue, then the relationship is of the form $\mathbf{Ax} = \mathbf{b}$. In this case $\mathbf{A}$ is a 3-by-3 matrix comprised of tristimulus values from the measured system

$$\left(\begin{pmatrix} X_r & X_g & X_b \\ Y_r & Y_g & Y_b \\ Z_r & Z_g & Z_b \end{pmatrix} \begin{pmatrix} R_{set} & 0 & 0 \\ 0 & G_{set} & 0 \\ 0 & 0 & B_{set} \end{pmatrix}^{-1} \right) \begin{pmatrix} R \\ G \\ B \end{pmatrix} = \begin{pmatrix} X \\ Y \\ Z \end{pmatrix}, \tag{3.15}$$

where $\mathbf{x}$ is the setpoint for controlling the intensity of the RGB system. Intensity values R_{set}, G_{set}, and B_{set} represent the intensity setting used at the time when the tristimulus values were measured, most often scaled to one. Solving Eq. 3.15 yields

$$\begin{pmatrix} X_r R_{set} & X_g G_{set} & X_b B_{set} \\ Y_r R_{set} & Y_g G_{set} & Y_b B_{set} \\ Z_r R_{set} & Z_g G_{set} & Z_b B_{set} \end{pmatrix}^{-1} \begin{pmatrix} X \\ Y \\ Z \end{pmatrix} = \begin{pmatrix} R \\ G \\ B \end{pmatrix}. \tag{3.16}$$

Using Eq. 3.16, we can specify the desired tristimulus value. Quite often, this tristimulus value is derived from the two-dimensional chromaticity coordinate of the desired correlated color temperature.

It is common to normalize the white point of matrix $\mathbf{A}$ such that the sum of the Y tristimulus sum to 100. In this case, every element in matrix $\mathbf{A}$ is multiplied by a scaling factor c, where

$$c = \frac{100}{Y_r + Y_g + Y_b}. \tag{3.17}$$

This centers the fixture's whitepoint such that $Y = 100$. The solution $\mathbf{x}$ is of the set $\{\mathbf{x} \in \mathbb{R}^n : 0 \leq \mathbf{x} \leq 1\}$. If $\mathbf{x}$ is outside of this set, then it represents a point in space unachievable with the current configuration.

If we add a fourth wavelength to the system, a simple approach is fix the ratio of this fourth wavelength to its closest color. For example, if we add an amber color, we make amber a fixed ratio, α, of the red setpoint. In this example, the solution is

$$\begin{pmatrix} X_r(\lambda_1) + X_r(\lambda_2) & X_g & X_b \\ Y_r(\lambda_1) + Y_r(\lambda_2) & Y_g & Y_b \\ Z_r(\lambda_1) + Z_r(\lambda_2) & Z_g & Z_b \end{pmatrix}^{-1} \begin{pmatrix} X \\ Y \\ Z \end{pmatrix} = \begin{pmatrix} R \\ G \\ B \end{pmatrix}, \tag{3.18}$$

where

$$\begin{pmatrix} R \\ A \\ G \\ B \end{pmatrix} = \begin{pmatrix} R \\ \alpha R \\ G \\ B \end{pmatrix}. \tag{3.19}$$

Similarly, we can do the same for five wavelength system. However, these are naive techniques, which constrain the radiant energy to a linear system in which the output color is the only concern. This problematic approach is only slightly mitigated by removing this fixed ratio, and minimizing the sum-squared error.

Overdetermined Systems

If we consider a linear system of the form $\mathbf{Ax} = \mathbf{b}$ that contains four wavelengths than we can rewrite matrix $\mathbf{A}$ as a 3-by-4 system. However, $\mathbf{A}$ is now rectangular and has more equations than unknowns, $\mathbf{x}$ is overdetermined, and, no exact solution exists. But, we could seek a solution of $\mathbf{x}$ that minimizes the sum-squared error between $\mathbf{Ax}$ and $\mathbf{b}$, such as $J_s(\mathbf{x}) = \|\mathbf{Ax} - \mathbf{b}\|^2$. In this classical problem, the norm has a closed form solution, and we solve for the Jacobian by taking the derivative of $J_s(\mathbf{x})$ and setting the solution to equal to zero. Solving this leads to the pseudoinverse:

$$\begin{aligned} \mathbf{x} &= (\mathbf{AA})^{-1}\mathbf{A}^T\mathbf{b} \\ &= \mathbf{A}^{\dagger}\mathbf{b}. \end{aligned} \tag{3.20}$$

Using the four wavelength example to illustrate a red, amber, green, and blue system:

$$\begin{pmatrix} R \\ A \\ G \\ B \end{pmatrix} = \left(\begin{pmatrix} X_r & X_a & X_g & X_b \\ Y_r & Y_a & Y_g & Y_b \\ Z_r & Z_a & Z_g & Z_b \end{pmatrix} \begin{pmatrix} S_1 & 0 & \dots & 0 \\ 0 & S_2 & \dots & 0 \\ \vdots & \vdots & \ddots & \vdots \\ 0 & 0 & \dots & S_4 \end{pmatrix}^{-1} \right)^{\dagger} \begin{pmatrix} X \\ Y \\ Z \end{pmatrix}, \tag{3.21}$$

where the 3-by-4 tristimulus matrix is measured with some intensity setting denoted here as S_i, where i corresponds to the specific wavelength, with a typical intensity such that solution $\mathbf{x}$ is of the set $\{\mathbf{x} \in \mathbb{R}^n : 0 \leq \mathbf{x} \leq 1\}$ where the dimension of the space is n, the number of wavelengths.

Using this method, we are guaranteed that for any T_c, a minimum square error solution exists. Therefore, in contrast to the method in Eq. 3.18, we are no longer tasked with finding the ratio α such that we minimize error for any arbitrary T_c.

The use of this method, which is a improvement over the ratio-based technique is nearly non-existent in literature regarding spectral control of LEDs.

3.3 Proposed Method of Control: Direct Search

Here we consider an entirely new approach for solving the optimal setpoint in a system composed of an arbitrary number of wavelengths. The key insight here is that linear models are efficient (for the most part) at accurately controlling the intensity for a specified correlated temperature, yet this solution, due to the nonlinear nature of calculating the color rendering index, leads to a chromatically accurate white light with a low color rendering index. This is not desireable.

The reason is that parameter R_a is the average color difference of eight different color samples illuminated by both the test light source and a perfect illuminant (perfect meaning a CRI of 100). Often times, a setting obtained using a linear method may have a good score ($R_i > 80$) for less than quarter of the color samples. Finding the optimal R_a means finding a feasible set of solutions in the search space, while at the same time meeting the illuminance constraints and desired color temperature.

In this section, we briefly introduce direct search algorithms, describe a subset of two relatively new methods, pattern search and mesh adaptive search, and their application to solve the problem detailed in Sec. 3.1.

Background

Direct search methods are a class of optimization algorithms that require only a numerical answer, supplied by the iterative evaluation of the objective, that guides the search. In general, these methods are applicable to problems that lack a closed form solution, or non-convex, or discontinuous. In the words of Audet et al.,

> "There is a wide spectrum of optimization methods. At one of the spectrum, there are those designed to exploit a specific known structure of the optimization problem. For example, the simplex method [19] is designed to exploit the linearity of both the objective and constraint functions to solve large problems efficiently. At the other end of the spectrum are methods that do not or cannot exploit any structure. This is often the case when the objective and/or the constraints are evaluated through computer code (such as process simulator) or by an experiment...Direct search methods belong to the end of the spectrum [7]."

The first published papers on direct search appeared in the early 1960s, yet they lacked rigorous convergence analysis and were dismissed by the community for almost 30 years until the award winning work of Torczon [74] on the convergence of pattern search algorithms, which are a generalization of algorithms used by Hooke and Jeeves [27]. Powell [53] describes the many forms of direct search: line search, discrete grid, simplex methods, conjugate direction, linear approximation, quadratic approximation, and simulated annealing. Some well known direct search methods documented by Audet et al. are: Jones et al. [31], Hooke

and Jeeves [27], Rosenbrock [56], and Nelder and Mead [46]. Kolda, Lewis, and Torczon [32] also provide a historical and technical review of these methods.

Pattern Based Algorithms

The generalized pattern search algorithm described in [74] proves the convergence of an iterative algorithm most analogous to the classic "compass search." In this work, Torczon established global convergence, that is, subsequent iterates (i.e., progressively decreasing the objective function) that guaranteed first order convergence and hence proved the algorithm's optimality. Recently (2006), the mesh adaptive direct search algorithm (MADS) published in [10, 9] extends the work of Torczon, but calculates the search points at random. Both methods allow for both linear and nonlinear constraints and bounds, however the algorithms perform exceedingly well in unconstrained cases. The algorithms are implemented in MATLAB as part of the Global Optimization Toolbox [71].

Algorithm Description

Both pattern search and the mesh adaptive algorithm are iterative algorithms that evaluate a *mesh* centered around the *current point*. A mesh is formed by the multiplication of the current point with a set of vectors called a *pattern*. Typically these patterns are of the maximum basis $2n$ or minimum basis $n+1$, where n is the total number of dimensions in the search space. The size of mesh, *mesh size*, is used along with the pattern and *incumbent solution* in a *poll step*, where the new points in the mesh are tested to see if they are smaller than the present solution. Both algorithms have the ability to grow or shrink the size of mesh such that the search can expand and contract based upon the results of the user-supplied evaluation function. With each incumbent solution, the algorithm shrinks the mesh, and when the mesh size decreases beyond a threshold, the algorithm terminates. Of course, there are many more details that are omitted in this discussion. These are found in [74, 37, 36, 1, 10, 8, 2].

3.4 Lighting Network Control

In order to evaluate the methods of spectral control and test the closed loop control of the lighting network (detailed in Secs. 3.1 and 3.2) a custom toolbox was written in MATLAB. The spectrometer processing and optimization toolbox (SPOT) is a collection of functions that calculate and evaluate illuminance, color temperature, color rendering, and the new color quality scale (CQS) [20]. These functions were used in the evaluation and control of lighting parameters in this work. It is planned to release this package to the community under open source license.

1. *Measurement* (*once per lamp*)
    a) Perform a calibrated radiometric measurement for each of the wavelengths in the system to obtain the spectral power distribution, E_e or P_e. Measure system quiescent current, (I_q) and the maximum forward current (I_λ) for each wavelength.
2. *Calibration*
    a) Perform room calibration. Measure E_{dark} and E_v for an arbitrary set point for all the controllable fixtures in the area and calculate the contribution of each light source at the sensor node. (Sec. 3.1).
3. *Calculate Optimal Setpoint*
    a) Specify an objective function (Eq. 3.11) and select what parameter will be maximized (CRI or Efficacy), then specify a target color temperature T_c and desired illuminance $E_{desired}$. The objective function operates using a model of the system using the spectral data acquired in step 1.
    b) Obtain results and set light fixtures.
4. *Update*
    a) Continuously monitor for changes in intensity or color temperature at the sensor node or requests for recalibration.
        i. If $E_{desired}$ or T_c change but the sensor node is not displaced go back to step **??**.
        ii. If sensor node is displaced or recalibration is requested, go back to step 2.

Figure 3.1: The lighting control algorithm.

Control by Optimization Workflow

The control problem is summarized in Fig. 3.1. The process begins with step 1. Controlling the spectral output of a single or group of light fixtures requires a one time step of measuring either the radiant flux with symbol P_e (W), which requires the use of an integrating sphere, or the irradiance E_e ($\mathrm{W} \cdot \mathrm{m}^{-2}$) and distance of the measurement, the latter of which is used in this work. Additionally, in this step, the voltage, quiescent current $I_{p,q}$, and maximum current I_p, for each wavelength are also recorded. Step 2 is the calibration step. Here, the E_{dark} of the room is measured, as well as the individual illuminance of each of the fixtures measured by the sensor node. In step 3, the direct search algorithm is called using the information in collected in steps 1 and 2 with additional information about what to maximize. Finally, in step 4, the system continuously monitors for changes and returns to either step 2 or step 3, depending on what happened.

3.5 Sensor Feedback in a Lighting Network

If a sensor was introduced that measures color, for example, red, green, and blue, then Eq. 3.22 can be written to include the color sensor information. Assuming a calibration step is taken where the intensity of the system is set to maximum, we omit writing the setpoint matrix and define the problem as:

$$\left(\begin{pmatrix} X_r & X_g & X_b \\ Y_r & Y_g & Y_b \\ Z_r & Z_g & Z_b \end{pmatrix} \begin{pmatrix} R_r & R_g & R_b \\ G_r & G_g & G_b \\ B_r & B_g & B_b \end{pmatrix}^{-1} \right) \begin{pmatrix} R_s \\ G_s \\ B_s \end{pmatrix} = \begin{pmatrix} X \\ Y \\ Z \end{pmatrix}, \tag{3.22}$$

where the vector of interest is found by the red, green, and blue measurements from the color sensor. In this case, the solution is of the form $\mathbf{A^{-1}b} = \mathbf{x}$, where $\mathbf{b}$ represents the tristimulus values of the desired color and $\mathbf{x}$ the corresponding sensor values. Thus, the expected sensor values can be obtained by first performing a calibration step where the fixture is set to a maximum intensity and the corresponding trimstimulus and sensor values are recorded for later computation. Once these values are obtained, closed loop operation is maintained by comparing the expected color sensors values to the measured sensor values. Typically a proportional, integral and derivative (PID) type controller is used to minimize error between the setpoint and measured values [3, 5].

If the system is comprised of more than three wavelengths, then the color levels can be approximated using a similar channel such as red for amber, or blue for cyan, at the cost of decreased responsivity (this sacrifice in dynamic range reduces the ability to converge on particular solutions). This could be augmented by using additional sensors and placing a tinted filter over the array to reject wavelengths not in the desired bandpass. For example, using a five wavelength system, we pose to color-feedback and control as:

$$\begin{pmatrix} R_s \\ A_s \\ G_s \\ C_s \\ B_s \end{pmatrix} = \left(\left(\begin{pmatrix} X_r & X_a & X_g & X_c & X_b \\ Y_r & Y_a & Y_g & Y_c & Y_b \\ Z_r & Z_a & Z_g & Z_c & Z_b \end{pmatrix} \mathbf{S}^{-1} \right)^{\dagger} \begin{pmatrix} X \\ Y \\ Z \end{pmatrix}, \right. \tag{3.23}$$

where $\mathbf{S}$ is a square matrix containing the color sensor readings for the five channels each measured for a particular wavelength,

$$\mathbf{S} = \begin{pmatrix} R_r & R_a & R_g & R_c & R_b \\ A_r & A_a & A_g & A_c & A_b \\ G_r & G_a & G_g & G_c & G_b \\ C_r & C_a & C_g & C_c & C_b \\ B_r & B_a & B_g & B_c & B_b \end{pmatrix}. \tag{3.24}$$

The results of Equations 3.22 and 3.23 produce a result that is the sum of the sensor readings for every channel. This means that the solution cannot be used to explicitly set the intensity of each channel. If we take into account the sensitivity of a single wavelength to the other wavelengths, then assuming there is no wavelength shift, we can decouple the system. Using Equation 3.23 as an example, we extend the results of [5] to five wavelengths and compute the sensitivity matrix as

$$\Gamma = \begin{pmatrix} 1 & R_a/A_a & R_g/G_g & R_c/C_c & R_b/B_b \\ R_a/R_r & 1 & A_g/G_g & A_c/C_c & A_b/B_b \\ R_g/R_r & G_a/A_a & 1 & G_c/C_c & G_b/B_b \\ R_c/R_r & C_a/A_a & C_g/G_g & 1 & C_b/B_b \\ R_b/R_r & B_a/A_a & B_g/G_g & B_c/C_c & 1 \end{pmatrix}, \tag{3.25}$$

and solve $\mathbf{Ax} = \mathbf{b}$ for $\mathbf{x}$, that is,

$$\Gamma^{-1} \begin{pmatrix} R_s \\ A_s \\ G_s \\ C_s \\ B_s \end{pmatrix} = \begin{pmatrix} \hat{R}_s \\ \hat{A}_s \\ \hat{G}_s \\ \hat{C}_s \\ \hat{B}_s \end{pmatrix}. \tag{3.26}$$

The decoupled sensor readings can now be used to directly set the intensity of the individual channels.

Chapter Four

Physical Implementation

The hardware, firmware, and software developed in this research phase aims to break new ground in the control of energy efficient lighting networks by researching and implementing highly configurable light sources and determining the proper feedback sent from the sensor network. In this chapter, we present a novel pentachromatic lighting and control system to test the theory defined in Chapter 3.

4.1 Requirements

The ideal system is comprised of a sensor node, daylight, incandescent, fluorescent, and LED technologies. The sensor node measures the intensity and color temperature of all sources and sends the data to a controller (in this research, a computer). The controller processes these data and, taking into account the user's preferences, sets the lighting to the optimal conditions (Figure 4.1 on page 41). This method can be extended for multiple control nodes. However, with some adaptation, the enhanced processors utilized in both the sensor and lighting controllers can perform most of the lookup routines and some floating point calculations. Additionally, an embedded processor (i.e., ARM 9, Atom, or OMAP) running an operating system could perform the same optimization algorithms as the computer.

To solve the problem outlined in Section 3.1, we designed a prototype LED lighting system and sensor board. The intensity of the LED fixture is controlled using pulse width modulation (PWM). This requirement is crucial, since much of the theory requires that the power and intensity relationship of the light fixture be linear. A digital signal processor (DSP) with microcontroller-type peripherals controls the intensity, monitors onboard LED operating temperature, intensity and color, and has a bidirectional data link to the computer. The sensor node measures intensity and color. These data allow the controller to estimate the illuminance and correlated color temperature of each light source. The sensor node also features basic controls for the user (e.g., intensity and color control), and detects occupancy. The LED array is comprised of five dominant wavelengths; four of the LEDs are active emitters and and one is a phosphor based device. This enables a wide range of possible

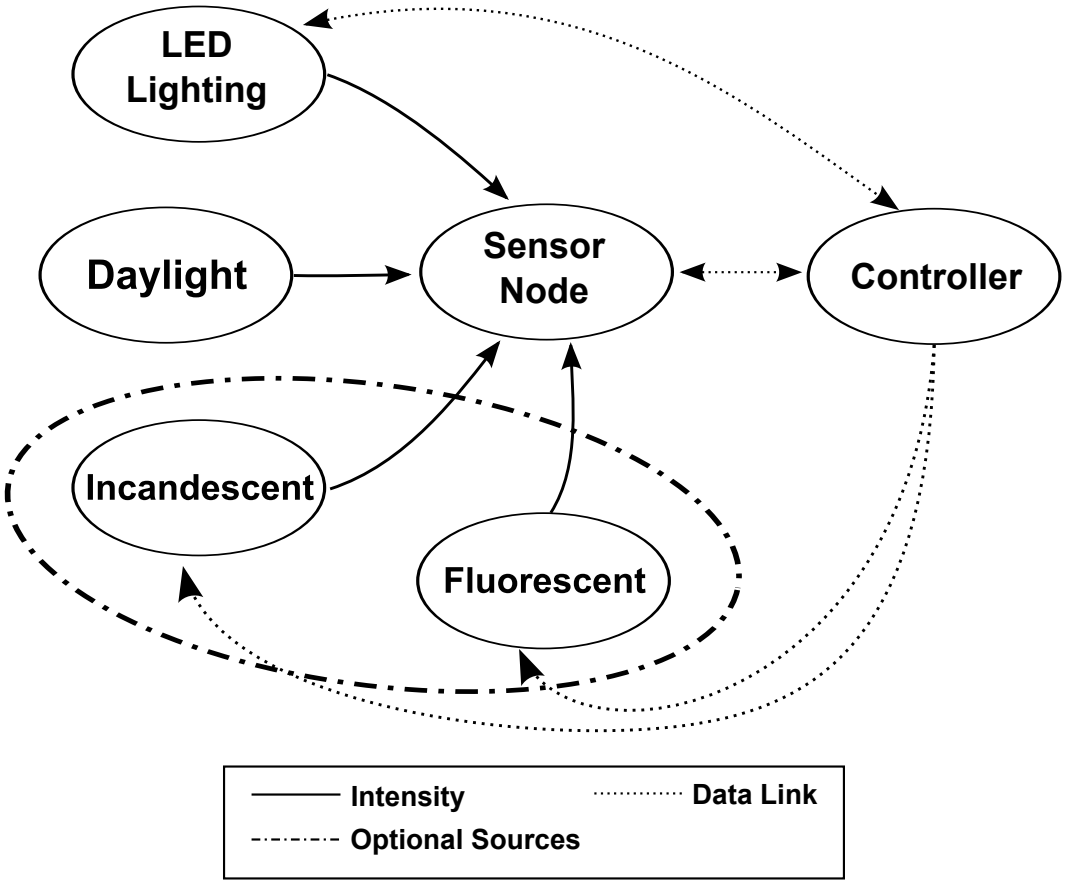

Figure 4.1: System diagram. The lighting network consists of LED light sources, optional incandescent and fluorescent sources, and ambient room conditions (daylight), that are measured by a single or group of sensor nodes. The sensor nodes return intensity and color information back to the control node (e.g., a computer) for processing. Here, the intensity is controlled via a link to the artificial light sources. The data link is bidirectional from either the sensor node or the LEDs.

color temperatures and serves a second purpose – the broad spectral range ensures an exceptionally high color rendering index.

4.2 Sensor Node

The sensor node is controlled by a TMS320F28027 controller from Texas Instruments and is comprised of multiple sensors. The device detects occupancy via a passive infrared sensor (AMN11111, Panasonic), as well as measures the illuminance and color of incident light (Table 4.1 on page 43). The sensor also features a basic user interface, realized using linear potentiometers and buttons. These serve to specify the intensity and color temperature of the adjustable light sources.

Measuring the illuminance is achieved using three analog linear illuminance sensors (ISL29006, Intersil) with different sensitivities and one digital sensor (TCS3414CS, Taos). The analog sensors are sampled by the system at 30Khz using a 12 bit successive approximation converter. Oversampling of the sensors is user configurable (up to 256×). Two of the sensors are filtered using a second order unity gain low pass with a cut off frequency of 50 Hz which ensures illuminance data is accurately measured when fixture intensity is less than 100% (the circuit integrates the duty cycle of the LEDs). The integration time (e.g., update rate) of the digital color sensor is a function of an internal timer which controls the acquisition time of the digital color sensor. This is nominally set to 120 Hz. The digital color sensor measures the irradiance of a photodiode array consisting of red, green, blue, and clear filters. Figure 4.2a on page 44 is an image of the prototype sensor node. The prototype is on two layer 1.65 mm (0.065 in) thick circuit board and measures 178×119 mm (7×4.7 in). Near-future modifications include drastically reducing board size, adding an accelerometer, and reducing power consumption.

4.3 LED Controller

A TMS320F28027 from Texas Instruments runs custom firmware to control the LEDs and read the sensors. The system requires the use of a 24V supply and is powered by a laptop power supply rated at 24V, 2.2A. Five BuckPlus DC-DC buck converters from LEDdynamics drive the LEDs. The intensity is controlled by five independent 16-bit PWM signals with a fundamental frequency nominally set at 120Hz. A single pixel digital color sensor (TCS3414CS, Taos) samples the LED array from within the fixture in certain cases, and updates color data at 20Hz. This is useful for closed loop control of color at the fixture. Optionally, an internal linear analog lux sensor (ISL29006, Intersil) is also sampled at 30Khz. These sensors are used for closed loop control of the LEDs. Full duplex communication is handled by the system's asynchronous receiver and is interfaced using either a wired or wireless link. Measuring the on-board color sensor requires precise timing. The integration of the color sensor is controlled via hardware, which is synchronized to the LED fundamental

Sensor	Type	Output Bandwidth	Range	ADC Resolution	mlx / mV[a]
ISL29006, Intersil	analog, linear	50 Hz (external filter)	2000 lux	2^{12}	606 mlx/mV
ISL29006, Intersil	analog, linear	600 Hz (no filter)[b]	2000 lux	2^{12}	606 mlx/mV
ISL29006, Intersil	analog, linear	50 Hz (external filter)	10000 lux	2^{12}	3030 mlx/mV
TCS3414CS, Taos	digital (I2C), linear	50 Hz (internal filter)	5000 lux	2^{16}	1515 mlx/mV

Table 4.1: Illuminance sensor table for the sensor node in Section 4.2. The sampling frequency of the analog sensors is 30 kHz. The sampling frequency (integration time) of the digital sensor is controlled by the sensor node. It is nominally set to 120 Hz, with variable oversampling set at 2×(up to 10×).

[a] $(V_{refh} - V_{refl}) = 3.3\,V$
[b] Based on manufacturer data at 1000 lux.

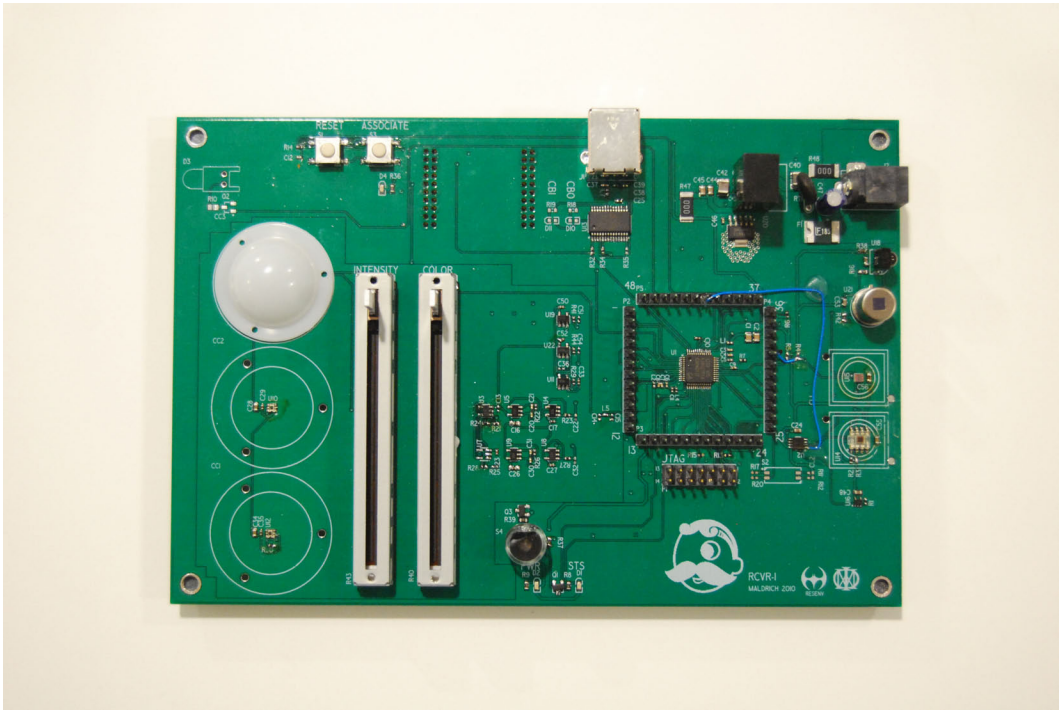

(a) Sensor Node.

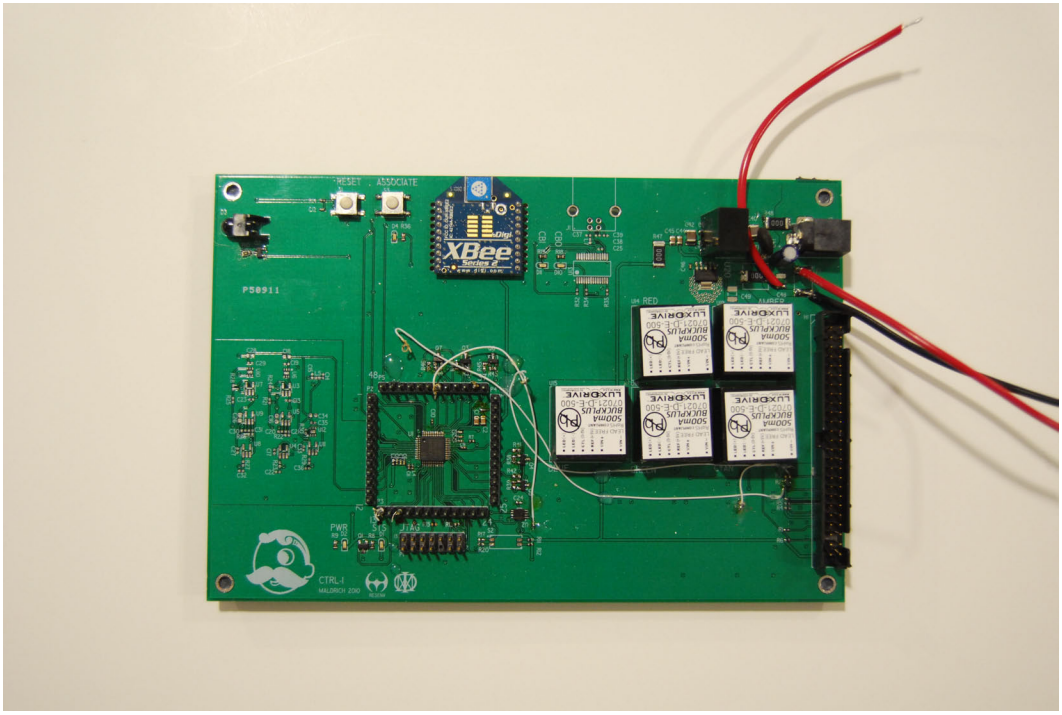

(b) LED Control Board.

Figure 4.2: The prototype sensing and control hardware used in the experiments.

frequency. This ensures color measurement precision. Figure 4.2b on page 44 is an image of the prototype controller with its input protection circuitry removed. The prototype is on a two layer 1.65 mm (0.065 in) thick circuit board and measures 178×119 mm (7×4.7 in). This board can also be reduced in size.

4.4 LED Array

The primary LED array used in this research consists of five unique wavelengths, four of which are active emitters and one that is phosphor-converted (Table 4.2 on page 46). The five colors employed are royal blue, cyan, green, phosphor-converted amber, and red. Selecting a phosphor-converted amber allows for a higher efficiency. The intensity of the red, orange, and amber wavelengths (AlGaInP compounds) are quite temperature sensitive. The efficiency of the device (i.e., conversion of electrons to photons) decreases in these compounds with shorter wavelengths. This is an unfortunate phenomenon, as our eye's sensitivity peaks at 555 nm. The blue, cyan, and green wavelengths (InGaN) compounds do not exhibit the same temperature dependence as the AlGaInP devices, however they too suffer from decreased quantum efficiency near our eye's peak sensitivity. Krames et al. [33] detail the recent breakthroughs in high efficiency optoelectronics and discuss the status and future of these devices for lighting applications. Moreover, the phosphor-converted (PC) amber uses an ultra-violet pumped blue LED to excite the organic phosphor which, re-radiates at longer wavelengths. This fixes the problem of systems with decreasing efficiency utilizing wavelengths in the neighborhood of 580 nm. The LED array also has on board temperature sensors (to estimate LED junction temperature) and can measure, using filters, the red, green, blue, and clear values of the irradiance using a TCS3414 color sensor (Table 4.1 on page 43). Figure 4.3 shows the actual array used in the research.

Informally, using discrete emitters creates a light source in which there is no scattering of the discrete wavelengths. This leads to "fringing" on the outer edge of light incident to a surface. This effect is not desireable, as it produces individual shadows cast by the LEDs near the edges of the light field. Ramer et al. [55] and Rains et al. [54] utilize constructive interference to reduce these effects. This technique requires the use of a reflective and diffuse hemisphere to scatter the photons before they emerge from the LED array aperture. However, this improvement comes at significant cost, as scattering loss lowers the total candelas of the lamp. In this research, this technique is tested and presented in Chapter 5 but ultimately, a direct view method (i.e., the LED array is facing downwards) is selected for efficiency. Figure 4.4 on page 48 shows the dome mounted on the LED array, which in turn is mounted to aluminum heatsink.

Color	Dominant Wavelength	FWHM[a]	lm / W[b]	Lumiled Part
Royal Blue	440nm - 460nm	30 nm	350 mW/W[c]	LXML-PR01-0350
Cyan	490nm - 520nm	30 nm	70 lm/W	LXML-PE01-0070
Green	520nm - 550nm	24 nm	70 lm/W	LXML-PM01-0070
Amber (Phosphor)	587.8nm - 595.4nm	80 nm	70 lm/W	LXM2-PL01-0000
Red	620.5nm - 645nm	20 nm	40 lm/W	LXML-PD01-0040

Table 4.2: Description of the color, dominant wavelength, full width half maximum, efficacy and full part number of the LEDs used to test the system.

[a] Full Width Half Maximum (FWHM) describes the bandwidth of the spectral output. It is related to the standard deviation (σ) of a Gaussian distribution such that: FWHM $= 2\sqrt{2\ln 2}\sigma$.

[b] forward current is 350 mA

[c] published as radiometric power (mW)

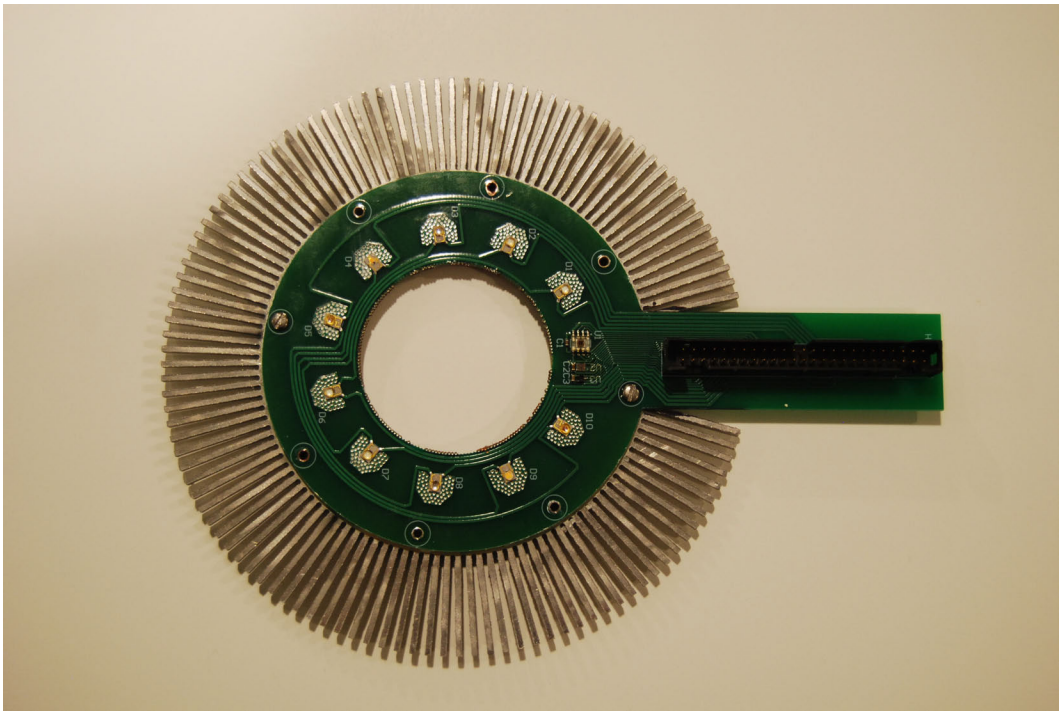

(a) LED Ring comprised of Luxeon Rebel emitters

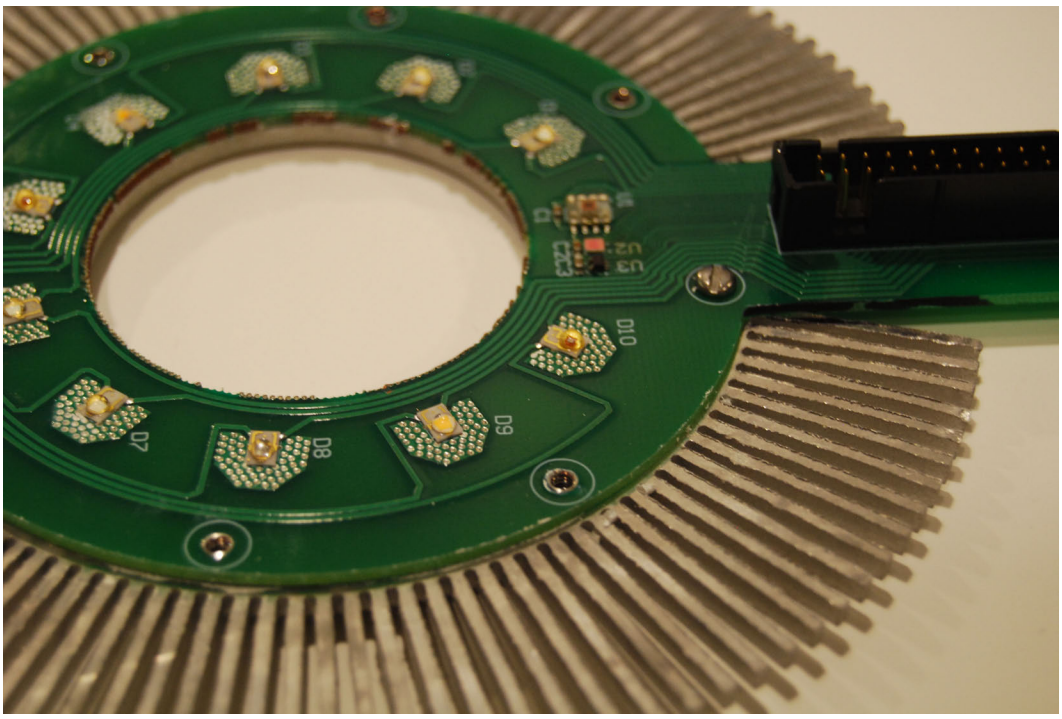

(b) Close up of LED array

Figure 4.3: The LED ring comprised of five wavelengths with on-board color and temperature sensors (mounted on a concentric heat sink).

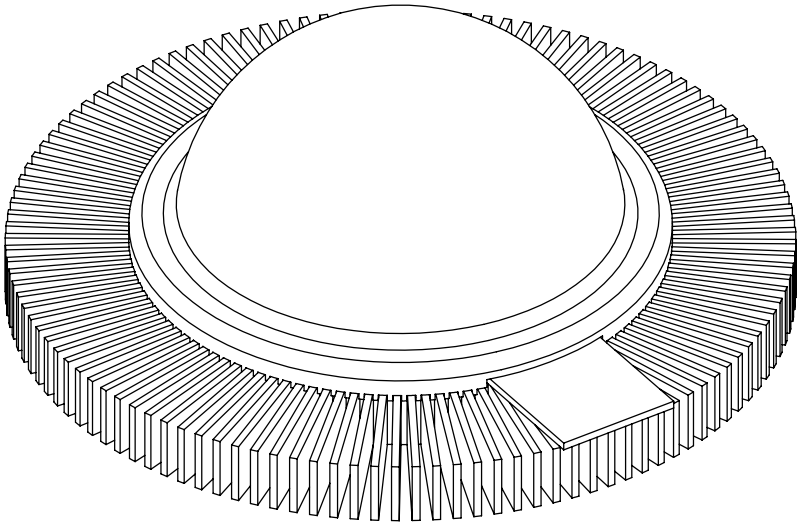

(a) Rendering of dome and heatsink [62, 73].

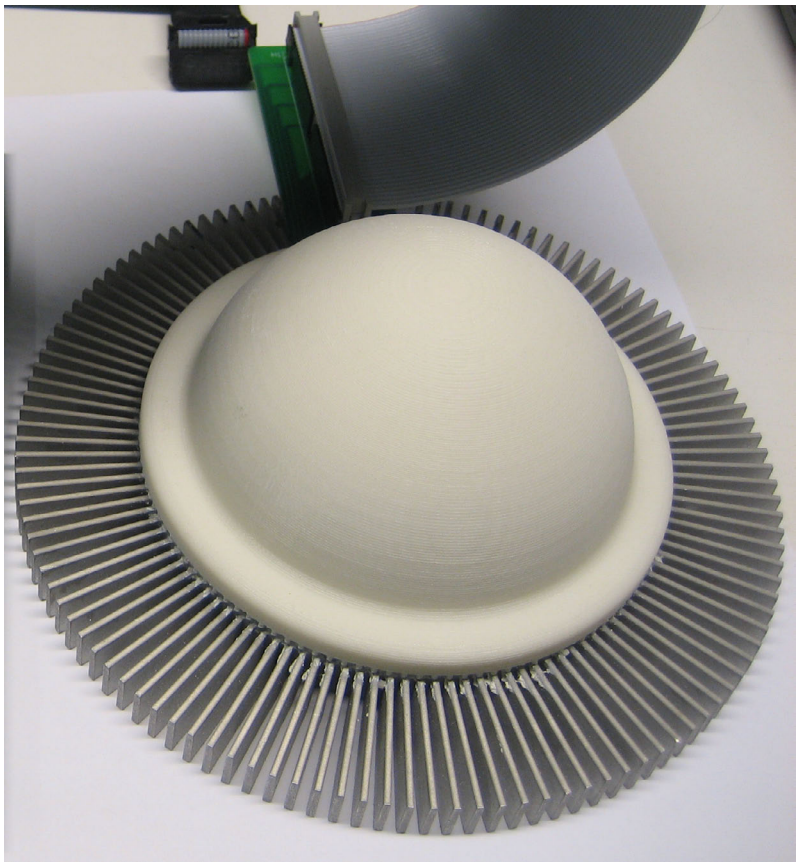

(b) LED array with dome mounted and heatsink.

Figure 4.4: Interference dome mounted on the LED array with aluminum heatsink. The interference technique is adapted from [55, 54].

Chapter Five

Observations

The experimental results are presented in this section. Where needed, theoretical predictions are provided for comparison.

5.1 Experiment Setting

For two weeks, a "dark room" conveniently located in building E14 served as the testing area to acquire the LED spectra. The generic setup utilized an adjustable light source, a fixed sensor node (with illuminance sensors), and a cosine-corrected spectrometer head. A laptop interfaced the electronics and stored the data using MATLAB. The testing environment was not necessarily ideal due to reflected light (there were reflective aluminum objects in the room) and lack of baffling, but sufficed to take the data. The wide field of view for both the sensor node and spectrometer are somewhat sensitive to reflected light from the the source. These data in the experiments were downsampled to 1 nm resolution for processing.

5.2 LED Measurement

A series of experiments to measure the linearity of the system were conducted. These experiments measured absolute irradiance and the power of each channel of the system. A cosine-corrected USB4000 spectrometer radiometrically calibrated against a NIST traceable radiometric standard measured system irradiance (see Appendix D). The spectrometer data are sampled at 0.1 nm resolution and downsampled to 1.0 nm for all subsequent processing. The spectrometer data were used to create a model of the light source for the computer-optimized control of the system.

Observing the Inverse Square Law

The light source (light source A) was set to maximum intensity and the distance of the light from the from the spectrometer and sensor node was varied. The objective of this

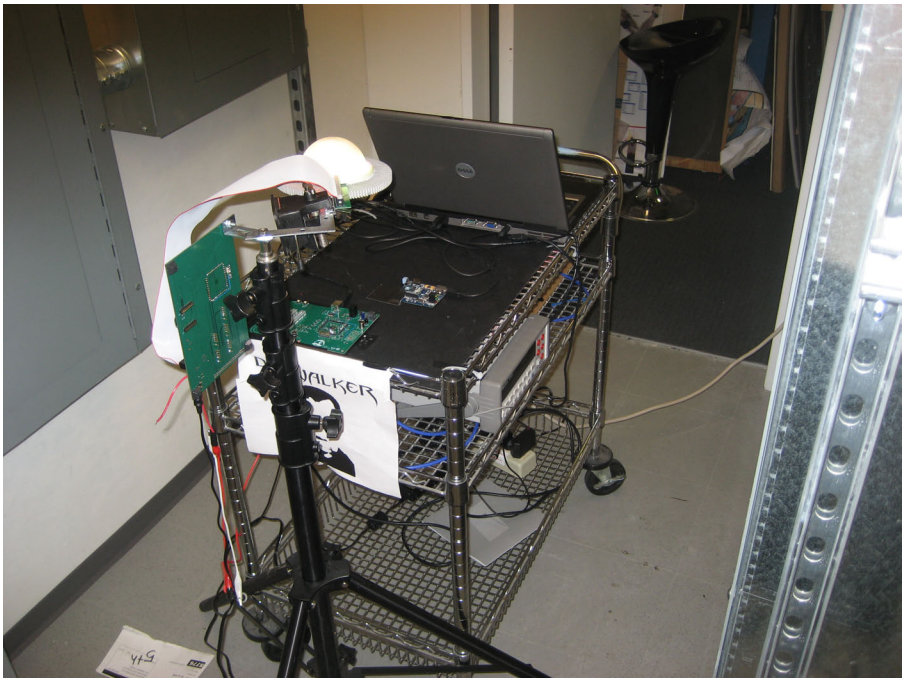

(a) Testing with the dome.

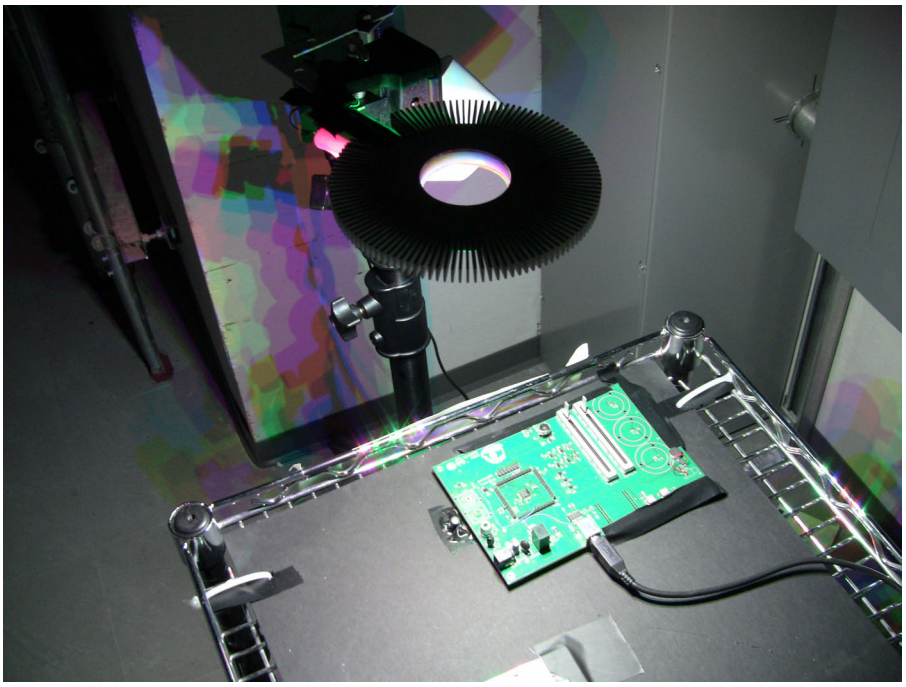

(b) Testing without the dome (notice fringing effects).

Figure 5.1: The makeshift "dark room" for acquiring LED spectra. In most experiments, the distance was fixed at 30 cm and the illuminance and power of the setting is measured.

experiment is to confirm the assumption that the light source acts like a point source (see Fig. 5.2).

Linearity and Superposition

Experiment #1

In this experiment, the distance was fixed at 30 cm and the intensity of the individual LEDs, as well as, the "all on point" of light source A was varied. The illuminance was measured using the TCS3414 sensor (clear channel) and a HP 34401A multimeter measured the current. The supply voltage was 24 V. The spectrometer data from this experiment were obtained incorrectly, so a second set of experiments were conducted (Fig 5.5 is a graph of this error). The problem was determined to be an electronic dark correction setting on the spectrometer. In effect, this setting subtracted too much irradiance from the individual LED measurements such that there was a large error between the whitepoint and the superposition of the individual spectra. This problem was fixed in experiment 2. However, data acquired using the sensor node's digital color sensor are still valid (see Fig 5.3 and Fig 5.4). Although the sensor does not report an absolute measurement, it still captures the effects of temperature (measured in sensor counts). The measured quiescent power consumption, $P_q = 2\,W$, is subtracted from the measurements in Fig 5.3.

Experiment #2

To revise the errors in the spectrometer data from the previous experiment, the maximum intensity for each wavelength was acquired, this time disabling the electric dark correction and calibrating the spectrometer integration time for each wavelength. Measurements were taken at 30 cm from the source. The experiment was conducted for both the dome and no dome versions of light A (see Fig .5.6). Additionally, the optical efficiency of the dome is given in Table 5.1.

5.3 Theoretical Limits of Operation

To prepare a set of test points to prove the effectiveness of the proposed direct search algorithm, a series of experiments were devised. First, a Monte Carlo simulation was performed using the data taken in Sec. 5.2 to understand the relationship between these variables before applying the direct search algorithm. The resulting contours highlight the difficulty encountered when randomly searching in this space, namely getting stuck in local minima. Next, the individual LED spectra acquired in Experiment #2 were used to create a model similar to that in the Monte Carlo experiments. Using this model, a standard set of test points for comparing and contrasting the linear equality, pseudoinverse, and direct search with linear inequality constraints methods was created. In short, the goal was to determine if direct search was a feasible nonlinear method for controlling a single fixture.

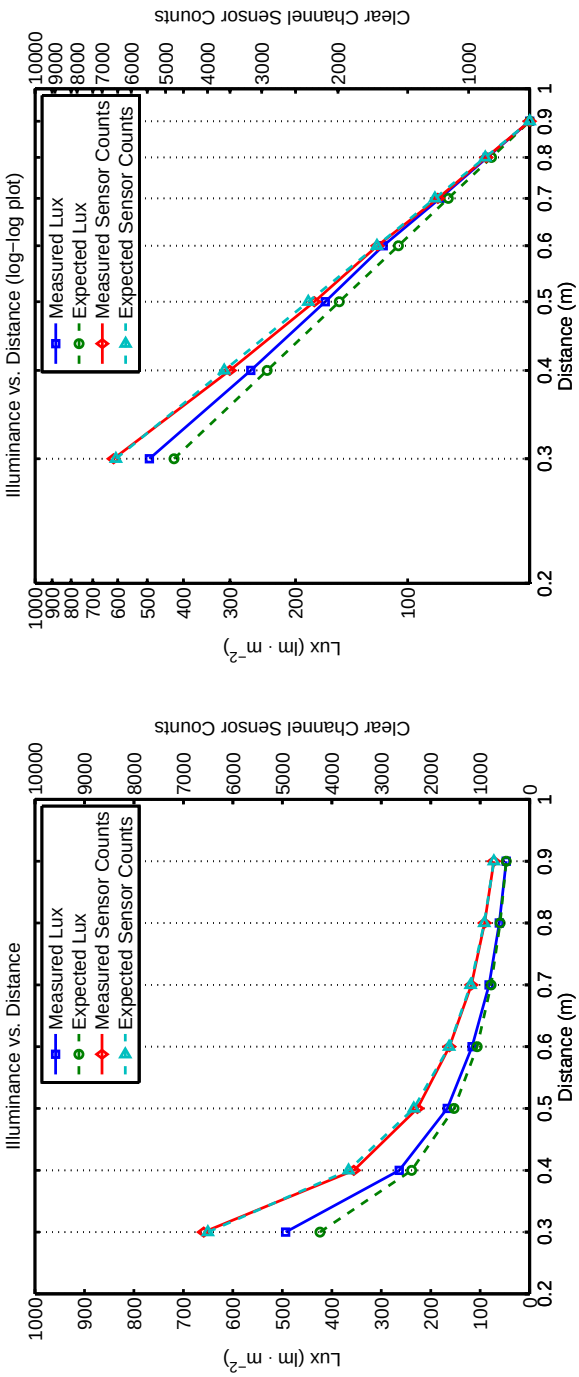

(a) A linear plot of the experiment.

(b) A log-log plot of the experiment.

Figure 5.2: Lux and TCS3414 clear channel measurements. The distance between the sensors and light source was incremented at 10 cm steps for a total of seven measurements. The expected measurements, of the form $E_v = \frac{I_{cp}}{d^2}$, are the derived from the last data point (the lux and sensor counts at 90 cm).

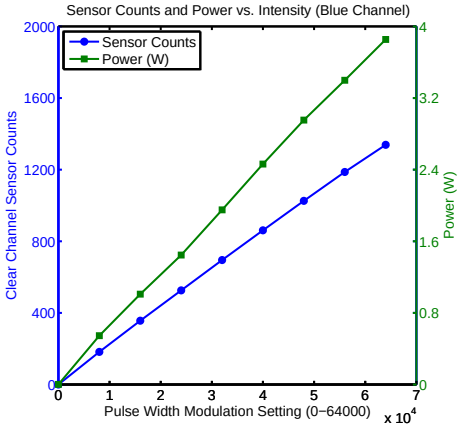

(a) Results for royal blue LEDs.

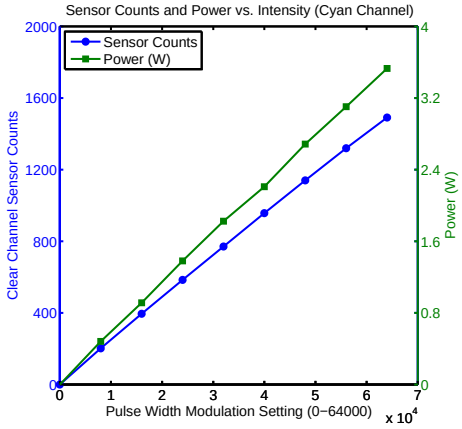

(b) Results for cyan LEDs.

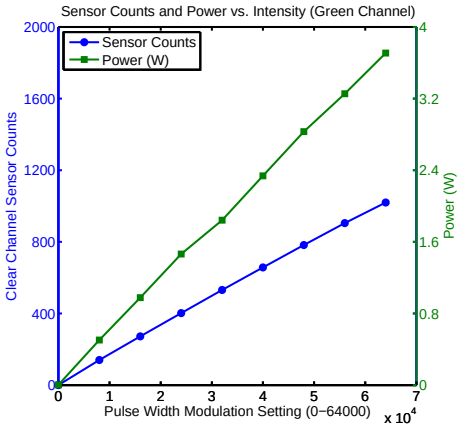

(c) Results for green LEDs.

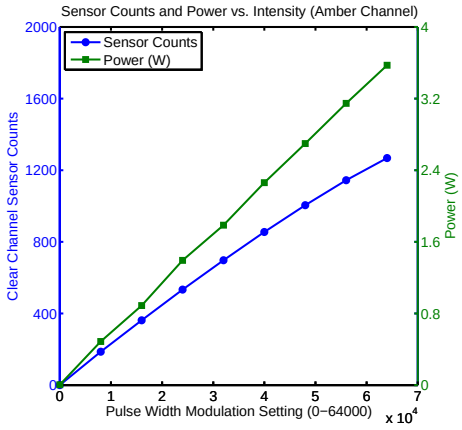

(d) Results for amber LEDs.

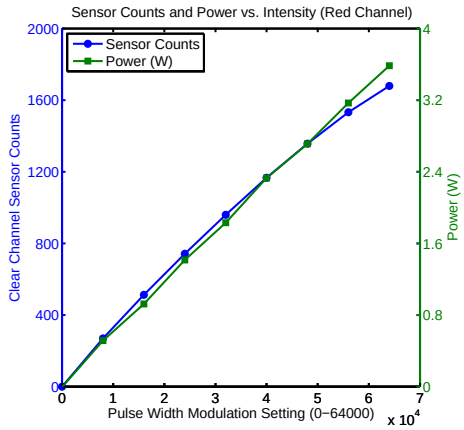

(e) Results for red LEDs.

Figure 5.3: Results of measuring each of the five wavelengths for light source A as sensed by the digital color sensor and multimeter.

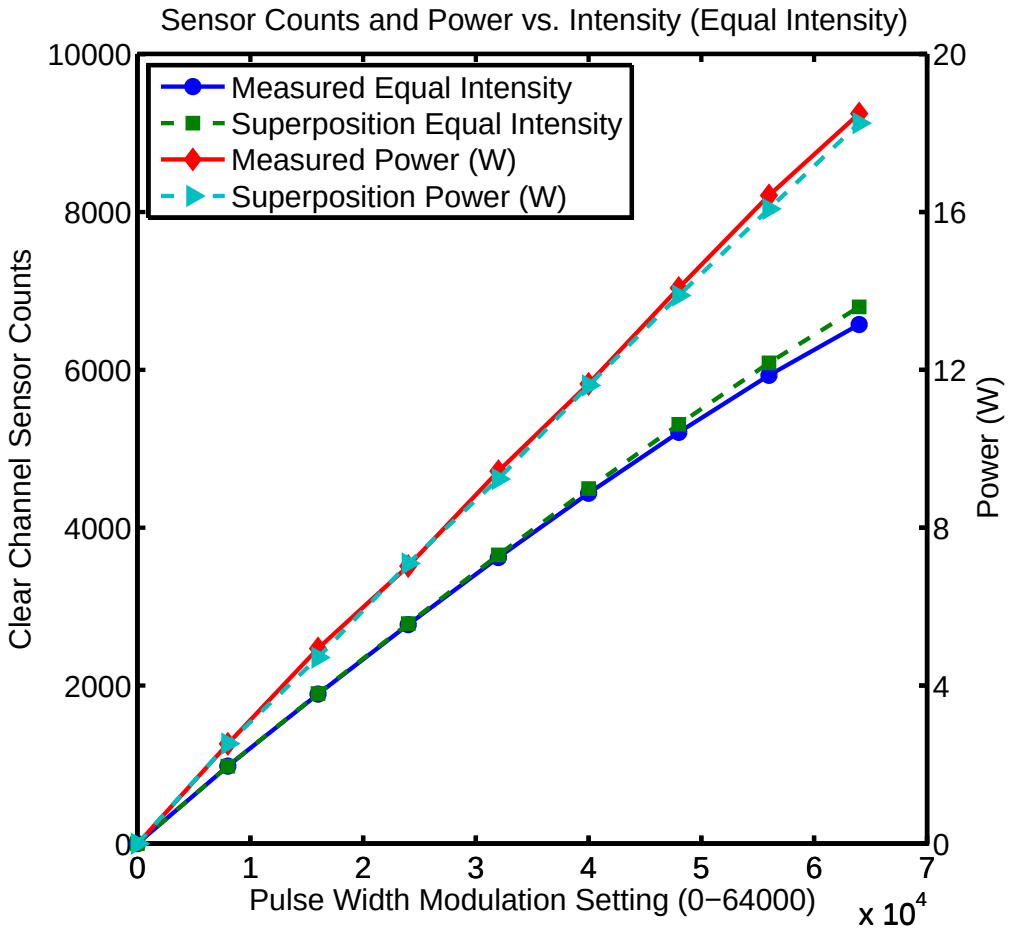

Figure 5.4: In an experiment designed to test the linearity and superposition of the individual wavelengths, all LEDs were set to the same intensity then progressively increased. The observed sensor counts and observed current were recorded. In this graph, the data acquired previously (figure 5.3) are compared to the equal intensity test. These experiments are useful to quantify the errors of the underlying linear assumption.

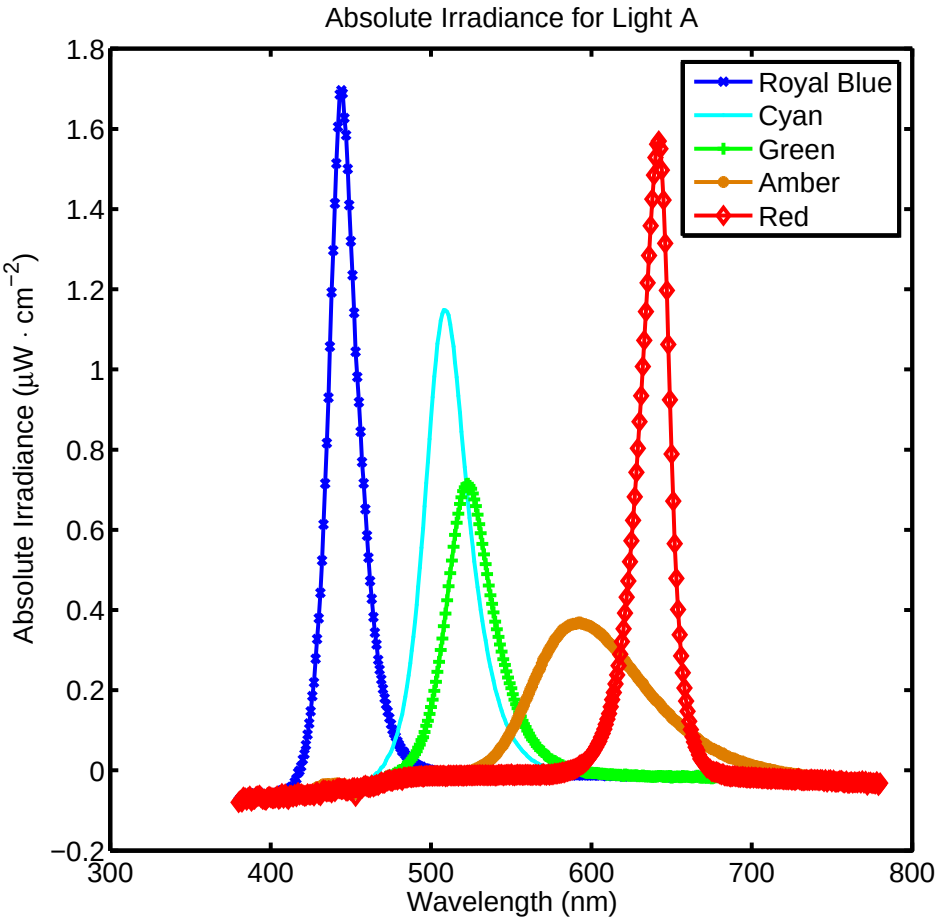

Figure 5.5: This graph shows the individual acquired spectra from experiment #1. It was later determined that an incorrect electronic dark setting in spectrometer led to incorrect readings of the individual spectral components, thus these measurements were not used to create the model of the system. Yet, the spectra adequately depict the visible energy of the system. In subsequent experiments, the electronic dark setting was disabled and the spectrometer integration time was specified for each wavelength measurement.

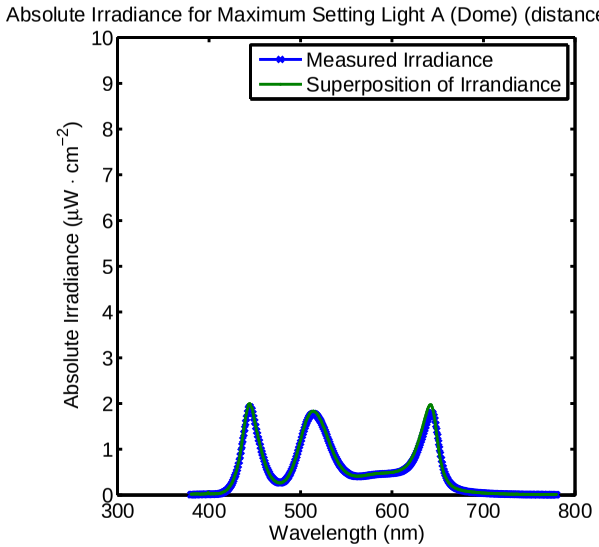

(a) Results of measured white point and sum of individual wavelength spectra with interference dome and distance=30 cm

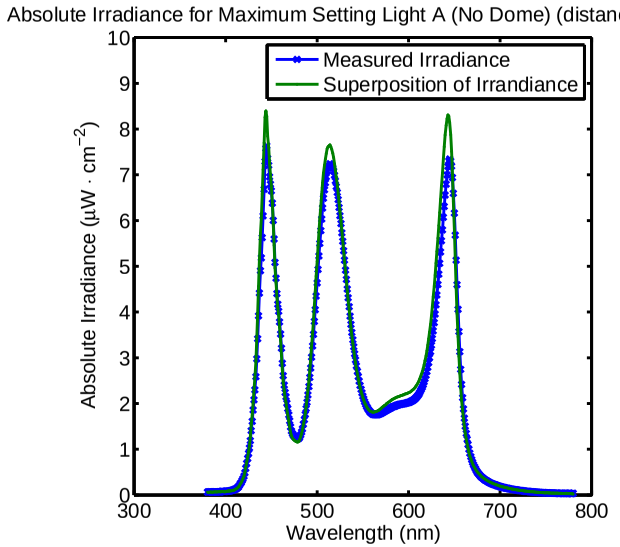

(b) Results of measured white point and sum of individual wavelength spectra without interference dome and distance=30 cm

Figure 5.6: In this experiment, the spectrometer integration time was set for each wavelength to measure the error between estimating a white point using superposition. The graphs also show the difference in radiant energy between the same light source with a dome and without. The data acquired in these experiments are used for all subsequent modeling.

Test Method [a]	**Measured Lux**	**Estimated Lux** [b]	**% Difference**	**Efficacy**
Dome	555 lux	572 lux	3%	30 (lux / W)
No Dome	2323 lux	2443 lux	5%	126 (lux / W)

Table 5.1: Summary of results for the second absolute irradiance measurement.

[a] distance=30 cm
[b] Found using the superposition of the five wavelengths

Dataset	Mean CRI	Mean lux	Mean Efficacy	Mean Δuv
linear:500 lux	65	500 lux	136 (lux·W^{-1})	0
linear:1000 lux	65	1000 lux	136 (lux·W^{-1})	0
linear:1500 lux	65	1500 lux	136 (lux·W^{-1})	0
overdetermined:500 lux	76	500 lux	141 (lux·W^{-1})	0
overdetermined:1000 lux	76	1000 lux	141 (lux·W^{-1})	0
overdetermined:1500 lux	76	1500 lux	141 (lux·W^{-1})	0

Table 5.2: Summary of linear equality testpoints. Each data set is comprised of 11 white points ranging from warm (2800 K) to cool white (10000 K). These datasets were generated using irradiance measurements with no dome at a distance of 30 cm. The measurement, mean Δuv, is the Euclidean distance to the actual chromaticity coordinate of the color temperature in CIE 1964 color space. In this test dataset, we supply the precise coordinates corresponding to the color temperature and seek an exact solution of the form $\mathbf{A^{-1}b} = \mathbf{x}$ (exact) or $\mathbf{A}^{-\dagger}\mathbf{b} = \mathbf{x}$ (overdetermined), thus we expect that Δuv is zero.

Predicted Results using Monte Carlo Simulations

Figure 5.7 and Figure 5.8 show the resulting contours for randomly picked setpoints based upon the absolute irradiance experiments using the interference dome. In these graphs, the illuminance of the system is fixed at an arbitrary point and the resulting R_a is given as a function of T_c and efficacy. In this experiment the illuminance, E_v is "constrained" by limiting which lux values are within the range we want to graph. This is analogous to the linear inequality constaints given in Sec 3.1. In these experiments the system does not employ dynamic efficacy. Instead based on our assumptions of the wavelengths present in the system, two sets of simulations are performed. One set uses five wavelengths and the other set uses three wavelengths. Figures 5.7 and 5.8 are the contour plots representing possible solutions.

Predicted Results using Linear Methods

Using the techniques discussed in Section 3.2, we proceed to generate the setpoints using linear methods. These setpoints correspond to 11 different color temperatures (warm to cool) for 500 lx, 1000 lx, and 1500 lx. These data were generated using both the exact solution and pseudoinverse methods (see Figure A.1 in Appendix A for the test spectra). They are summarized in Table 5.2.

Predicted Results using Direct Search

The Global Optimization Toolbox in Matlab [71] contains the generalized pattern search and mesh adaptive direct search optimization algorithms. As discussed Chapter 3, the Mesh

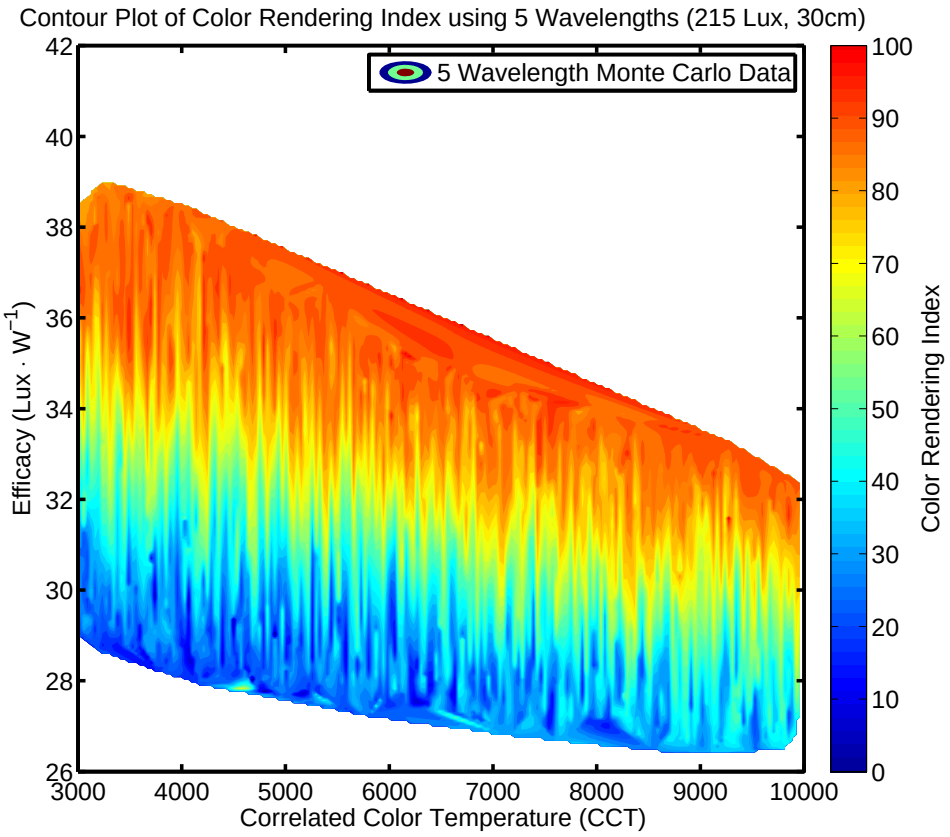

Figure 5.7: Results of Monte Carlo simulation using five wavelengths for approximately 215 lux. These results are from the irradiance data using the interference dome and distance=30 cm. For any given color temperature, there exists plenty of local minima to make maximizing the color rendering index a difficult problem. 1,000,000 data points were generated, and then filtered to ANSI white point standards and limited to approximately 215 lux. The simulation took eight hours to complete on a Intel Core 2 Quad.

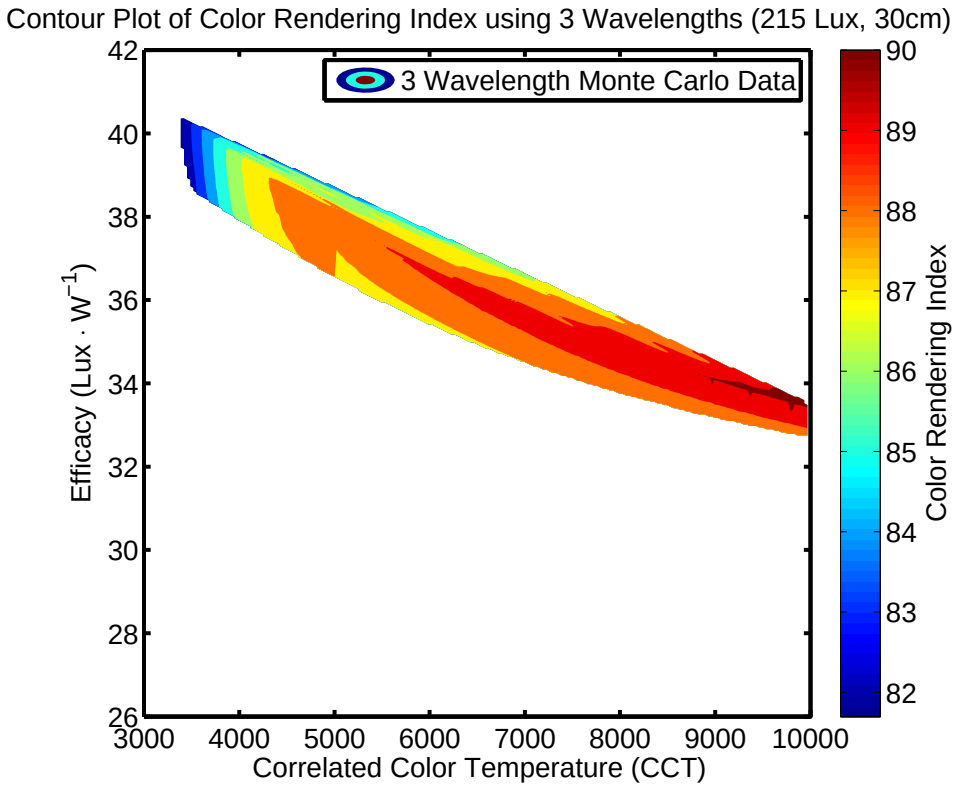

Figure 5.8: Results of Monte Carlo simulation using three wavelengths for approximately 215 lux. These results are from the irradiance data using the interference dome and distance=30 cm. For any given color temperature, there exists plenty of local minima to make maximizing the color rendering index a difficult problem. 1,000,000 data points were generated, and then filtered to ANSI white point standards and limited to approximately 215 lux. The simulation took seven hours to complete on a Intel Core 2 Quad.

Adaptive Direct Search algorithm generated the testpoints summarized in this section (see Sec. 3.3, as well as, [8] and [74]). Using the objective function defined in Chapter 3, the optimal setpoints for the five wavelengths of light A were found. Six data sets were generated for a range of color temperatures (Figure A.3 on page 88). These are: optimized efficacy at 500 lux, optimized efficacy at 1000 lux, optimized efficacy at 1500 lux, optimized color rendering index at 500 lux, optimized color rendering at 1000 lux, optimized color rendering at 1500 lux (see Table 5.3 on page 61). Each data set completed in just under three minutes using an Intel Core Duo Quad. The settings used for the solver are given in Table 5.4.

Dataset	Mean CRI	Mean lux	Mean Efficacy	Mean Δuv
Efficacy:500 lux	67	490 lux	191 (lux·W^{-1})	0.0472
Efficacy:1000 lux	50	923 lux	200 (lux·W^{-1})	0.0645
Efficacy:1500 lux	48	1416 lux	191 (lux·W^{-1})	0.0706
CARI:500 lux	94	500 lux	155 (lux·W^{-1})	0.0070
CRI:1000 lux	94	996 lux	155 (lux·W^{-1})	0.0076
CRI:1500 lux	93	1523 lux	157 (lux·W^{-1})	0.0199

Table 5.3: Summary of testpoints obtained from the nonlinear solver (MADS). Each data set is comprised of 11 white points ranging from warm (2800 K) to cool white (10000 K). These tests points were determined using the irradiance measurements in Sec. 5.2 with no dome at 30 cm. The measurement, mean Δuv, is the Euclidean distance to the actual chromaticity coordinate of the color temperature in CIE 1964 color space. It is a quantitative way of describing the error in chromaticity for a particular color temperature.

Setting	Value
Search Step	MADSpositivebasisNp1
Poll Step	MADSpositivebasis2N
Max Iterations	4000
Complete Poll	On
Complete Search	On

Table 5.4: Specific settings used in the configuration MATLAB function `patternsearch()`, a nonlinear solver (capable of handling linear and nonlinear constraints, as well as, bounds), that is part of the Global Optimization Toolbox. Specifically, the MADS algorithm [8] was used to obtain the direct search testpoints.

5.4 Measured Results

Here we present the measured results of of the linear and direct search test methods for setting light fixture A, with no dome.

Linear Methods

The results of the setpoint found using linear methods is summarized in Table 5.5. The acquired spectra are found in Figure A.2 on page 87.

Dataset	Mean CRI	Mean lux	Mean Efficacy	Mean Δuv
linear:500 lux	55	504 lux	130 (lux·W^{-1})	0.0100
linear:1000 lux	57	964 lux	126 (lux·W^{-1})	0.0072
linear:1500 lux	62	1358 lux	120 (lux·W^{-1})	0.0020
overdetermined:500 lux	67	499 lux	132 (lux·W^{-1})	0.0085
overdetermined:1000 lux	70	935 lux	127 (lux·W^{-1})	0.0047
overdetermined:1500 lux	70	1351 lux	124 (lux·W^{-1})	0.0029

Table 5.5: Summary of the measured results of the testing data sets. Each data set is comprised of 11 white points ranging from warm (2800 K) to cool white (10000 K). These datasets were generated using irradiance measurements with no dome at a distance of 30 cm.

Dataset	Mean CRI	Mean lux	Mean Efficacy	Mean Δuv
Efficacy:500 lux	68	457 lux	173 (lux·W^{-1})	0.0429
Efficacy:1000 lux	52	827 lux	176 (lux·W^{-1})	0.0616
Efficacy:1500 lux	47	1264 lux	167 (lux·W^{-1})	0.0689
CRI:500 lux	92	490 lux	143 (lux·W^{-1})	0.0021
CRI:1000 lux	92	933 lux	139 (lux·W^{-1})	0.0047
CRI:1500 lux	90	1378 lux	138 (lux·W^{-1})	0.0174

Table 5.6: Summary of the measured results of the testing data sets found using the direct search method. Each data set is comprised of 11 white points ranging from warm (2800 K) to cool white (10000 K). These datasets were generated using irradiance measurements with no dome at a distance of 30 cm.

Direct Search

The results of the setpoint found using the MADS algorithm is summarized in Table 5.6. The acquired spectra are found in Figure A.4 on page 89.

5.5 Sensor Data

For one week, a mobile cart (the same cart in Figure 5.1b on page 50) was used to collect daylight and artificial light indoors at the Media Lab. Additionally, direct sunlight was also collected, but resulted in sensor saturation. The experiment was designed to collect a dataset of different color temperatures and lux values used for optical calibration. Using these data, we calibrate a sensor node able to measure the lux and color temperature of daylight, incandescent, fluorescent, and LED sources (Figure 5.9 on page 63).

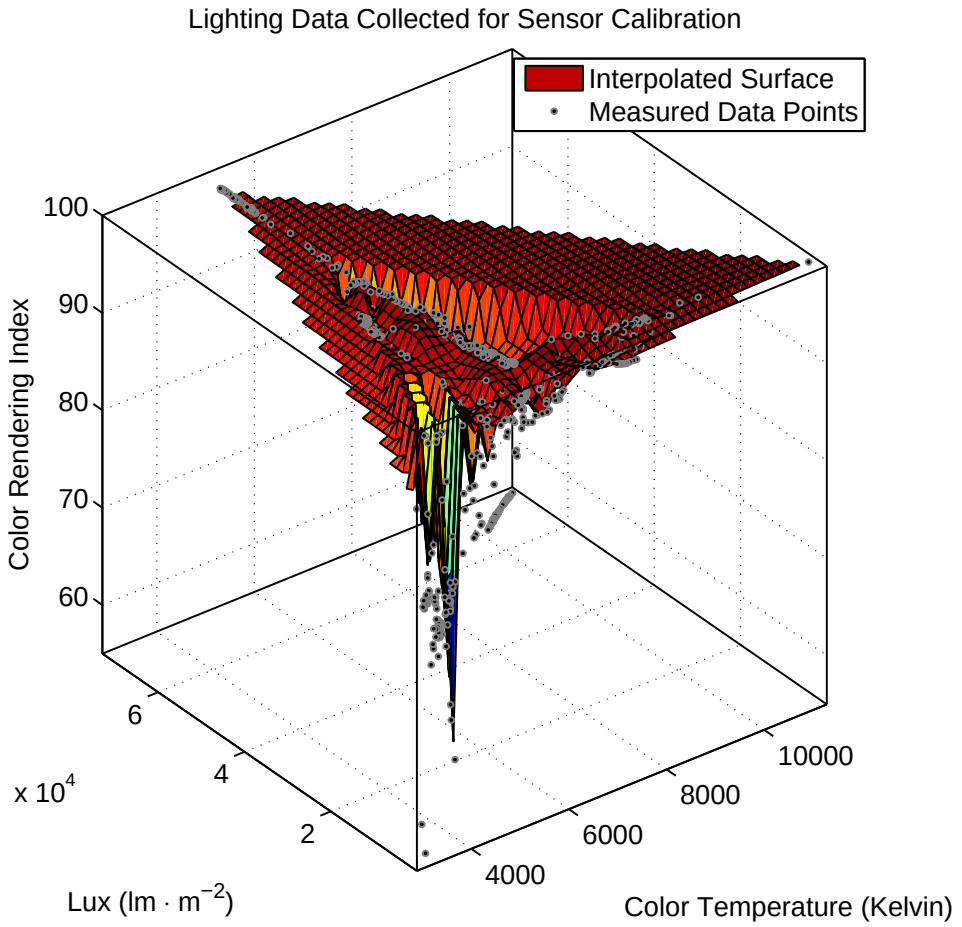

Figure 5.9: Using a spectrometer, absolute irradiance was collected and then processed to estimate the color temperature, lux, and color rendering index of multiple light sources.

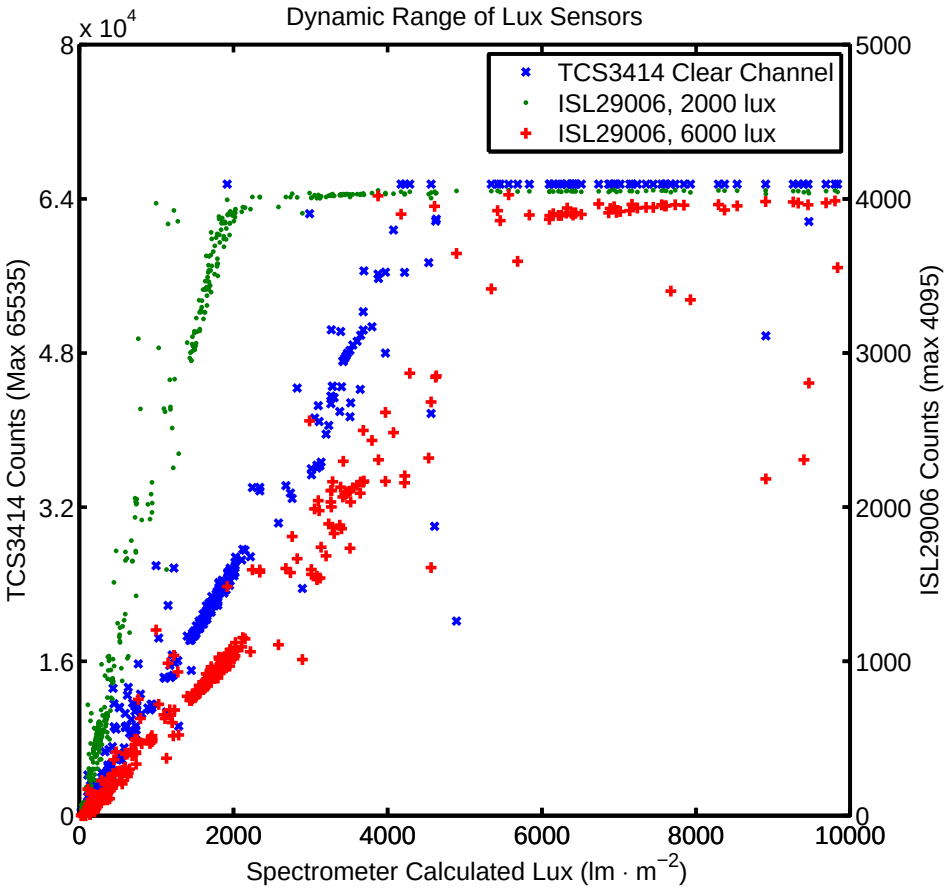

Figure 5.10: Dynamic range of the TCS3414 and two ISL29006 optical sensors set to different sensitivities. The TCS3414 has an on board analog to digital converter. The ISL29006 are measured by the on board analog to digital converter. In this experiment, the TCS3414 was set to oversample 10 times (the highest sensitivity) in order to estimate the level of illuminance required to saturate the sensor. Nominally, the range is set to approximately $10,000$ lx.

The lux measured by the optical sensors (TCS3414 clear channel, and ISL29006) is given in Figure 5.10. The corresponding color-filtered data are given in Figure 5.11.

5.6 Estimating the Ambient Light

Several tests were conducted with light source A, with no dome, mounted at 30 cm from the sensor node to study the time it takes to calibrate a single light and measure the ambient lighting (see Table 5.7 on page 67). In this study, the unfiltered analog lux sensor, set

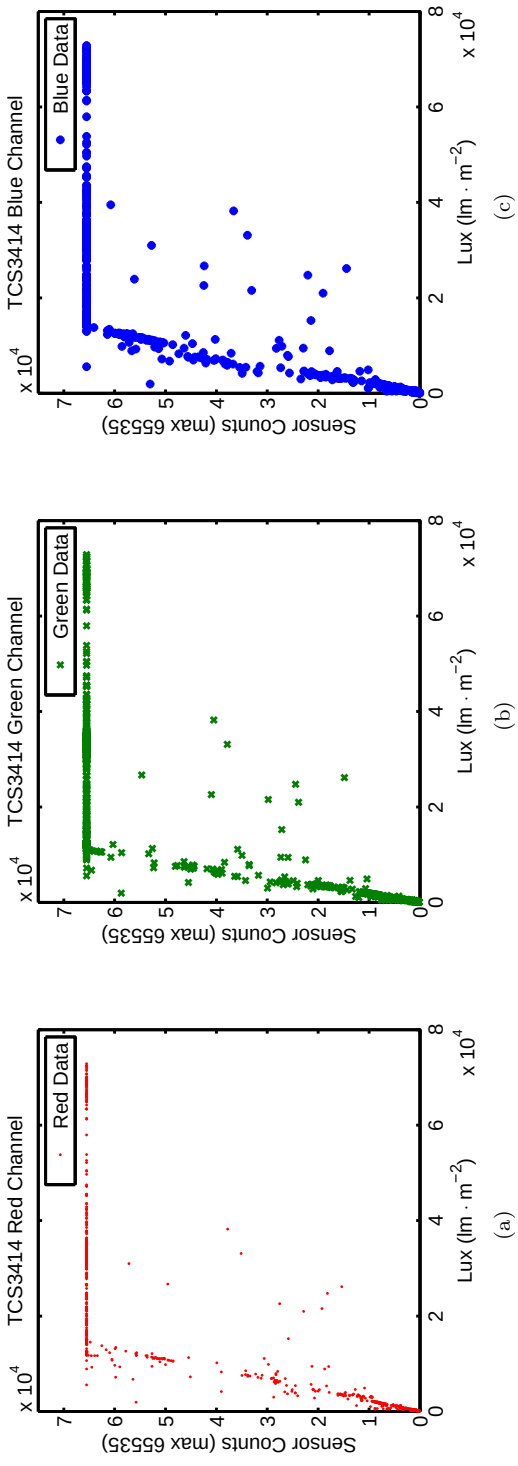

Figure 5.11: Red, green, and blue channel readings from the experiment in Figure 5.9.

to a sensitivity of approximately 5000 lx, was tested. This purpose of this experiment was to measure the total system update rate (including read and writes from MATLAB) and to choose an integration time for the digital color sensor depending on the results of the experiments. In each experiment, 200 data points were gathered by toggling the light source and querying the sensor board in MATLAB. No oversampling of the sensors was used. Instead, these data were averaged post-experiment. In each experiment, the delays were set such that the light source was on and off for an equal amount of time. The poll time in the table is the total period of each experiment step. Therefore, 150 ms means the light was on for 75 ms and off for 75 ms.

Condition	**Lux**
Ambient	0 lx
Overhead Lights	221 lx
LEDs	2044 lx

(a)

Test	μ_{off} **(Counts)**	σ_{off} **(Counts)**	μ_{on} **(Counts)**	σ_{on} **(Counts)**	μ_{poll} **(ms)**	σ_{poll} **(ms)**
Lights On 150ms	57	4	1709	7	156.3	2.1
Lights Off 150ms	0	3	1646	3	156.2	2.1
Lights On 90ms	48	2	1706	3	93.9	3.0
Lights Off 90ms	0	0	1641	3	93.8	3.0
Lights On (none)	1025	829	885	830	31.3	2.1
Lights Off (none)	890	825	815	824	31.3	2.1

(b)

Table 5.7: In (a), the ambient and testing conditions are given. These were measured using the spectrometer. The LED light source was placed 30 cm away from the head. In (b), the mean and standard deviation are given for different polling frequencies and different conditions.

Chapter Six

Analysis

6.1 Sources of Error

This section begins by reviewing the sources of error in both the test setup and the spectrometer. Park et al. [50] provide a complete discussion of uncertainty and error propagation in spectrometer-based LED measurement. Hwang et al. [30] provide an analogous treatment of uncertainty in color measurement using a spectrometer.

Measurement Error

All subsequent calculations in this thesis are derived from the primary step of measuring the absolute irradiance of the test fixture (see Figure 5.1 on page 50). There are four primary sources of error in the test setup. The first source of error is the estimated distance between the LED array and the spectrometer head. The second source of error is the accuracy of the LED forward current. The third source of error is the specific junction temperature of the LEDs on the array. The fourth source of error relates to the actual spectrometer irradiance measurement itself. In [50], the major components of uncertainty governing the irradiance measurement error are: spectral irradiance reference data, calibration lamp detector distance, calibration lamp current, repeatability, wavelength accuracy, linearity, and spectral stray light.

Spectrometer Induced Error

All experiments in this work are preformed using a USB4000 spectrometer from Ocean Optics. The monochromator is an Czerny-Turner (see Wyszecki and Stiles [79]) with a 25 μm entrance slit and a diffraction grating blazed at 500 nm (Ocean Optics grating number H3). The spectral bandwidth (Full Width Half Maximum) of the monochromator is approximately 1.5 nm with stray light estimates of <0.05% at 600 nm; 0.10% at 435 nm. The detector is a Toshiba TCD1304AP (200-1100 nm) with a corrected linearity of >99.8%. The

sensitivity of the CCD is approximately 130 photons/count at 400 nm; 60 photons/count at 600 nm. The calibration source is Ocean Optics HL-2000 Tungsten Halogen (traceable to NIST S/N: F-211), with a drift of approximately .3% per hour of use. The radiometric calibration source used in this research has an initial uncertainty of approximately 2.36%. The supply is regulated to within 0.5% of rated specifications.

Assuming a 3% certainty on mechanical setup and a 4% uncertainty regarding reflected and scattered light, a back of the envelope calculation of the major sources of error allow us to estimate the expanded uncertainty ($k = 2$) of 14%, with the individual uncertainties of stray light, linearity, etc., accounting for only 2% to 4% of the uncertainty. However, without formal testing of the individual sources above, these are only estimates. In a similar setup, Park et al. estimated the expanded uncertainty ($k = 2$) of their calculations to be: 4.33% for red wavelengths, 4.22% for green wavelengths and 5.54% for blue wavelengths. As a general rule, 10% uncertainty is considered very good for spectrometer measurements. Uncertainties less than 2% are achievable only by NIST [57]. Additionally, the transferred uncertainty in the calibration source was initially estimated to be close to 1-2% in the visible range. In order to properly validate the test setup, the prototype light source should be sent to a third party, such as Luminaire Testing Laboratory (LTL).

Error in Linearity Assumptions

Although understanding the sources of absolute error are important for comparison to other systems (i.e., how this calibrated light source may appear at another optical instrument) it is also important to quantify the error introduced into the system due to assumptions of linearity. There are two major sources of error. The first is exemplified in Figure 5.3 on page 53. In a strictly linear system, the only information needed to estimate the intensity of any given light wavelength is the maximum intensity and the PWM setting. With no linear fit to minimize square error, when the wavelength is dimmed, the effect on the system is that the light source is brighter than the model anticipated. Accordingly, this manifests itself as chromaticity error and intensity error in setting the color temperature of the light source. Warmer colors, which use more red intensity, are strongly affected.

The second major source of error is estimating the white point, or the "all-on" setting, of the system. This is exemplified in Figure 5.6 on page 56 where the graph depicts the measured white point and the estimated white point, which is found by summing the total spectra for the individual wavelengths. Not surprisingly, the peaks of the five wavelengths in the system are lower for the measured white point. This effect, like the deviation from linearity in Fig 5.3, is due to temperature. The effect here is that the overall lux of the light source will be less than expected, particularly at the sensor node some distance from the light source. Additionally, this also affects the color temperature of the system.

Previous work attempted to compensate for these temperature effects by directly measuring the temperature and following the intensity derating curve for the LEDs [6, 43, 3].

Yet, it is difficult to properly estimate the junction temperature with only a single temperature sensor on board. One reasonable approach is closing the loop (e.g., using feedback to tune the individual wavelengths as discussed in Sec. 3.5). Additionally, we may also want to remove as much open loop error as possible. It may be desireable to begin with a correct model of the system, therefore we present a technique to correct the individual wavelengths based on a white point measurement, or series of white point measurements. We begin by correcting the acquired spectra to account for the worst case operating temperature (assumed to be the white point) such that

$$\min_{\mathbf{x}} f(\mathbf{x}) = \|E_{e,wp}(\lambda) - \sum_{i=1}^{m} \mathbf{x}_i E_{e,i}(\lambda)\|^2, \tag{6.1}$$

subject to $\{\mathbf{x} \in \mathbb{R} : 0 \leq \mathbf{x} \leq 1\}$. In this case, we seek a solution to minimize the square error between the measured whitepoint and the weighted sum of the individual intensities. Yet, because this only captures a single white point, we go one step further and write

$$\min_{\mathbf{x}} f(\mathbf{x}) = \sum_{j=1}^{n} \|E_{e,wp}(\lambda) - \sum_{i=1}^{m} \mathbf{x}_i E_{e,i}(\lambda)\|^2, \tag{6.2}$$

subject to $\{\mathbf{x} \in \mathbb{R} : 0 \leq \mathbf{x} \leq 1\}$. In this case, n represents the total number of white points taken, for example with increasing intensity. The reasoning behind Eq. 6.2 is that in Eq. 6.1, we assume that this relationship is fixed for all the operating points, when in fact it is dynamic. By taking into account multiple white points, we achieve an open loop accuracy theoretically higher than any line fitting method of a single LED. If we applied a linear fit to the data in Fig. 5.3, it will be incorrect because it does include the heating effect of the other LEDs. If the system is going to be running open loop color control, it is critical to perform these steps. Yet, even with many acquired white points, there are too many cases to take into account, and closed loop control may be required in certain cases.

Figure 6.1 shows the results of minimizing Eq. 6.1 for the data collected in Sec. 5.2. The corresponding correction factors are blue: 0.9373; cyan: 0.9255; green: 1.0000; amber: 0.9120; red: 0.8901. Then, using these corrected spectra, the optimal setpoints using either the direct search or linear methods are computed. To see how these methods would improve the results obtained in Sec. 5.4, we can measure the difference between measured results obtained when using the temperature-compensated superposition and the measured results using just superposition.

6.2 Performance of the Sensor Node

The primary goal of collecting the data in Figure 5.9 on page 63 is to calibrate the digital color sensor so that the color temperature of ambient lighting can be inferred. Early models of performance predicted that a calibration source with a sufficiently high color rendering index would make a suitable adjustable calibration source for the digital color sensor. Using

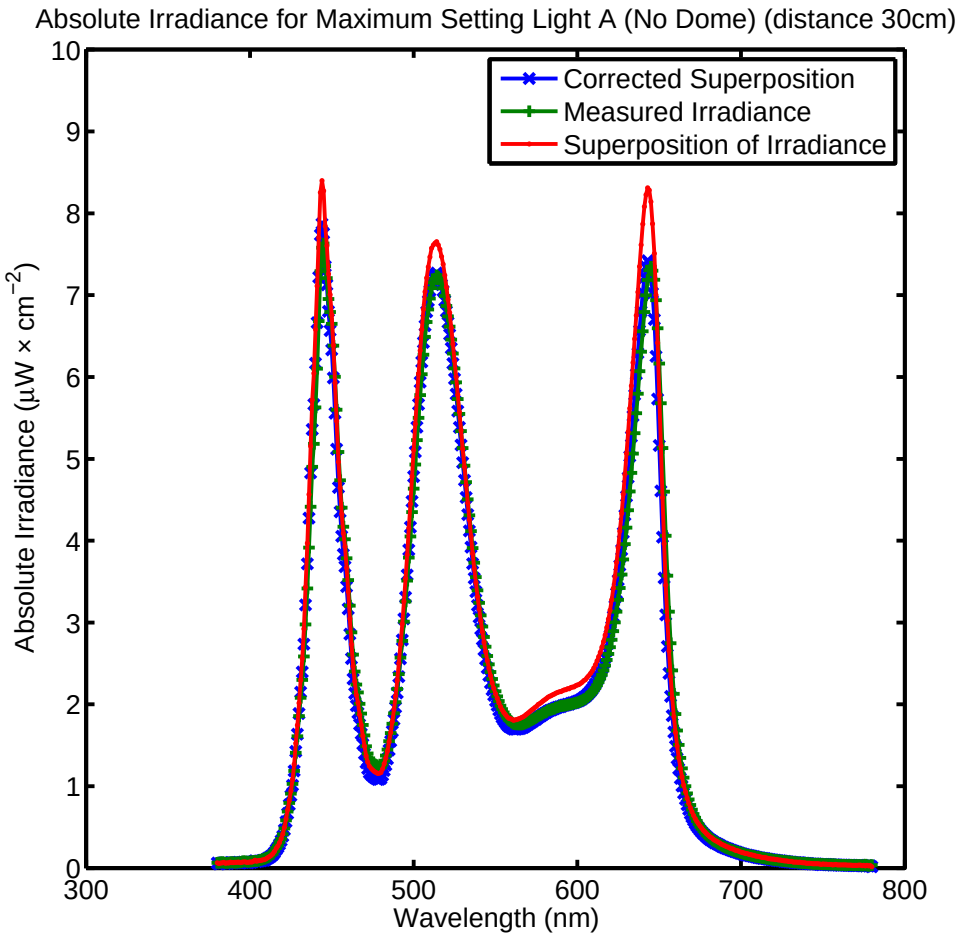

Figure 6.1: Results of minimizing the square error between the measured white point and the sum of weighted spectra taken during a calibration step. If this step is performed before using the linear and direct search methods to find the color temperature and intensity, the error between the model and the actual system will be decreased. The setpoints found during these steps will better reflect the worst case operating temperature.

the calibration methods described in Sec. 3.5, a single sensor was calibrated using 31 white points. This served as the LED calibration source. Additionally, daylight was collected (presented in Sec. 5.5) which served as the daylight calibration source (incandescent bulbs with multiple filters can function similarly). In Figure 6.2, the performance of the different calibration methods is given.

The results suggest that the method of calibration (either a five wavelength source or daylight) is the biggest predictor of error. For example, in Figure 6.2b we see that an LED source, even with an average color rendering index of 92, is not an adequate calibration source to correctly measure daylight. Of interest is the result in Figure 6.2a, in which the daylight calibration of the sensor produced a near linear output, but with a different slope than the ideal response. With an appropriate correction factor, the error between measuring daylight and artificial light sources could be minimized. More important here is the intended use of the sensor. Its purpose is not to measure with absolute certainty the correct color temperature (it would be nice if that were the case), but instead provide an output that could be used to synchronize the indoor lighting with daylight environment automatically.

The secondary function of the sensor node is measuring the illuminance of the ambient light and the adjustable light sources in the network to optimize the lighting at the point of measurement. From testing, it is clear that a query and response command for the analog lux sensors may not be the best solution for control via MATLAB. The reason is due to the lack of resolution in the MATLAB pause function.

In Section. 5.6, performance metrics were given for the unfiltered lux sensor. It was determined that because of the poor resolution of MATLAB's pause function, strict timing was not achievable. Therefore, the limitations of update rates (at present 11Hz) are too slow in order to perform a room calibration without noticing the flickering of the lights. There exists the possibility of continued use of MATLAB with an augmented pause function that utilizes Microsoft Window's high resolution clock. Thus, it may still be possible to achieve flicker-free calibration with only a minor software change. More testing needs to be performed to firmly comment if this is possible using MATLAB. If not, another solution must be found. Additionally, the RC time constant of the 50 Hz low pass filters (approximately 3 ms) theoretically would not hinder operation, but the present limitations of the timing resolution in MATLAB prevented any significant exploration.

The data presented in Figure 5.10 on page 64 were fit to the linear equation $y = mx + b$. From Fig. 5.10, it is clear that the analog sensors saturate close to 2000 lx and 6000 lx. The digital sensor was set to 10× integration time for maximum sensitivity, and it saturated close to 5000 lx. The ambient light levels on the fifth floor of the Media Lab average between 250 lx to 2000 lx near a window. Reporting the answer in lux rather then sensor counts may not be an issue, as the user is concerned only about the lighting on the surface. It is the goal of the system to minimize the other parameters to match what the user expects to be present. The main issue here is not sensitivity, but update rate. Increasing the integration time of the digital sensor may lead to poor response times as transitions across the lighting

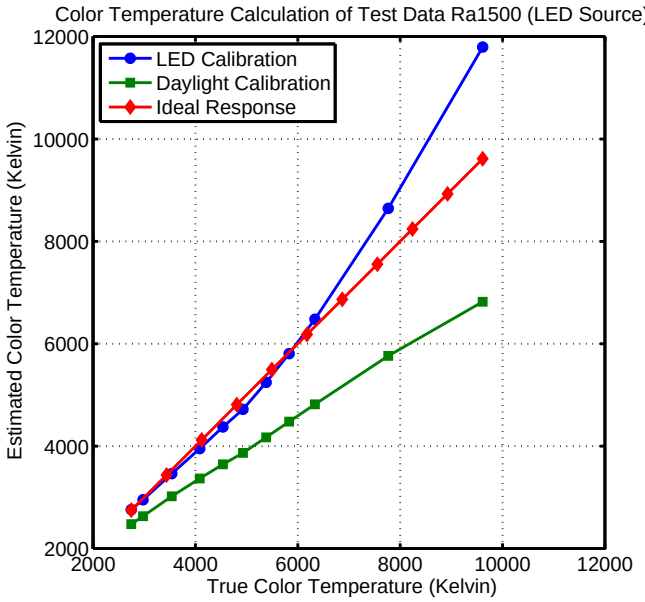

(a) Results of calibration methods when measuring an LED source.

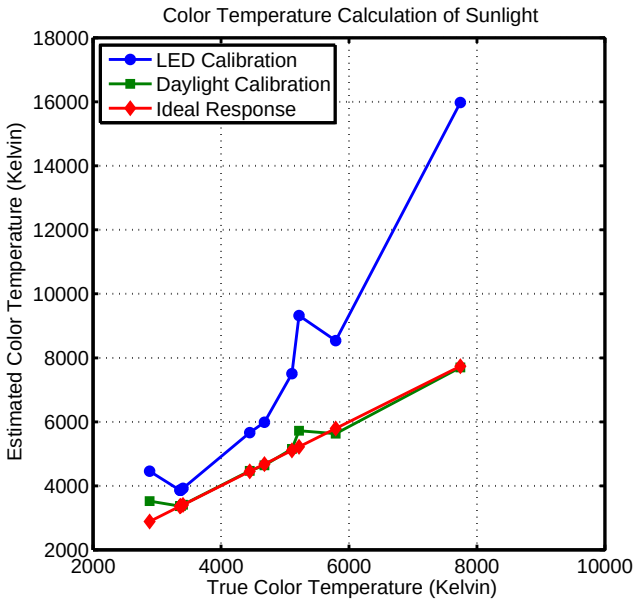

(b) Results of calibration methods when measuring daylight.

Figure 6.2: Comparison of calibration results. In (a) the color sensor is calibrated using either an LED source or daylight and its response to LED irradiance is given. In (b), the color sensor is calibrated the same way, but its response to daylight irradiance is given. Clearly, the results correlate well with the calibration method employed. However, in (a) the linearity of the daylight calibration method may make it applicable in measuring a broad range of sources.

network will be averaged by the sensor. More testing is required to settle on the correct integration time.

6.3 Performance of Control Methods

The experiments conducted in Sec. 5.4 are considered proof of concept measurements. They are intended to validate direct search as a new method of polychromatic intensity control for both a single fixture and a network of lights. Additionally, as discussed in Sec. 6.1 the measurements were conducted with datasets that were not temperature compensated, so in some cases there are significant chromaticity errors. It was decided, for brevity, that the results in Table 5.5 and Table 5.6 be given as an average so that a general sense of performance could be quickly ascertained. Because the average results are presented, specific color comparisons (11 colors were tested) are not possible. These tables of results are only appropriate once the model used to generate the datasets is temperature compensated so that the true open loop response can be measured. In Figure 6.4, the mean CRI and efficacy are presented for the tested light source.

Indeed, as suggested in Chapter 3, the direct search method finds the intensities for the individual wavelengths such that CRI and Efficacy are maximized (see Fig. Figure 6.3 on page 75). In theory, the variation across the three intensity groups (500 lx, 1000 lx, and 1500 lx) occurs due to errors in the linearity assumptions discussed in Sec 6.1. Neither CRI nor efficacy should vary if the model is perfect. In the worst case estimate, using direct search results in a 45% improvement of the color rendering ability of the light source over the linear method. Similarly, maximizing the efficacy results in a light source 28% more efficient than its linear counter part. It is clear that these methods have great potential for controlling the spectral composition of the source.

On the other hand, in Figure 6.4b, we see the effect of maximizing efficacy. The objective function will attempt to use the most efficient and fewest wavelengths possible to create the correct color temperature. Depending on the intensity and color, this could be two or three wavelengths. The penalty incurred for such efficiency is that we lose the quality of the white point. The Δuv reported in the figure is a measure of how close the measured white point is to the blackbody curve. As a rule of thumb, a $\Delta uv < .01$ is considered acceptable. Given the uncertainty of the spectrometer measurements to begin with it is difficult to comment about the true error regarding the white point (there is much room for improvement here). But qualitatively, we would notice a significant change of color if these white points were to be used. This could be improved by adding a coefficient in the evaluation function of the optimization problem, or by defining Δuv as a nonlinear inequality contraint in the optimization routine, or even by fixing the minimum number of wavelengths to be three, and not two (redefining the lower and upper bound of the optimization problem). This is a relatively small problem and is easily fixed (potentially at the cost of run-time performance).

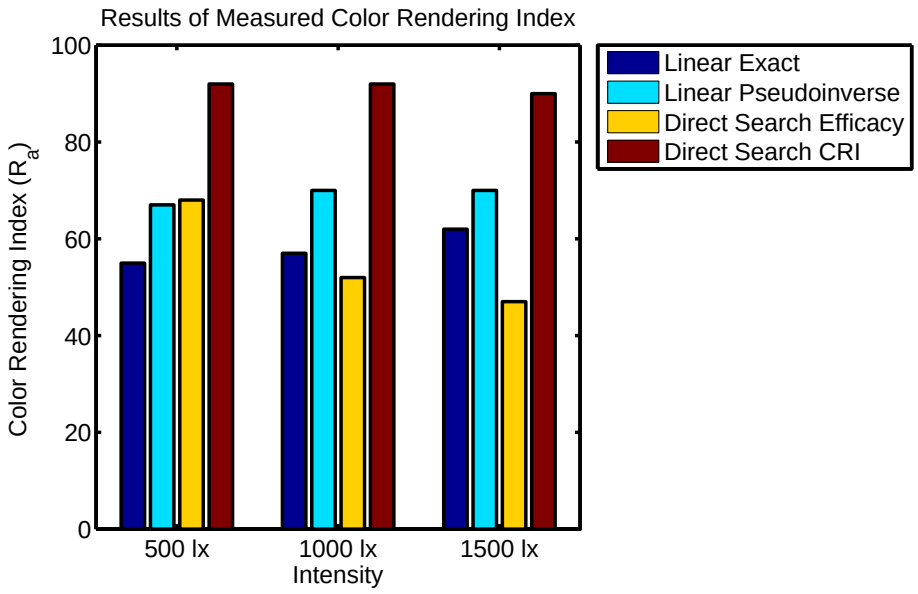

(a) Results of average CRI.

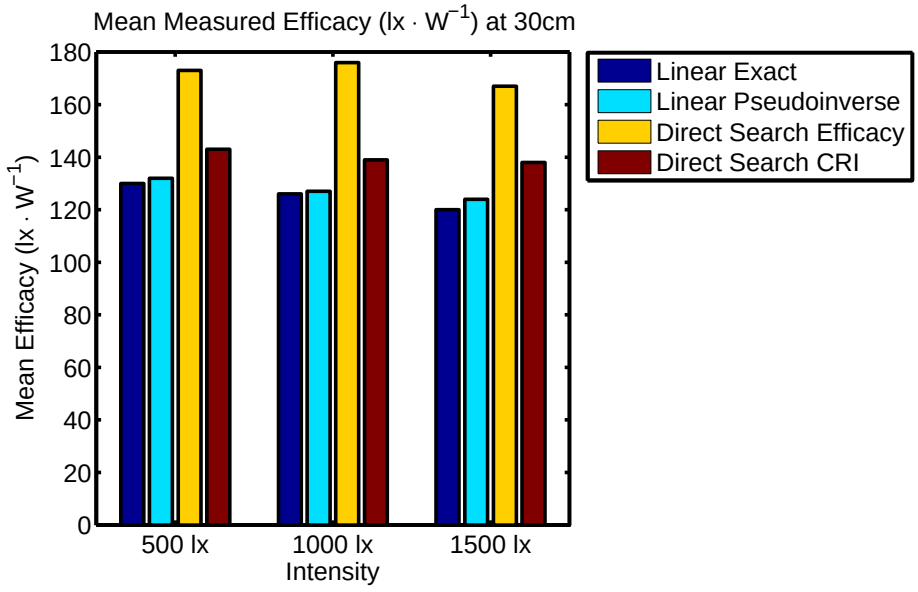

(b) Results of average efficacy.

Figure 6.3: Results obtained from study of linear and nonlinear methods of color control. Here, we see the effectiveness of the direct search algorithm. It is capable of outperforming the exact and overdetermined methods of control. A CRI score of 100 is considered perfect. In (b), the algorithm is able to create colors 28% more efficiently then the other methods.

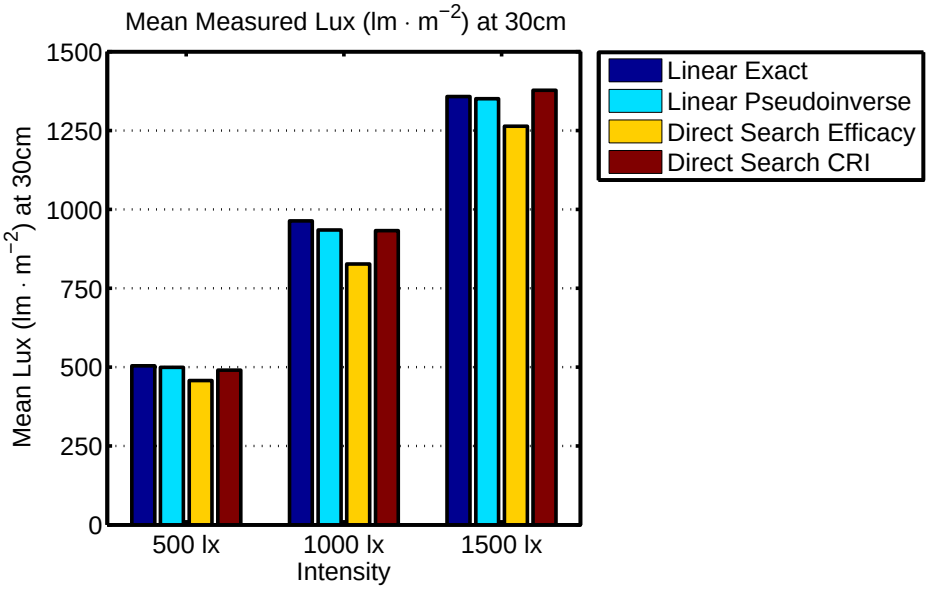

(a)

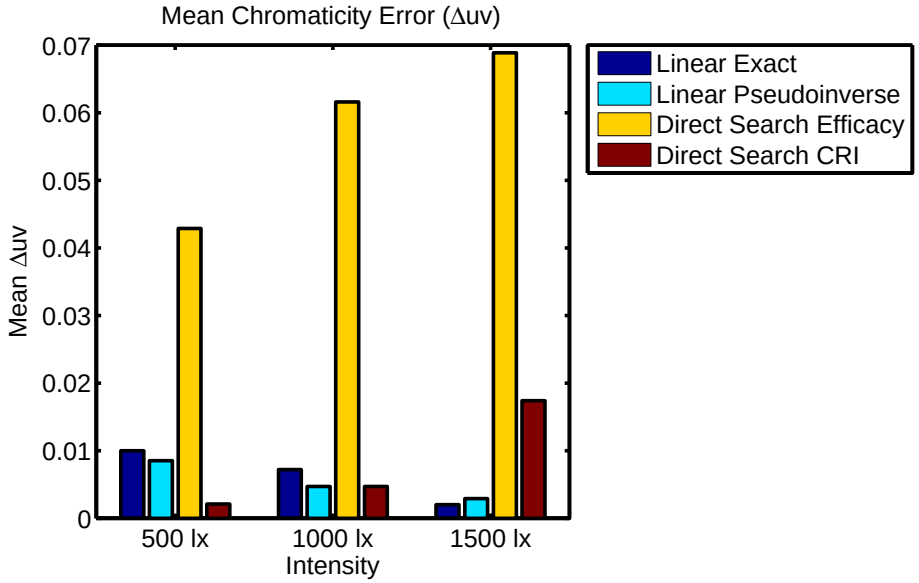

(b)

Figure 6.4: Results obtained from study of linear and nonlinear methods of color control. In (a), the variation in illuminance is due to open loop error. In (b), the large Δuv error means that the resulting color temperature is not exactly on the blackbody curve. Maximing efficacy resulted in lower quality white light.

6.4 Comparison to Commercial Systems

The Caliper program, sponsored by the US Department of Energy, is responsible for documenting the progress and developments with SSL-related technology. In a recent publication (2009), it was reported that:

> "The general trend of increasing efficacy continues, with Round 9 products averaging 46 lm/W and ranging from 17 to 79 lm/W. Unfortunately, wide disparities are still observed in the accuracy of manufacturer specifications. SSL recessed downlights are now capable of meeting or exceeding light output levels and light distribution characteristics of downlights equipped with 45-75W incandescent and halogen lamps, and the SSL products are meeting or exceeding color quality of CFL recessed downlights [48]."

These fixtures are all phosphor-based designs. The color rendering index of the fixtures in the Caliper report range from 63 to 93, with a majority of the tested fixtures having a CCT ranging from 2700 K to 6500 K, none of them being color adjustable.

We can estimate the performance of the prototype presented in this thesis for a range of color temperatures as well (see Table 6.1). In this case, we consider the results obtained in Table 5.6 to serve as our comparison. In Figure 5.2 on page 52, we measured the test source to study if the relationship $E_v = I_v/d^2$ holds. Using this assumption, we can estimate the total candelas of the test fixture at a desired operating point (we assume we measured the lux directly under the source). First we estimate the total lux at a distance of 1 m from the source by applying Eq. 3.2 rewritten to estimate the illuminance at two different distances measured from the same source. The illuminance, now estimated at 1 m, can be converted into candelas. The next step involves calculating the solid angle of lamp (in steradians) which is $2\pi(1 - \cos(\alpha/2))$, where α is the beam angle of our source, which is estimated by be roughly 110 degrees. We obtain the lumens by multiplying the intensity with the solid angle, $I_v 2\pi(1 - \cos(\alpha/2))$.

Several Color Kinetics iW Blast Powercore lamps were obtained and characterized in a set of experiments outlined in Chapter 5 as a commercial test fixture most analogous to the one developed. The iW Blast Powercore is a phosphor-converted adjustable white fixture. It consists of LEDs at two color temperatures, 2700 K and 6500 K, and allows the channels to be mixed. The fixture is rated at 50 W at maximum intensity, and consists of two banks of warm white LEDs and one bank of cool white LEDs. The range of achievable output is fixed between these two color temperatures. The user controllable resolution of three channels is limited to eight bits where the input/output relationship (PWM versus intensity) follows the power law, $y = x^k$. The measured CRI of the light source varies with temperature and has a range of 72 to 83 and an efficacy of 35 lm/W.

Phosphor-based designs already dominate the market and the chronological Caliper data suggests that improvements across the board are happening. Phillips et al. [52] discuss the

$\mathbf{T_c}$ (kelvin)	**Lux** ($\mathbf{lm \cdot m^{-2}}$)	**Lumens** (**lm**)	**power** (W)	**efficacy** (lm/W)
2748	98	263	8	33
2978	101	271	8	34
3538	108	289	8	36
4085	117	313	9	35
4538	124	332	10	33
4930	132	354	10	35
5382	135	362	11	33
5830	137	367	11	33
6335	138	370	12	31
7768	137	367	12	31
9613	137	367	12	31

Table 6.1: Estimated luminous efficacy of prototype light source for the measured lux obtained in Sec. 5.4.

future of phosphor and active emitter designs. The LED systems in the latest Caliper report surpass most compact fluorescent designs, both in terms of efficacy and quality. Yet we are still left with the problem of intelligent control and to some degree, the mixing of color. There more than likely will still be a need in niche markets for adjustable systems, especially ones in which the reproduction of color temperature and color rendering are important. Over time, commercially available systems with the color adjustable range and color quality of the prototype presented in this thesis will begin to surface. From a design standpoint, especially with regard to the lighting industry, color-adjustable systems are complex, both mathematically and physically. Above all, lower efficacy and higher cost make them less appealing to the mass consumer market. Certainly, if the goal is to maximize the $/Klm ratio, it is not achieved using active emitters. In order for active emitters to become dominant in a large cross section of the market, the quantum efficiency of the green emitters will need to improve to the levels of near ultra-violet emitters. From a engineering perspective, the techniques presented here are just as applicable to color tunable white systems as they are to polychromatic active emitter systems.

6.5 Energy Saving Potential

The affordances offered by color-adjustable systems are broad, yet a great barrier in the broad adoption of these devices is due in part to cost, lower efficacy and complexity. One idea explored in this work is dynamic efficacy, or the ability of the lighting system to optimize the number of wavelengths used to create the white point. From an engineering standpoint,

the technique works quite well, however one issue remains: if given the choice between a high quality light and a poor quality one, which one do you choose? In order to maximize the full potential of adopting a polychromatic system, the lighting must not burden the user. A probable answer is that either directly, or indirectly, we do not really care as long as we are satisfied.

We turn our attention to estimating the performance of the network considered in Figure 4.1. We consider a hypothetical illuminance profile of ambient light (e.g, daylight) collected in an office in MIT building E14 (Figure 6.5). In this example, the peak illuminance, estimated to be 500 lx is measured during midday. The offices in building E14 currently use compact fluorescent bulbs and the illuminance, 1.5 m from the plenum, was estimated at 325 lx. From Figure 6.5, we see that for 1/3 of the day, the lighting level is 300 lx or greater, which, to guarantee 325 lx at the work surface, would require 25 lx or less from the fixtures. By midday, according to the figure, the lights could be turned off. Although this is a completely a hypothetical situation, the implications are that the fixtures would require less than 3% of their total output during the course of the normal waking hours.

But, let us consider a case where the lighting network runs continuously for 24 hours each day and is configured to maintain 325 lx at the work surface. By compensating for daylight, we can infer that average illuminance in the room from the overhead lighting, over a period of a day, is 180 lx/h. This constitutes a 45% reduction if the lights were left running at full intensity, 24 hours a day. In theory, another 1/6 of that time no illumination is required, and in this case, the reduction is 59%.[1] The example given was extreme, as in most cases, the total ambient lux may never exceed the capabilities of the lighting system. Also of consequence is that the fact that the distribution will not be Gaussian, but erratic and most certainly, not smooth.

The idea behind dynamic efficacy is to augment closed loop intensity control by modulating the spectral composition of the source and automatically determining at which times a more efficient light, rather than higher quality light, satisfies the user's requirements. The important distinction between dynamic efficacy and closed loop intensity control is that a reduction in overall energy usage is achieved without reducing the intensity and output color. For example, let us consider the system whose results are described in table 5.6. Here, we see that the higher efficacy modes of operation are 23% more efficient than their high CRI counterparts. This means that for the same intensity, the high CRI mode uses 1.2 times more energy then the high efficacy mode.

If we reconsider the example above, we can imagine an operational scenario in which the network determined situations and times where, although it could not adjust the intensity, it could tune the efficacy instead. In the example above, we assume that maintaining 325 lx

[1]Here we computer the average of maintaining 325 lx 5/6 of the time, and 0 lx the other 1/6, which corresponds to an average of 244 lx/h. For the adjustable intensity it becomes 0 lx for 50% of the day which corresponds to an average of 100 lx/h.

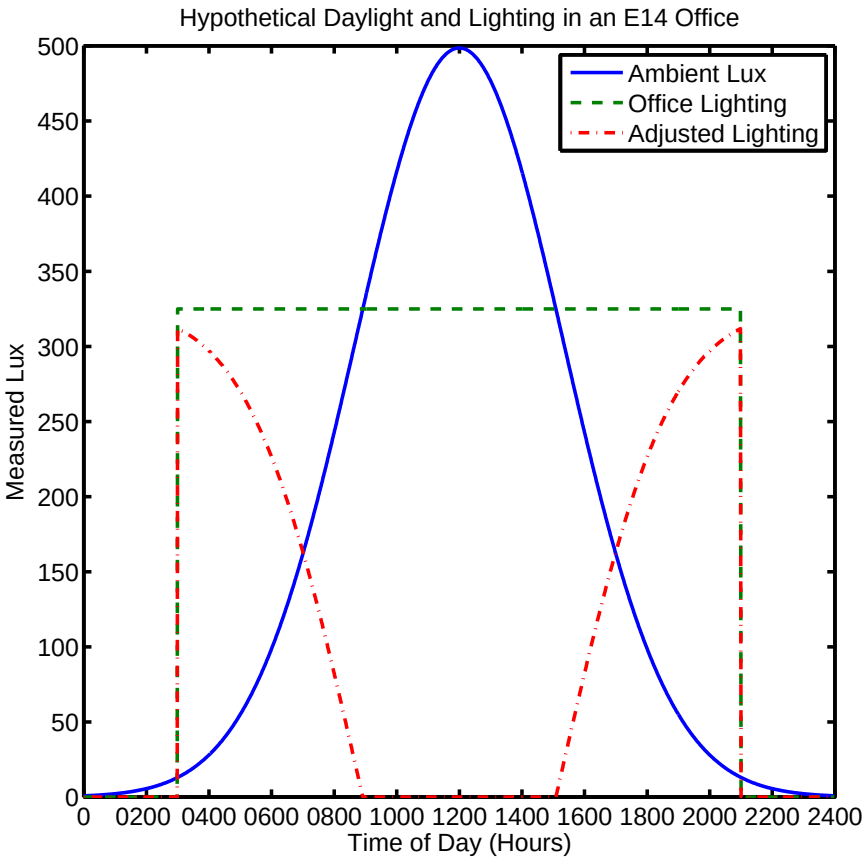

Figure 6.5: Hypothetical distribution of illuminance in an office in E14, with a maximum reading of 500 lx during midday. In this scenario, there are two lighting models used. The first model assumes the lights remain on at a constant intensity during the day. The second method assumes the intensity of the sources are adjustable.

on the surface of interest requires 40 W of electrical power and that decreasing the intensity of the system corresponds linearly with power, that is, 180 lx consumes 22 W of power. A 40 W light, left on for 18 hours a day uses 720 W·h. In the hypothetical 58% scenario, the equivalent power consumption of the light source is 16 W each hour (16 W·h). This leads to a total consumption of 400 W·h per day. By using feedback, we reduce the total energy consumed by the system by 44%.

By adjusting the intensity throughout the day, we changed the equivalent power consumption of the light source, that is, a 40 W lamp "became" a 16 W lamp. Earlier, it was stated that high CRI mode of operation uses 1.2 times the power of the high efficacy mode. If we assume that the equivalent 16 W source is running in high CRI mode, then for same light level, the rated power becomes 13 W, a change of 18%. If the fixture ran in high efficacy mode for 24 hours, this is equivalent to 312 W·h per day. Depending on the time spent using high efficacy or high CRI, we could save up to an additional 88 W·h. We could assume the efficacy mode is used 50% of time and our corresponding consumption becomes 356 W·h. Over a year, this saves 16 kW·h for just a single light source.

Compensating for ambient lighting and detecting occupancy in an office is not new; we are all familiar with the technology such as the building sensor that controls outdoor lighting when the sun sets or timer based lighting in the library stacks. However, these systems, lacking any cohesive infrastructure, cannot dynamically raise and lower the intensity in response to changing ambient conditions. Instead, for simplicity they are binary; either off or on (almost always off at the wrong time). For many systems this is adequate, but there are still plenty opportunities left to pursue. Larger systems, designed to control the lighting in office type environments, typically have the ability to zone the lighting and adjust the intensity of individual lamps on the network. By far, the most prevalent method of controlling these networks is human input, using either change on demand or pre-programmed sequences. One example is the Lutron Grafik Eye, installed in E14. Yet, this system, for all of its capabilities, lacks the "off the shelf" components to realize the dynamic adjustment of intensity to compensate for daylight. However, these systems are capable of being controlled using a computer – it is not unreasonable to think that that the hardware and techniques presented here could one day control the overhead fluorescent lighting at the Media Lab.

Chapter Seven

Conclusions

This thesis focused on the development, modeling, and testing of dynamic solid state lighting. In this work, state of the art methods were presented to optimize the optical and energy related parameters of an intelligent lighting system. A comparison of control techniques, both linear and nonlinear, provided quantitative evidence that the methods described in this thesis are optimal for the control and design of future polychromatic as well as phosphor-based lighting systems. In addition, the feasibility and current performance of room calibration and the performance of a novel method of measuring the correlated color temperature of daylight were also given. In short, the broad foundation for future research on the optimal control of lighting has been both quantitatively and qualitatively discussed. With the proper techniques, subsystems, and methodologies in hand, it is now time to consider dynamic interaction with the network. The next immediate portion of the research will study the effects of the computer-controlled network of multiple light sources.

7.1 Overview of Performance

The network, as designed right now, has several bottlenecks. These are manifested as query delays to sensor nodes and light fixtures, and timing expense incurred from roundtrip full duplex communication. A majority of the proposed control algorithms utilize MATLAB, which when combined with Windows, is hardly a real-time OS. In the short term, minor firmware revisions to correct expensive and consecutive read/write operations are critical. Because the optimal control of a single fixture and sensor node was considered, there may be unexpected delays as the network scales. Now, after testing and reporting on the performance of the sensor nodes, the gain of the analog and digital sensors can be locked down. The main hindrance in transparent operation of the network is going to be subtly measuring the ambient and current intensity of the uncontrolled and controlled lighting in the room. Currently, this update rate is 11 Hz.

In Chapter 3, the use of direct search was presented as an efficient nonlinear solver for the lighting network. It is not an issue of being able to accurately determine the correct intensity

for the total number of wavelengths present in a lighting network; this was demonstrated. It is an issue of speed. For example, one possible solution is use to the direct search method to calculate a table of intensities to be stored in each fixture, then the correct intensity of the network is determined via the control computer, and the intensity setting is transmitted to the fixtures. The lights themselves preform the linear adjustment to then correct their intensity.

The techniques discussed in this work can be generalized to the control of traditional lighting technologies. One goal of designing the polychromatic system was to develop a light source capable of best-in-class photometric and color related properties. It was also theorized that existing methods of measuring and sensing color lead to decreased performance of these systems. The development of a custom light source enabled a quantitative comparison of the methods and techniques proposed for control. Additionally, it extends the work on the optimal control of lighting in [64, 49] by considering spectrally tunable sources capable of dynamic energy consumption. These extra layers of difficulty prompted the development and testing of new models and techniques to control the network. Yet, LED lighting is not widespread. For example, in MIT building E14, a Lutron Grafik Eye controls the dimmable overhead fluorescent fixtures. Future work will focus on incorporating more diverse sources into the control of the system.

The benefits of using an adaptive approach to selecting the wavelengths of the source were mentioned, yet this extra degree of control presents some major concerns from a usability standpoint. At present, a single button press on the control node instructs the system to perform a calibration step. The user is then able to set the desired illuminance level and color temperature by adjusting a slider on the control node. These operations are more complicated than turning on or off a switch. Certainly, adding a fourth operation – the ability to switch between efficient and high quality light is overkill. So how can this be simplified? First, an experiment to derive the users' lighting preferences must be performed. In these experiments, it can be tested which light sources the user prefers under different situations. Ultimately, one conclusion may be that, although the dynamic efficacy offers additional energy savings, the quality of the light is not preferred by any users. Long term testing incorporating a large number of LED and other fixtures are required to report on the true energy savings employed by these techniques. In the short term, testing is planned to occur with the iW Blast Powercore from Color Kinetics.

7.2 Future Work

The work presented here leads to the "event horizon", so to speak, of researching the broader implications of sensor-enabled lighting networks. For every question answered here, several more exist. Missing from this discussion are the effects of reflected light (i.e., headmounted gaze tracking) on the control and performance of the network. Yet using a sensor board designed here, the preliminary effects of this type of control can be quickly studied. Also

missing are the quantitative results of the control of at least two fixtures and a full study of the actual energy saved by adjusting the intensity in response to changing ambient light. To get to this point, several illuminance studies of building E14 (concentrated primarily on the 5th floor) are required. These studies will provide actual illuminance data of the area, which we will use to build models of the expected energy savings. These will be performed in the short term and once complete, can be used to contrast the measured results of several tests in which the intensity is regulated according to ambient light. Going one step further, we plan to measure the energy savings when the user is able to adjust the color and illuminance as well. Also planned for the near-future is the redesign of the sensor node to make it compact and more energy efficient. Broader research ambitions include incorporating gesture-based control of the sensor node (i.e., create a light surface of this intensity and color quality here, similar to Bolt's classic "Put That There") [13]. In this manner a zone of lighting can be specified, for example, by moving the sensor node around the desired area (an accelerometer in the sensor node can detect motion) or video could enable gesture recognition and tracking.

Looking towards the future, the next phase of work will aim to utilize more complicated sensors and activity-recognition algorithms to better infer user context and light their environment accordingly. Room-mounted and wearable cameras, for example, will be used to track users and determine their zone of activity, lighting the area accordingly. Hands will be tracked, and gestural control (e.g., pointing, sweeping, framing, etc.) will be used to direct the room lighting when it is necessary to go beyond the assumptions made by the context engine [39]. Users can be tracked to within several meters by the wireless signal from their wearable system – correlating motion detected by their wearable accelerometers and local cameras can precisely identify and locate them [70, 69]. In the final phase of the work, the system will be installed into a suite of working offices to examine the interaction and control of this intelligent lighting system with other utilities (e.g., closed loop heating and air conditioning [22]) to create environments that automatically meet users' utility goals and comfort while minimizing energy. Also of interest are the persuasive interfaces to these environments, through which users will see the system working, explore their energy consumption, compare their energy usage with their past activity and to that of other subjects, and adjust the assumptions that the system makes about them. This phase of activity will also integrate with a ubiquitous interactive display system that we have installed throughout our building that identifies users when they approach and facilitates a variety of contact and non-contact interaction. Users of our system can employ these "portals" to invoke and interact with their energy-related information anywhere in the building. Although researchers have been exploring aspects of interactive lighting for several years, the agile control and rich sensor data afforded by these systems will inspire new means of interfacing with and controlling fine-grained utility infrastructure to maximize function while minimizing energy, illustrating a key application that will drive cyber-physical systems in the next decade.

Appendix A

Expanded Results

The Figures A.2, A.1, A.3, and A.4 contain the predicted and measured spectra used to describe the experiments in Chapter 5.

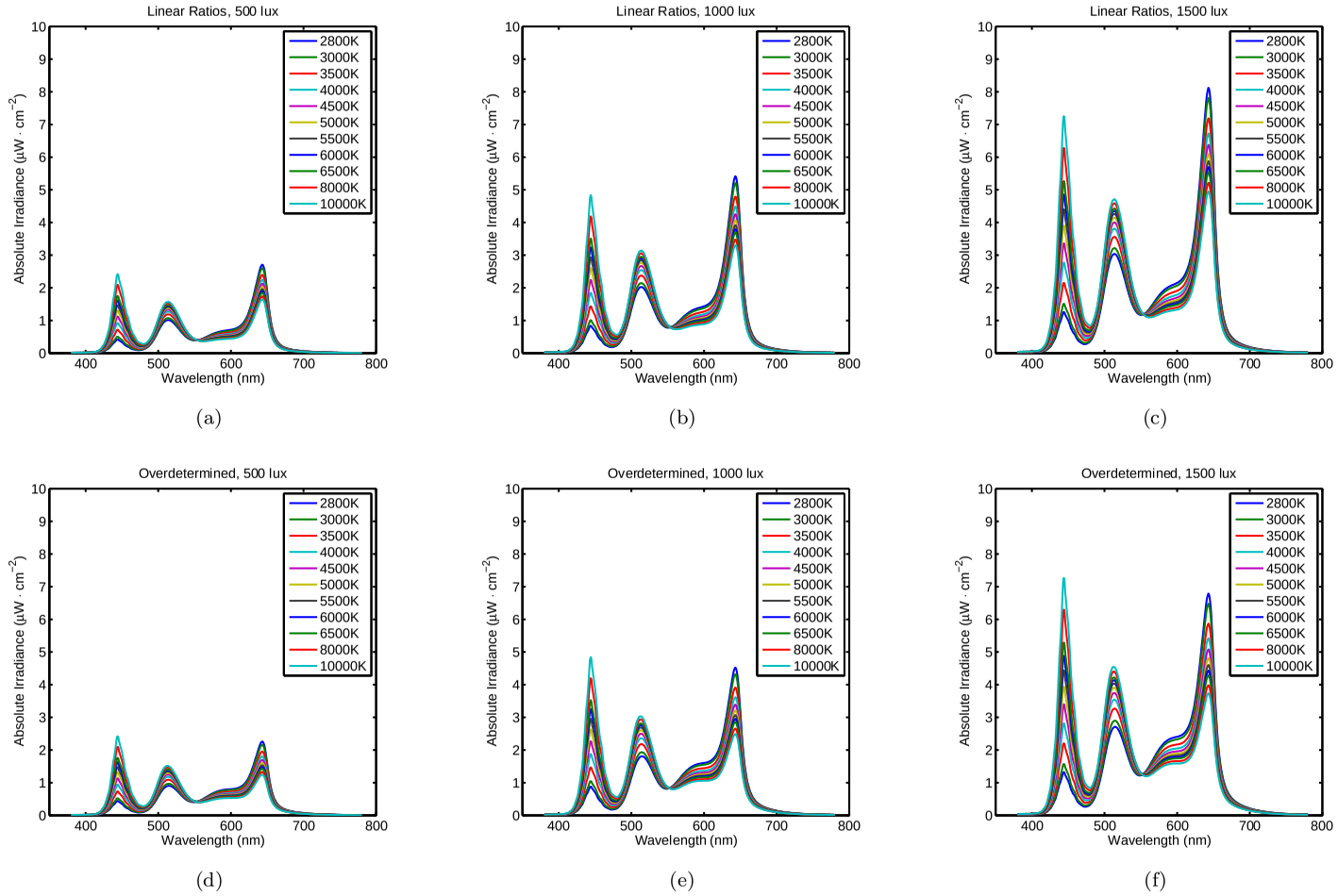

Figure A.1: Predicted spectral response for both linear and overdetermined methods for three different lux settings and 11 color temperatures.

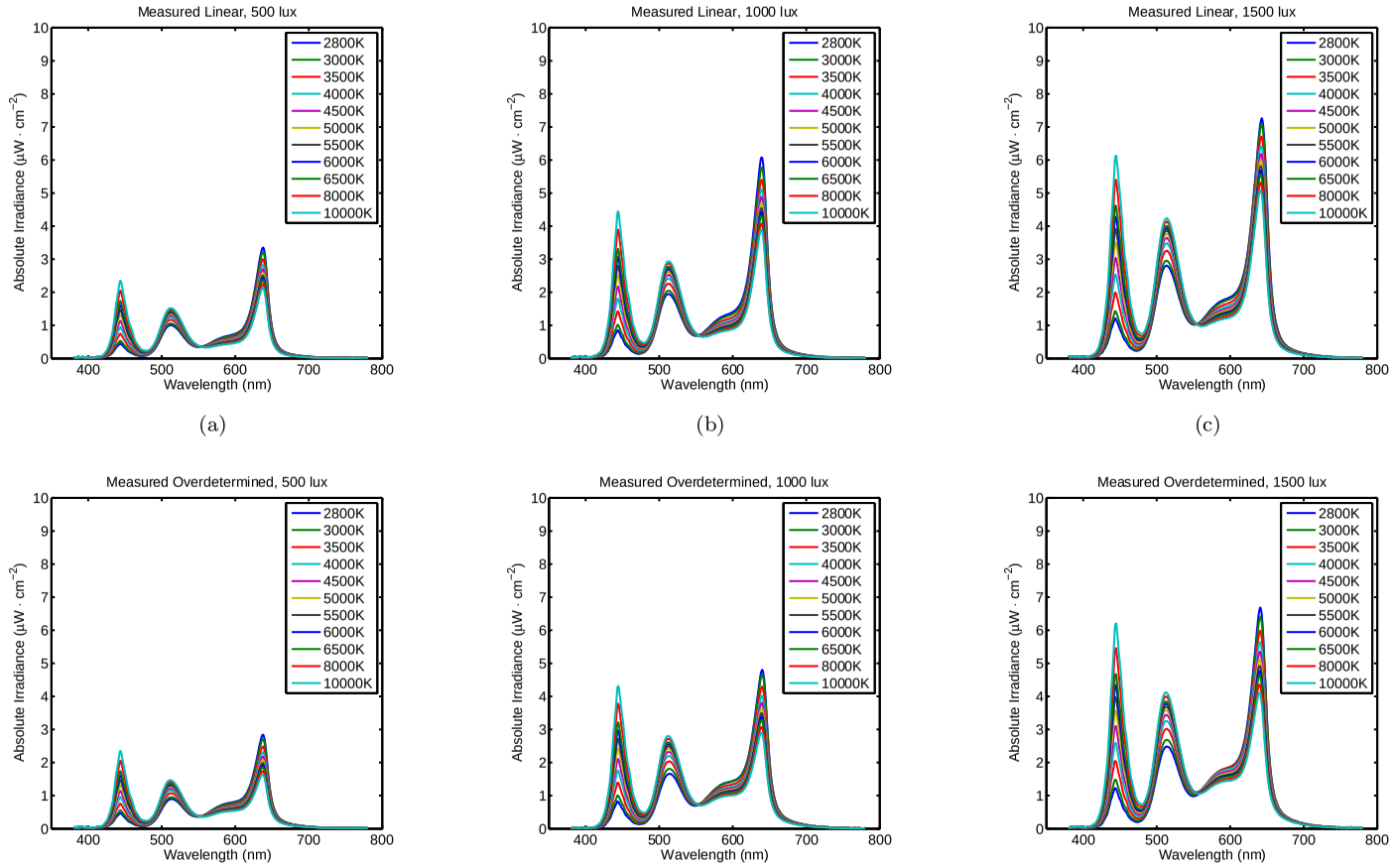

Figure A.2: Measured spectral response for both linear and overdetermined methods for three different lux settings and 11 color temperatures.

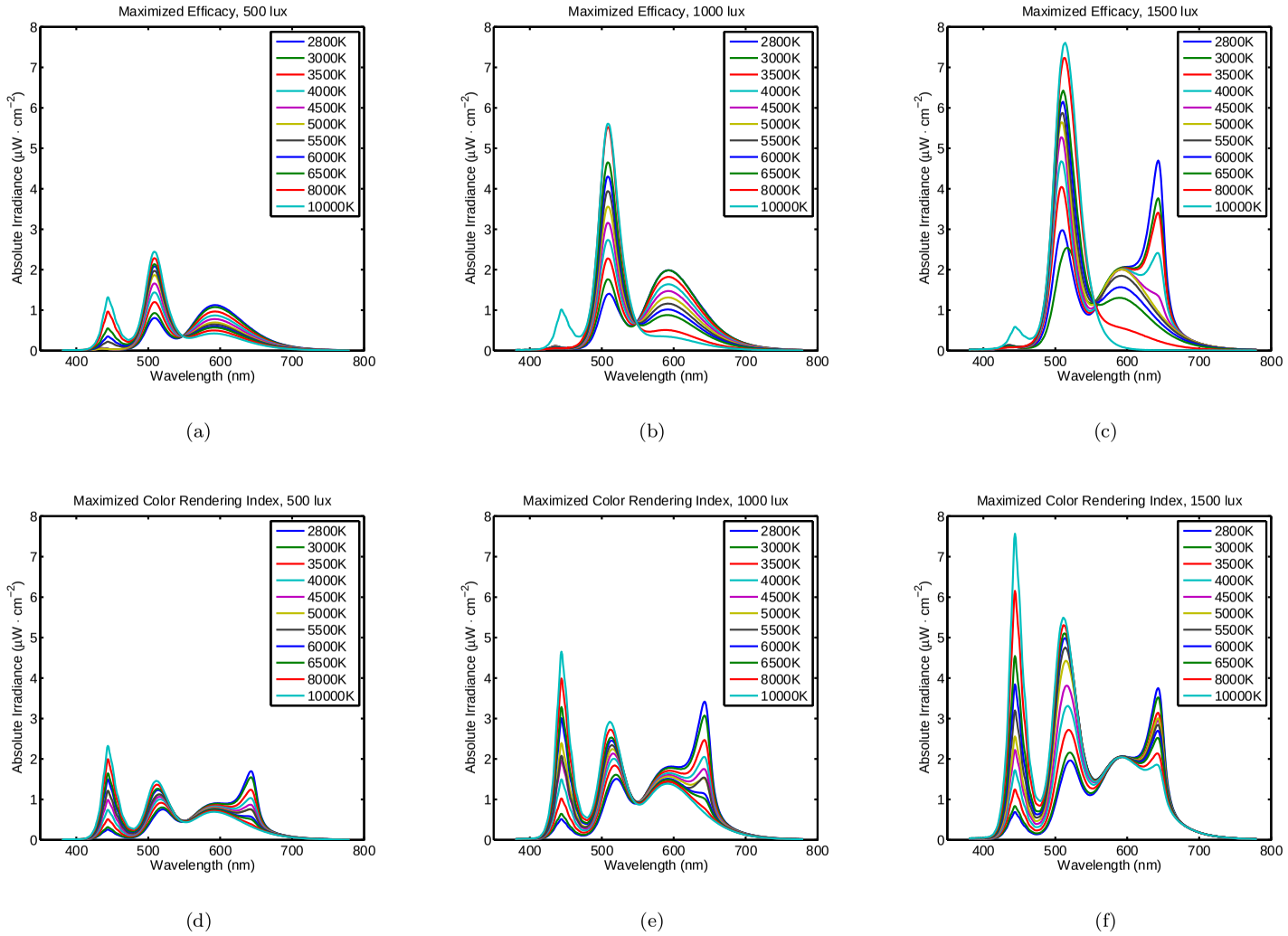

(a) (b) (c)

(d) (e) (f)

Figure A.3: Predicted spectral response using the MADS algorithm for maximizing efficacy or color rendering index for three different lux settings and 11 color temperatures.

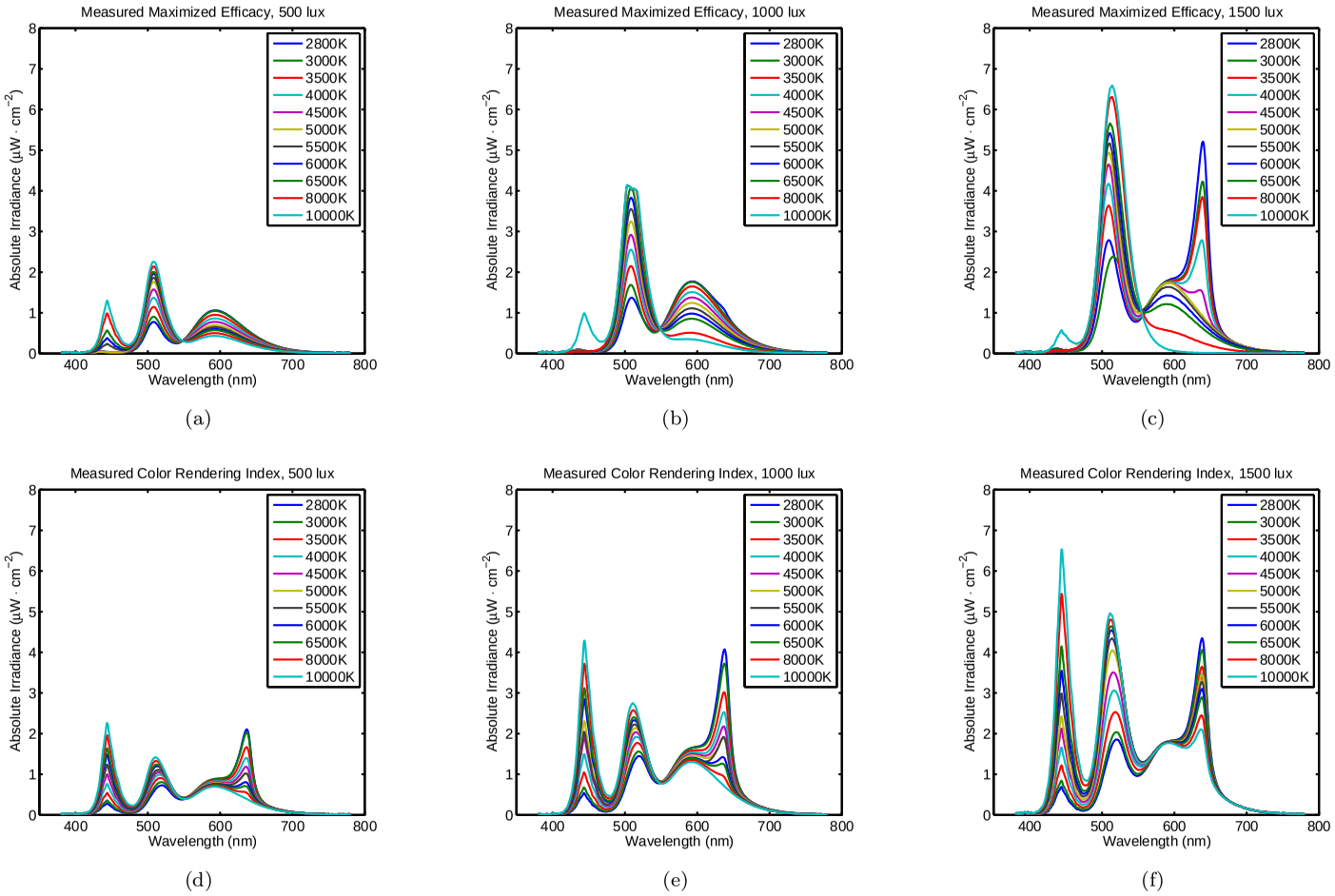

Figure A.4: Measured spectral response using the MADS algorithm for maximizing efficacy or color rendering index for three different lux settings and 11 color temperatures. In subfigure b, the spectrometer saturated for testpoints 8000 K and 10000 K.

Appendix B

Hardware Design

B.1 LED Controller Hardware Schematics

[follows on next page]

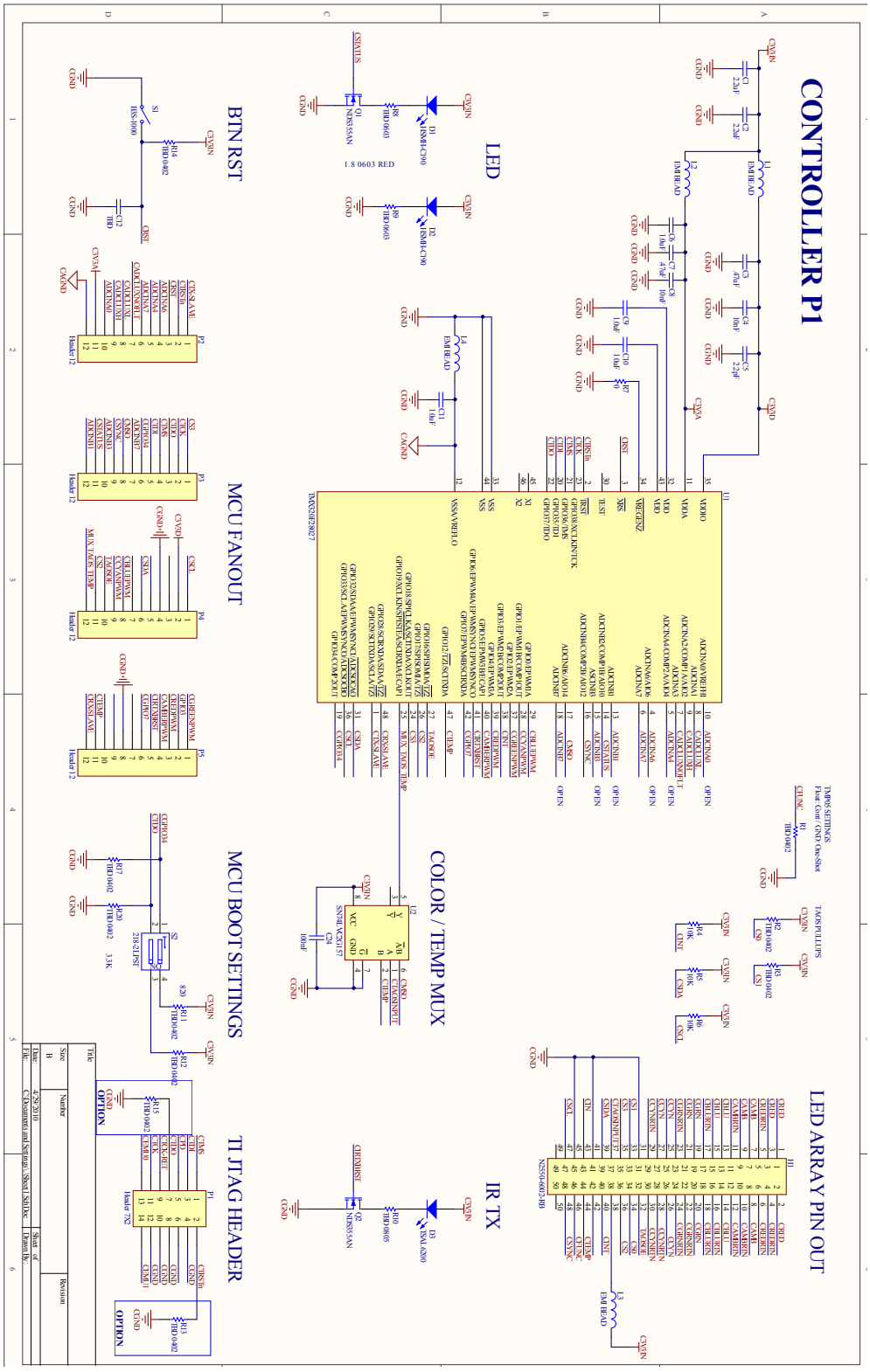
CONTROLLER P1
LED ARRAY PIN OUT
IR TX
COLOR / TEMP MUX
TI JTAG HEADER
MCU BOOT SETTINGS
MCU FANOUT
BTN RST
LED

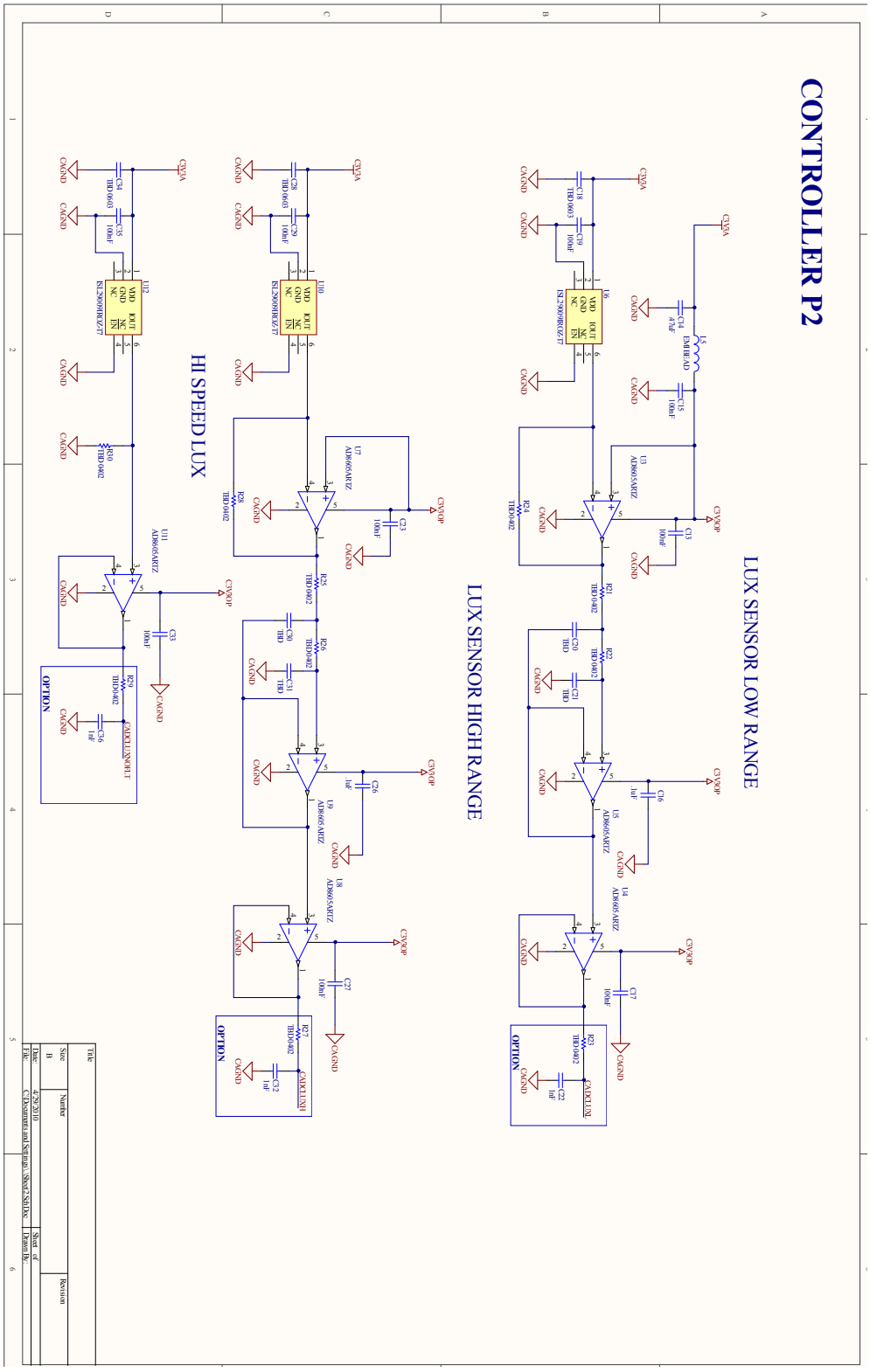
CONTROLLER P2
LUX SENSOR LOW RANGE
LUX SENSOR HIGH RANGE
HI SPEED LUX
OPTION
OPTION
OPTION
CAGND
C3VA
C3VAOP
Title
Size
B
Number
Revision
Date:
4/29/2010
File:
C:\Documents and Settings\...\Sheet4.SchDoc
Sheet of
Drawn By:

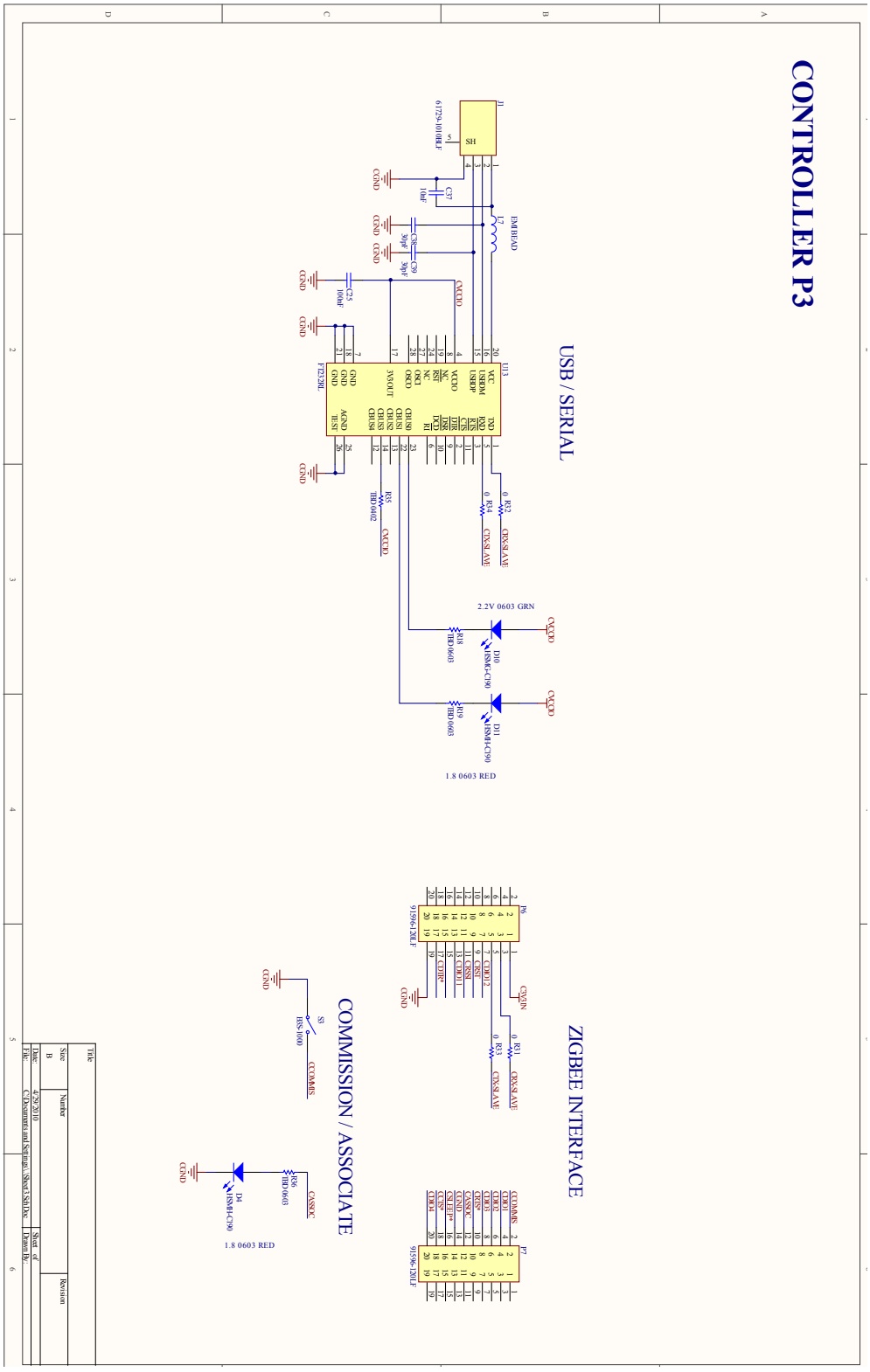
CONTROLLER P3
USB / SERIAL
ZIGBEE INTERFACE
COMMISSION / ASSOCIATE
2.2V 0603 GRN
1.8 0603 RED
1.8 0603 RED
Title
Size
B
Number
Revision
Date:
4/29/2010
File:
C:\Documents and Settings\...\Sheet1.SchDoc
Sheet
of
Drawn By:

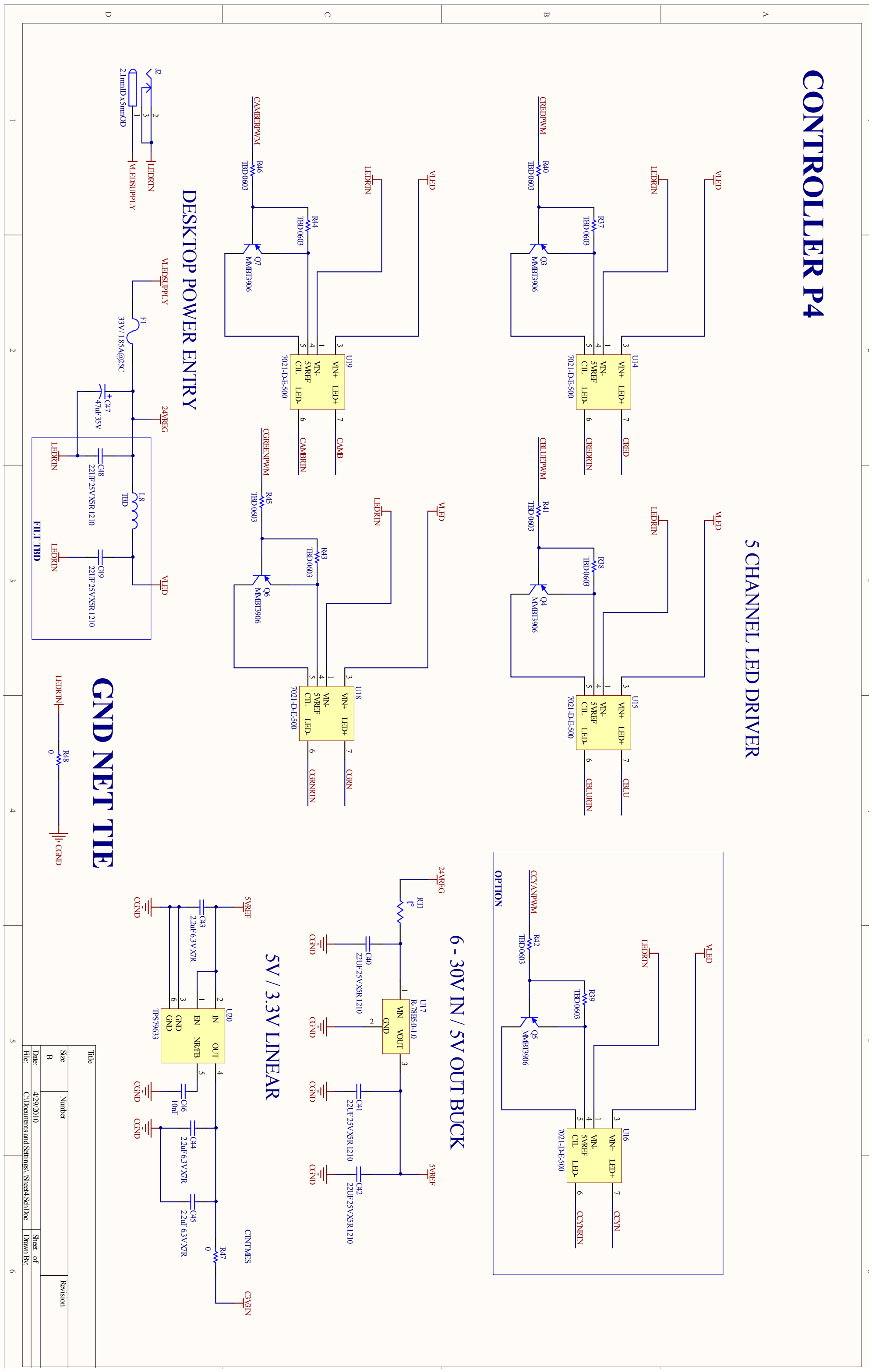
CONTROLLER P4
5 CHANNEL LED DRIVER
6 - 30V IN / 5V OUT BUCK
5V / 3.3V LINEAR
DESKTOP POWER ENTRY
GND NET TIE
FILT TBD
OPTION

B.2 LED Controller PCB

[follows on next page]

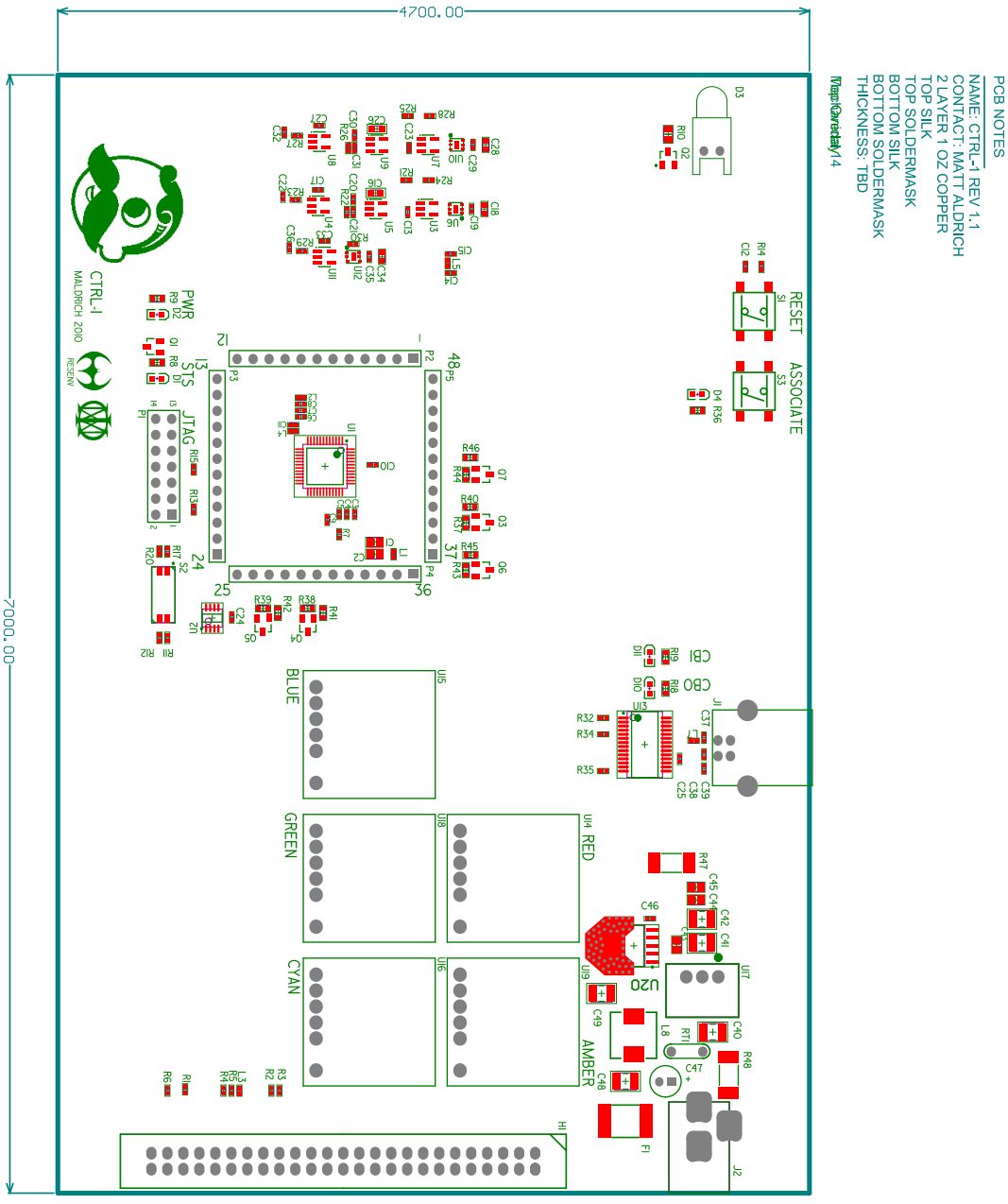
4700.00
7000.00
PCB NOTES
NAME: CTRL-1 REV 1.1
CONTACT: MATT ALDRICH
2 LAYER 1 OZ COPPER
TOP SILK
TOP SOLDERMASK
BOTTOM SILK
BOTTOM SOLDERMASK
THICKNESS: TBD
CTRL-1
MALDRICH 2010
RESENV
PWR
STS
JTAG
RESET
ASSOCIATE
BLUE
GREEN
CYAN
RED
AMBER
U20

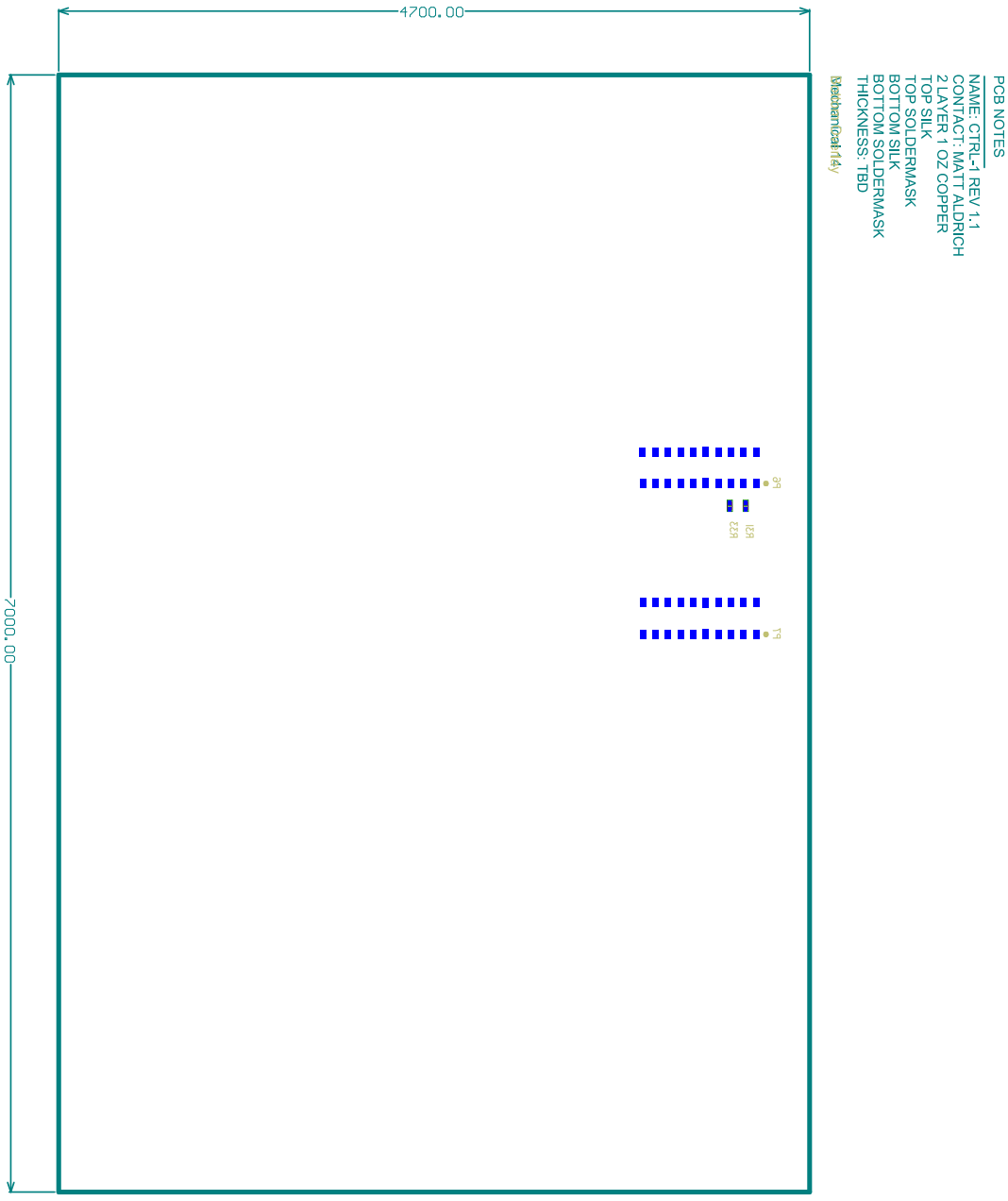
4700.00
7000.00
PCB NOTES
NAME: CTRL-1 REV 1.1
CONTACT: MATT ALDRICH
2 LAYER 1 OZ COPPER
TOP SILK
TOP SOLDERMASK
BOTTOM SILK
BOTTOM SOLDERMASK
THICKNESS: TBD
Mechanical1

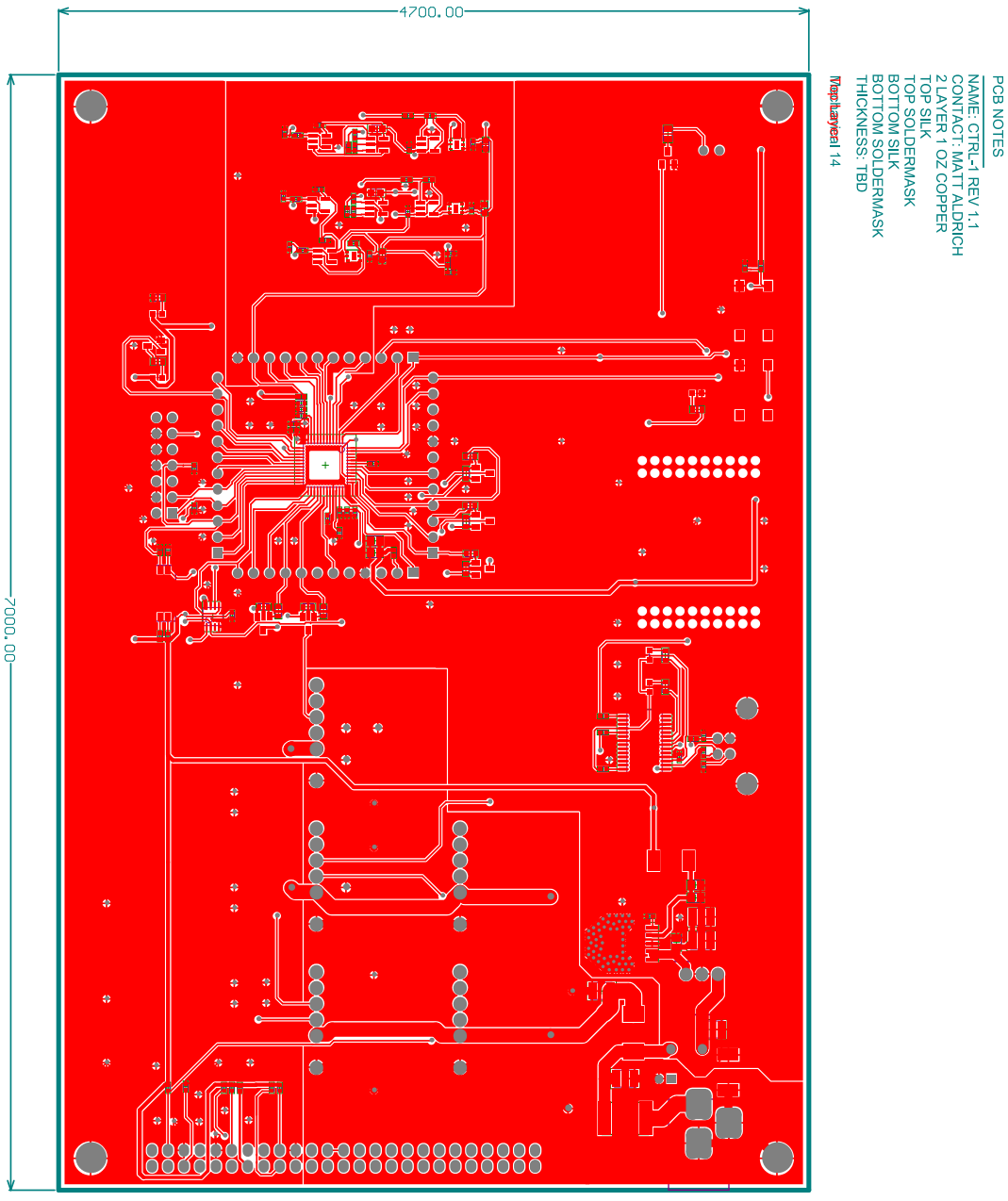
4700.00
7000.00
PCB NOTES
NAME: CTRL-1 REV 1.1
CONTACT: MATT ALDRICH
2 LAYER 1 OZ COPPER
TOP SILK
TOP SOLDERMASK
BOTTOM SILK
BOTTOM SOLDERMASK
THICKNESS: TBD
Top layer
Bottom layer

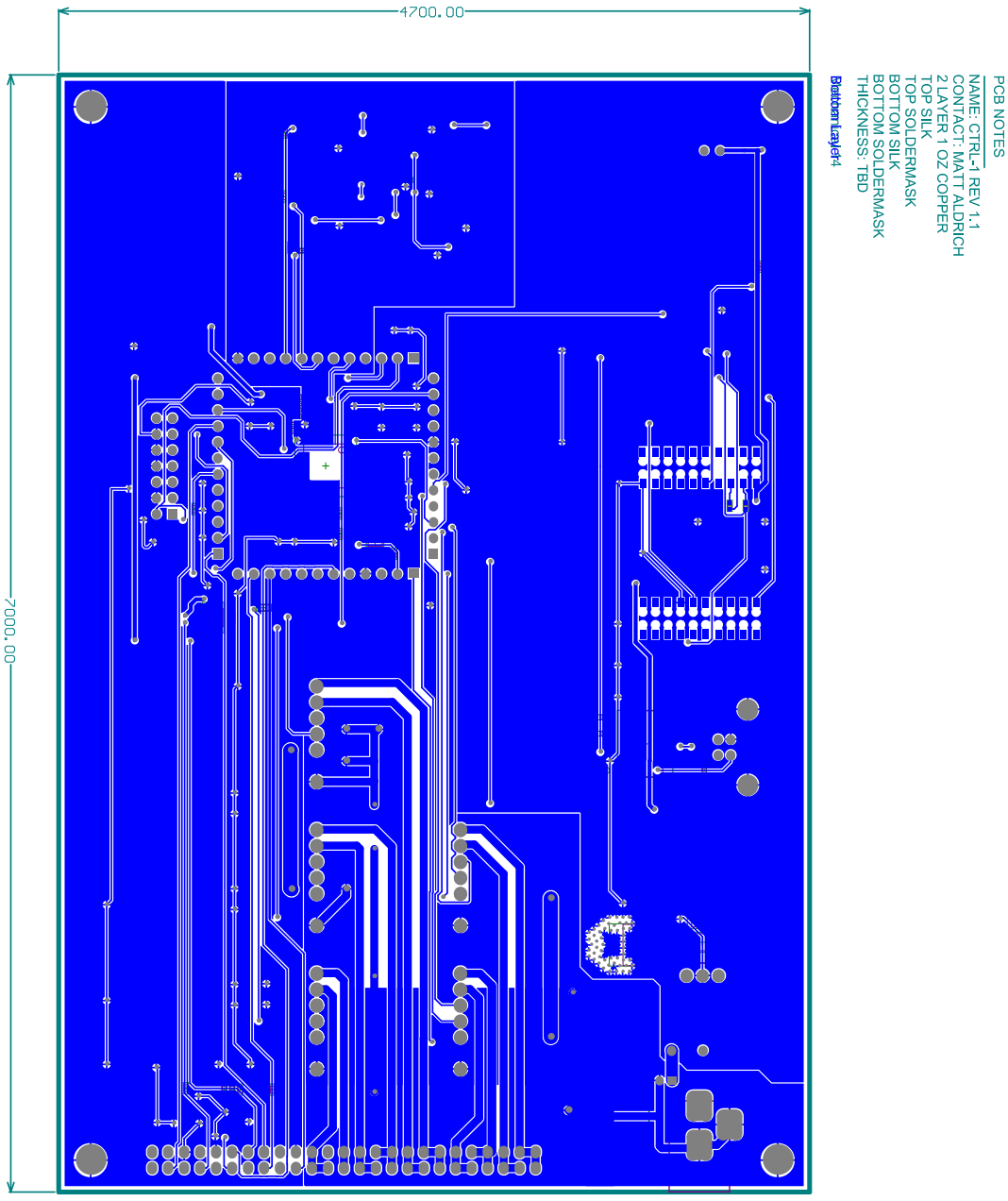
4700.00
7000.00
PCB NOTES
NAME: CTRL-1 REV 1.1
CONTACT: MATT ALDRICH
2 LAYER 1 OZ COPPER
TOP SILK
TOP SOLDERMASK
BOTTOM SILK
BOTTOM SOLDERMASK
THICKNESS: TBD

B.3 LED Controller Bill of Materials

[follows on next page]

Bill of Materials

Source Data From: LED Controller, Rev 1
Project: LED Controller, Rev 1
Design: M. Aldrich

Report Date: 1/12/2010 12:53:02 PM
Print Date: 29-Apr-10 6:39:26 PM

#	Designator	Description	Manufacturer 1	Manufacturer Part Number 1	Footprint	Supplier 1	Supplier Part Number 1	Quantity
1	N/A	LED Controller, PCB	Advanced Circuits	N/A	N/A	N/A	N/A	1
2	C1, C2	CAP CERAMIC 2.2UF 10V X5R 0805	Kemet	C0805C225K8PACTU	CAPC2012L	Digi-Key	399-3125-1-ND	2
3	C3, C7, C14	CAP CERM 1UF 6.3V X5R 0402	Kemet	C0402C105K9PACTU	CAPC1005L	Digi-Key	399-4873-1-ND	3
4	C4, C8, C37, C46	CAP CER 10000PF 25V 10% X7R 0402	Murata Electronics North America	GRM155R71E103KA01D	CAPC1005L	Digi-Key	490-1312-1-ND	4
5	C5	CAP CER 2.2PF 50V C0G 0402	Murata Electronics North America	GRM1555C1H2R2CZ01D	CAPC1005L	Digi-Key	490-1267-1-ND	1
6	C6, C9, C10, C11	CAP CERM 1UF 6.3V X5R 0402	Kemet	C0402C105K9PACTU	CAPC1005L	Digi-Key	399-4873-1-ND	4
7	C12	CAP CER 1000PF 50V C0G 0402,	Murata Electronics North America	GRM155R61A104KA01D,	CAPC1005L	Digi-Key	490-3244-1-ND	1
8	C20, C30	CAP CER .47UF 6.3V X5R 0402	Murata Electronics North America	GRM155R60J474KE19D	CAPC1005L	Digi-Key	490-3266-1-ND	2
9	C21, C31	CAP CER .22UF 6.3V X5R 0402	Murata Electronics North America	GRM155R60J224KE01D	CAPC1005L	Digi-Key	490-5407-1-ND	2
10	C20, C21, C30, C31	CAP CER .1UF 10V 10% X5R 0402	Murata Electronics North America	GRM155R61A104KA01D	CAPC1005L	Digi-Key	490-1318-1-ND	4
11	C13, C15, C17, C19, C23, C24, C25, C27, C29, C33, C35	CAP CER .1UF 10V 10% X5R 0402	Murata Electronics North America	GRM155R61A104KA01D	CAPC1005L	Digi-Key	490-1318-1-ND	11
12	C16, C26	CAP CER .1UF 50V 10% X7R 0603	Murata Electronics North America	GRM188R71H104KA93D	CAPC1608N	Digi-Key	490-1519-1-ND	2
13	C18, C28, C34	CAP CER 1.0UF 10V 10% X5R 0603	Murata Electronics North America	GRM188R61A105KA61D	CAPC1608N	Digi-Key	490-1543-1-ND	3
14	C22, C32, C36	CAP CER 3300PF 50V X7R 0402	Murata Electronics North America	GRM155R71H332KA01D	CAPC1005L	Digi-Key	490-3248-1-ND	3
15	C38, C39	CAP CER 30PF 50V 5% C0G 0402	Murata Electronics North America	GRM1555C1H300JZ01D	CAPC1005L	Digi-Key	490-1285-1-ND	2
16	C40, C41, C42, C48, C49	CAP CER 22UF 25V X5R 1210	Taiyo Yuden	TMK325BJ226MM-T	CAPC3225N	Digi-Key	587-2086-1-ND	5
17	C43, C44, C45	CAP CER 2.2UF 6.3V 10% X7R 0805	Murata Electronics North America	GRM21BR70J225KA01L	CAPC2012L	Digi-Key	490-1698-1-ND	3
18	C47	CAP 47UF 35V ELECT NHG RADIAL	Panasonic - ECG	ECA-1VHG470	CAPPR2-5x11	Digi-Key	P5550-ND	1
19	D2, D10, D11	LED 570NM GREEN DIFF 0603 SMD	Avago Technologies US Inc.	HSMG-C190	1608	Digi-Key	516-1425-1-ND	3
20	D1, D4	LED 630NM HE RED DIFF 0603 SMD	Avago Technologies US Inc.	HSMS-C190	1608	Digi-Key	516-1422-1-ND	2
21	D3	EMITTER IR 5MM HI EFF 940NM	Vishay/Semiconductors	TSAL6200	HLMP-5029	Digi-Key	751-1204-ND	1
22	(D3)	HOUSING RA FOR 5MM HIGH DOME LED	Avago Technologies US Inc.	HLMP-5029	N/A	Digi-Key	516-1395-ND	1
23	F1	PTC RESET 33V 1.85A SMD 2920	Littelfuse Inc	2920L185DR	2920L185DR	Digi-Key	F2871CT-ND	1
24	H1	CONN HEADER 50 POS STRGHT GOLD	3M	N2550-6002-RB	N2550-6002-RB	Digi-Key	MHC50K-ND	1
25	J1	USB RCPT B-TYPE R/A FULL BACK	FCI	61729-1010BLF	61729-1010BLF	Digi-Key	609-3656-ND	1
26	J2	MALE BARREL CONNECTOR 2.1x5.5	Switchcraft Inc.	RAPC722X	RAPC722X	Mouser	502-RAPC722X	1
27	L1, L3	FERRITE CHIP 60 OHM 1700MA 0402	Murata Electronics North America	BLM15PD600SN1D	1005	Digi-Key	490-5201-1-ND	2
28	L2, L4	FILTER CHIP 220 OHM 700MA 0402	Murata Electronics North America	BLM15EG221SN1D	1005	Digi-Key	490-4005-1-ND	2
29	L5	INDUCTOR MULTILAYER 330NH 0402	TDK Corporation	MLG1005SR33J	1005	Digi-Key	445-3077-1-ND	1
30	(L5)	INDUCTOR MULTILAYER 2.2UH 0402	TDK Corporation	MLF1005A2R2KT	1005	Digi-Key	445-3518-1-ND	1
31	(L5)	FERRITE CHIP 1000 OHM 200MA 0402	Murata Electronics North America	BLM15HG102SN1D	1005	Digi-Key	490-3999-1-ND	1
32	L7	FERRITE CHIP 40 OHM 550MA 0402	TDK Corporation	MMZ1005Y400C	1005	Digi-Key	445-2150-2-ND	1
33	L8	INDUCTOR 22UH 1.8A SMD SHIELDED	Murata Power Solutions Inc	46223C	46223C	Digi-Key	811-1173-1-ND	1
34	P1	CONN HDR DUAL 14POS .100 SRT AU	Molex Connector Corporation	10-89-7142	TH	Digi-Key	WM26814-ND	1
35	P2, P3, P4, P5	CONN HEADER 12POS .100 VERT TIN	Molex Connector Corporation	22-28-4120	TH	Digi-Key	WM6412-ND	4
36	P6, P7	CONN RECEPT 20POS 2MM STR DL SMD	FCI	91596-120LF	SMT	Digi-Key	609-2730-ND	2
37	Q1, Q2	MOSFET N-CH 30V 1.7A SSOT3	Fairchild Semiconductor	NDS355AN	SOT-23	Digi-Key	NDS355ANCT-ND	2
38	Q3, Q4, Q5, Q6, Q7	TRANSISTOR GP PNP AMP SOT-23	Fairchild Semiconductor	MMBT3906	SO-G3	Digi-Key	MMBT3906FSCT-ND	5
39	R10	RES 16.9 OHM 1/8W 1% 0805 SMD	Rohm Semiconductor	MCR10EZHF16R9	RESC2012L	Digi-Key	RHM16.9CCT-ND	1
40	(R10)	RES 4.32 OHM 1/8W 1% 0805 SMD	Vishay/Dale	CRCW08054R32FKEA	RESC2012L	Digi-Key	541-4.32CCCT-ND	1
41	R37, R38, R39, R43, R44, R40, R41, R42, R45, R46	RES 5.1K OHM 1/10W 5% 0603 SMD	Vishay/Dale	CRCW06035K10JNEA	RESC1608N	Digi-Key	541-5.1KGCT-ND	10
42	R24, R28, R30 (0-500 lx)	RES 820K OHM 1/16W 1% 0402 SMD	Vishay/Dale	CRCW0402820KFKED	RESC1005L	Digi-Key	541-820KLCT-ND	3
43	(R24, R28, R30) (0-2,000 lx)	RES 402K OHM 1/16W 1% 0402 SMD	Vishay/Dale	CRCW0402402KFKED	RESC1005L	Digi-Key	541-402KLCT-ND	3
44	(R24, R28, R30) (0-10,000 lx)	RES 182K OHM 1/16W 1% 0402 SMD	Vishay/Dale	CRCW0402182KFKED	RESC1005L	Digi-Key	541-182KLCT-ND	3

45	(R24, R28, R30) (0-35,000 lx)	RES 100K OHM 1/16W 1% 0402 SMD	Rohm Semiconductor	MCR01MZPF1003	RESC1005L	Digi-Key	RHM100KLCT-ND	3
46	R13, R15	RES 20.0K OHM 1/16W 1% 0402 SMD	Rohm Semiconductor	MCR01MZPF2002	RESC1005L	Digi-Key	RHM20.0KLCT-ND	2
47	R11, R12	RES 820 OHM 1/16W 1% 0402 SMD	Vishay/Dale	CRCW0402820RFKED	RESC1005L	Digi-Key	541-820LCT-ND	2
48	R14	RES 2.70K OHM 1/16W 1% 0402 SMD	Rohm Semiconductor	MCR01MZPF2701	RESC1005L	Digi-Key	RHM2.70KLCT-ND	1
49	R17, R20	RES 3.30K OHM 1/16W 1% 0402 SMD	Rohm Semiconductor	MCR01MZPF3301	RESC1005L	Digi-Key	RHM3.30KLCT-ND	2
50	R1, R7, R31, R32, R33, R34, R35	RES 0.0 OHM 1/16W 5% 0402 SMD	Rohm Semiconductor	MCR01MZPJ000	RESC1005L	Digi-Key	RHM0.0JCT-ND	7
51	R2, R3, R4, R5, R6, R21, R22, R25, R26	RES 10.0K OHM 1/16W 1% 0402 SMD	Rohm Semiconductor	MCR01MZPF1002	RESC1005L	Digi-Key	RHM10.0KLCT-ND	9
52	R23, R27, R29	RES 56.0 OHM 1/16W 1% 0402 SMD	Rohm Semiconductor	MCR01MZPF56R0	RESC1005L	Digi-Key	RHM56.0LCT-ND	3
53	R8, R9, R18, R19, R36	RES 560 OHM 1/10W 1% 0603 SMD	Rohm Semiconductor	MCR03EZPFX5600	RESC1608N	Digi-Key	RHM560HCT-ND	5
54	R47, R48	RES 0.0 OHM 1W 5% 2512 SMD	Vishay/Dale	CRCW25120000Z0EG	2512	Digi-Key	541-0.0XCT-ND	2
55	RT1	CURRENT LIMITER INRUSH 5 0HM 20%	Cantherm	MF72-005D7	MF72-005D7	Digi-Key	317-1148-ND	1
56	S1, S3	SWITCH TACT 6MM 160GF H=4.3MM	Omron Electronics	B3S-1000P	TH	Digi-Key	SW836CT-ND	2
57	S2	SWITCH DIP HALF PITCH 2POS	CTS Electrocomponents	218-2LPST	218-2LPST	Digi-Key	CT2182LPST-ND	1
58	U1	IC MCU 32-BIT W/FLASH 48-LQFP	Texas Instruments	TMX320F28027PTA	TSQFP50P900X900X145-48L	Digi-Key	296-24123-ND	1
59	U2	IC 2-1LINE DATA SELECT/MUX SM8	Texas Instruments	SN74LVC2G157DCTR	TSOP65P400X130-8L	Digi-Key	296-13266-1-ND	1
60	U3, U4, U5, U7, U8, U9, U11	IC OPAMP SNGL R-R I/O LN SOT23-5	Analog Devices	AD8605ARTZ	SOT23-5	Digi-Key	AD8605ARTZREEL7CT-ND	7
61	U6, U10, U12	IC PHOTO DETECTOR AMBIENT 6-ODFN	Intersil	ISL29009IROZ-T7	ISL29009IROZ-T7	Digi-Key	ISL29009IROZ-T7CT-ND	3
62	U13	IC USB TO SERIAL UART 28-SSOP	FTDI	FT232RL R	SOP65P780X200-28L	Digi-Key	768-1007-1-ND	1
63	U14, U15, U16, U18, U19	LED DVR BUCKPLUS 500MA 7SIP DIM	LEDdynamics Inc	7021-D-E-500	7021-D-E-500	Digi-Key	788-1009-ND	5
64	U17	SWITCHING REGULATOR, 5V, 1.0 A	Recom Power Incorporated	R-78B5.0-1.0	TH	Allied	394-0052	1
65	U20	IC LDO REG 3.3V 1A SOT223-6	Texas Instruments	TPS79633DCQR	SOT127P706X180-6L	Digi-Key	296-13766-1-ND	1
Approved			**Notes**					**169**
			Line Item (36) Eq. P/N: 3M, 953220-2000-AR-PR; 3M, 956220-2000-AR-PR; Sullins NPPN102GHNP-RC (DIGIKEY)					
			Line Item (65) Alternate Supplier: Mouser, PN: 595-TPS79633DCQ					

B.4 Sensor Node Hardware Schematics

[follows on next page]

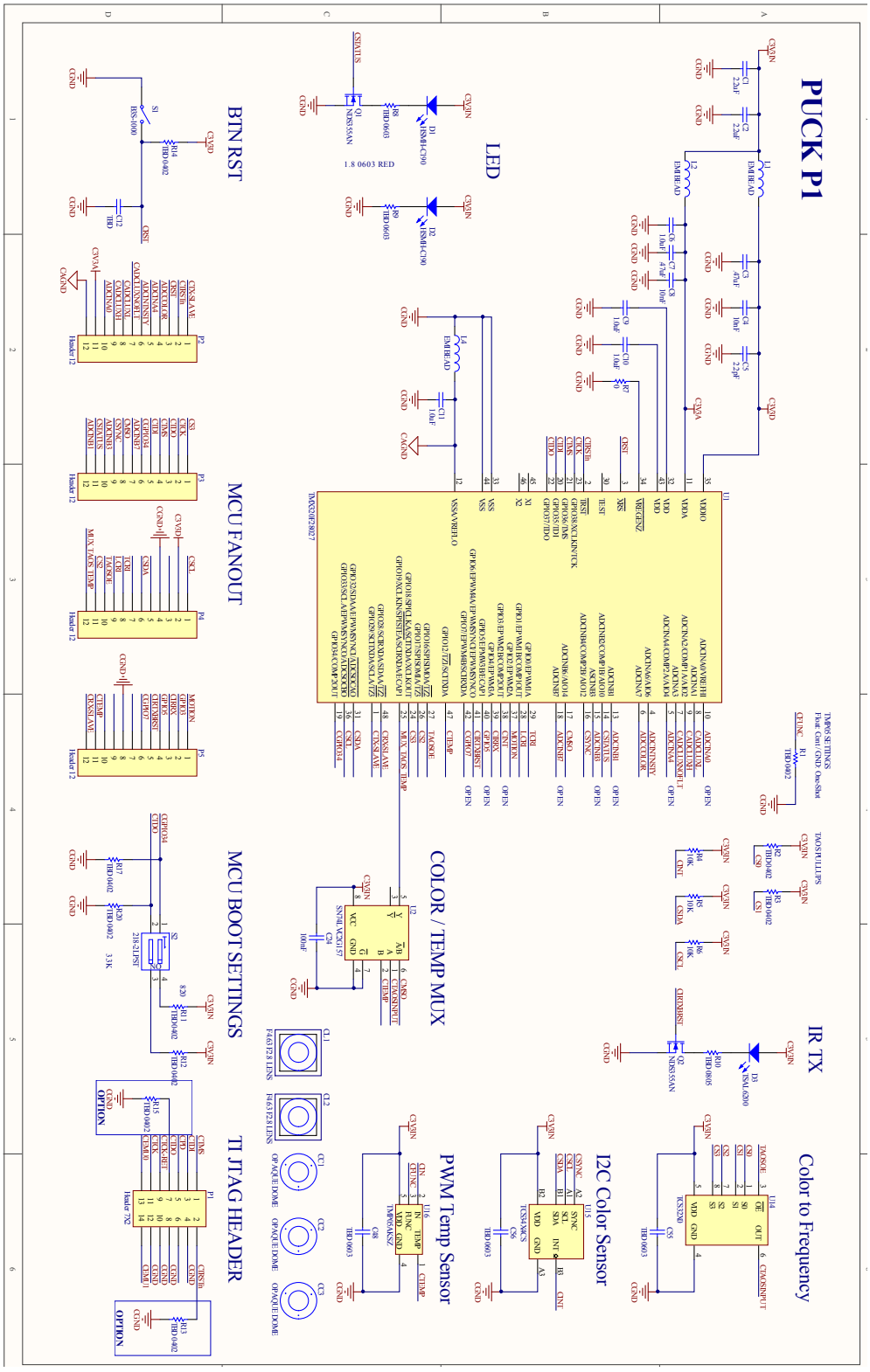
PUCK P1
LED
IR TX
Color to Frequency
I2C Color Sensor
PWM Temp Sensor
COLOR / TEMP MUX
TI JTAG HEADER
MCU BOOT SETTINGS
MCU FANOUT
BTN RST

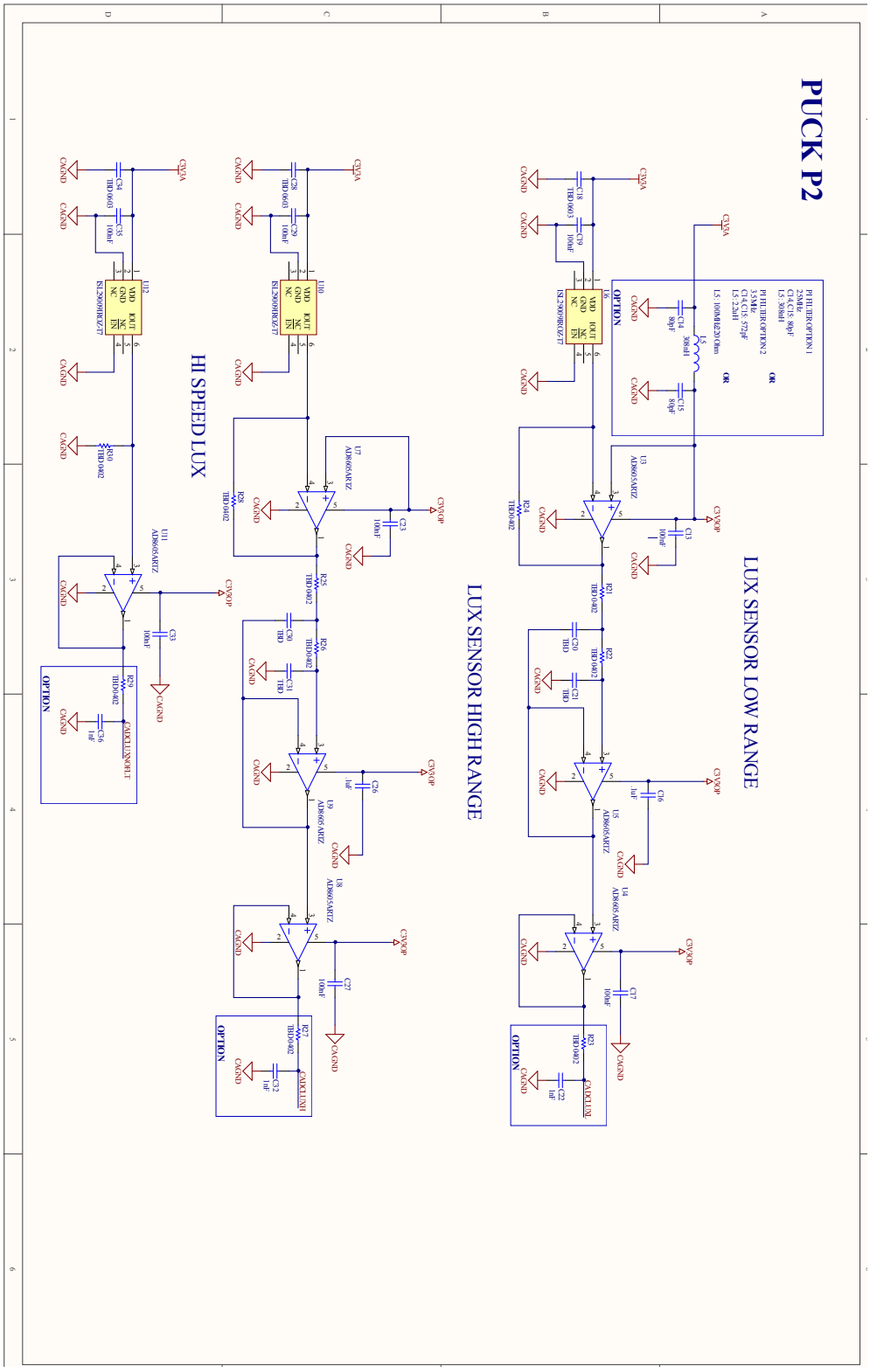
PUCK P2
LUX SENSOR LOW RANGE
LUX SENSOR HIGH RANGE
HI SPEED LUX
OPTION
OR

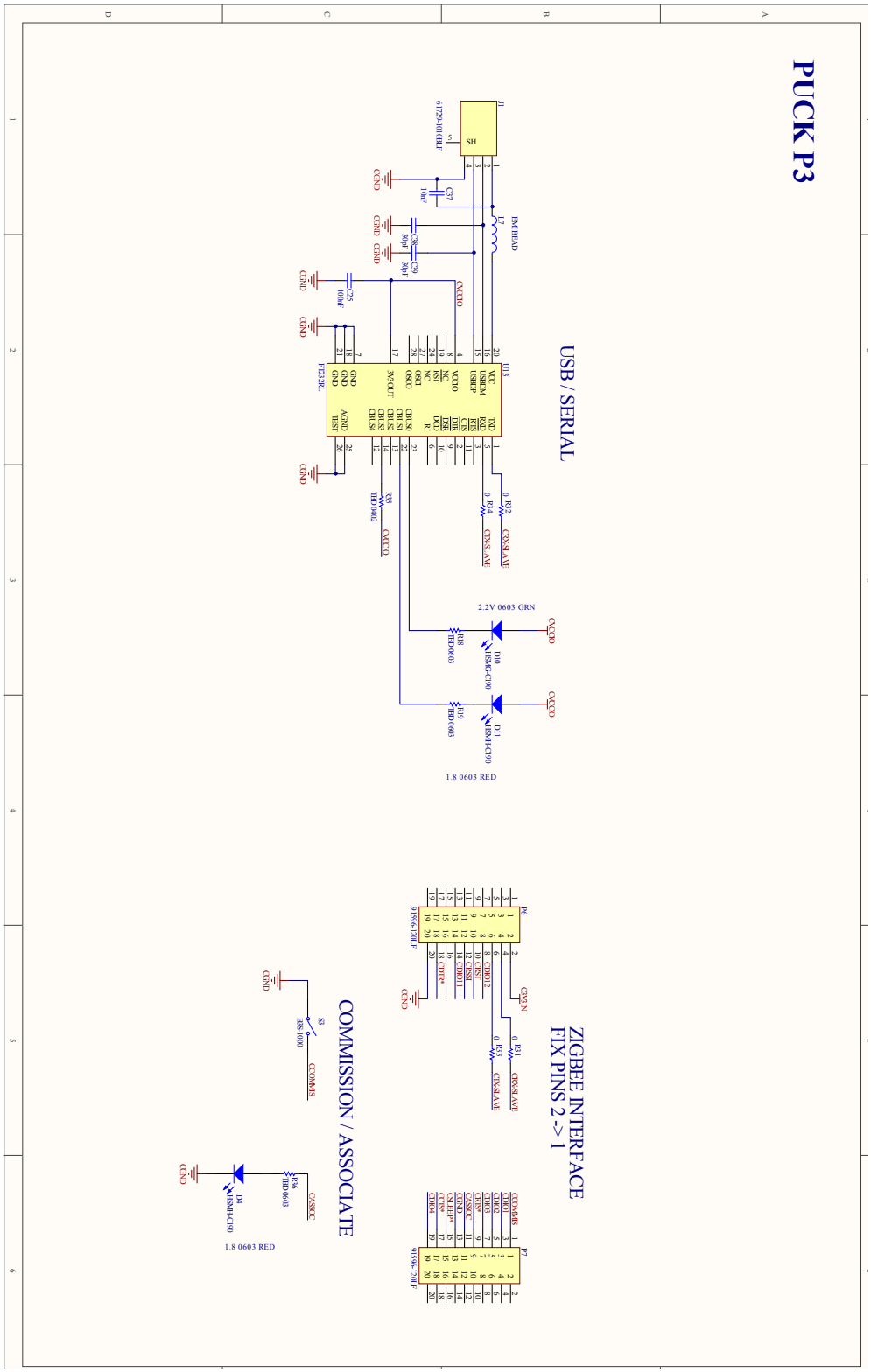
PUCK P3
USB / SERIAL
ZIGBEE INTERFACE
FIX PINS 2 -> 1
COMMISSION / ASSOCIATE
2.2V 0603 GRN
1.8 0603 RED
1.8 0603 RED
FT232RL
CGND
CXCDD
CTXSLAVE
CRXSLAVE
CXGIN
CXSSIZ
COMMRS

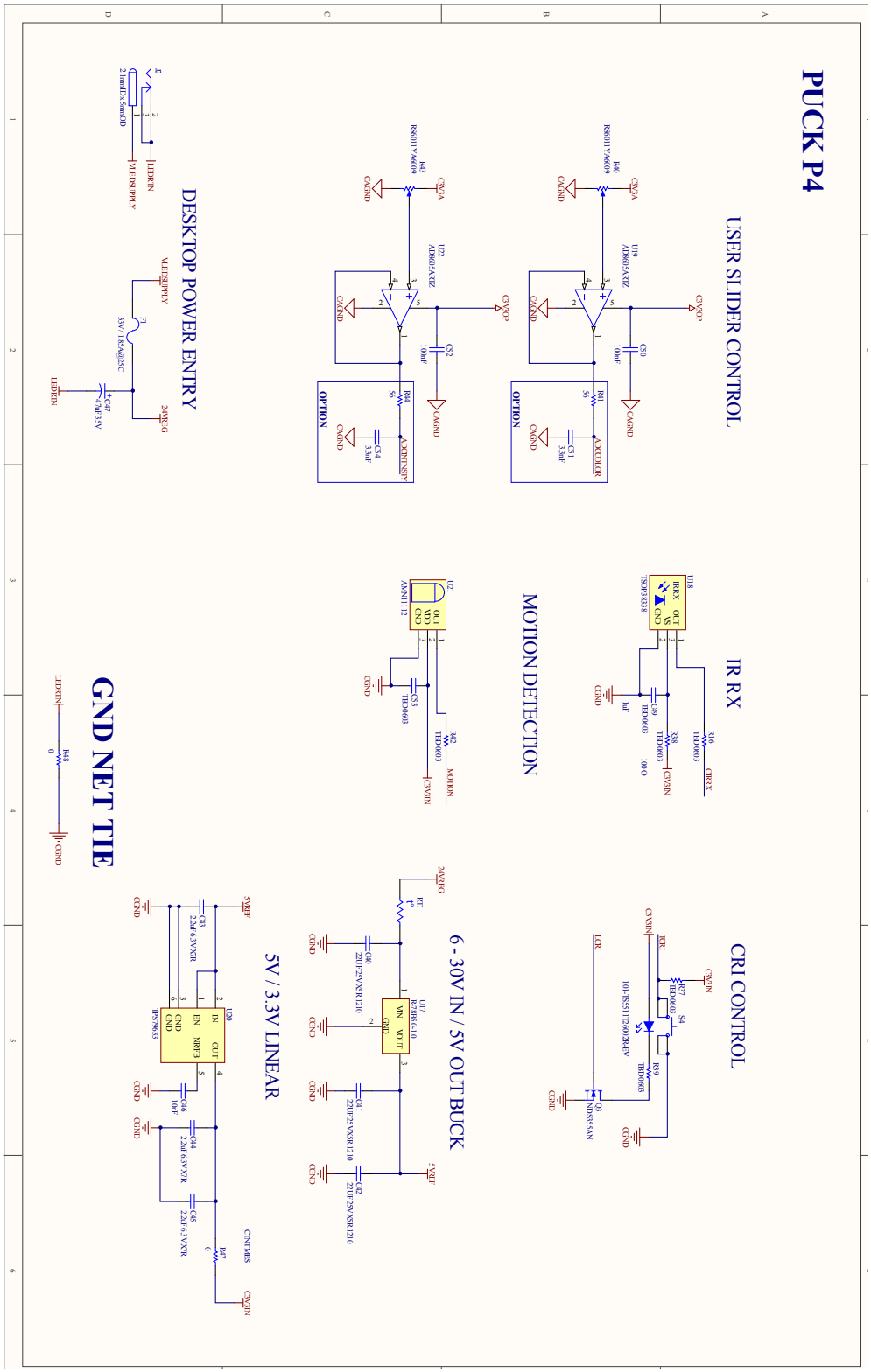
PUCK P4
USER SLIDER CONTROL
DESKTOP POWER ENTRY
IR RX
MOTION DETECTION
CRI CONTROL
6 - 30V IN / 5V OUT BUCK
5V / 3.3V LINEAR
GND NET TIE

B.5 Sensor Node PCB

[follows on next page]

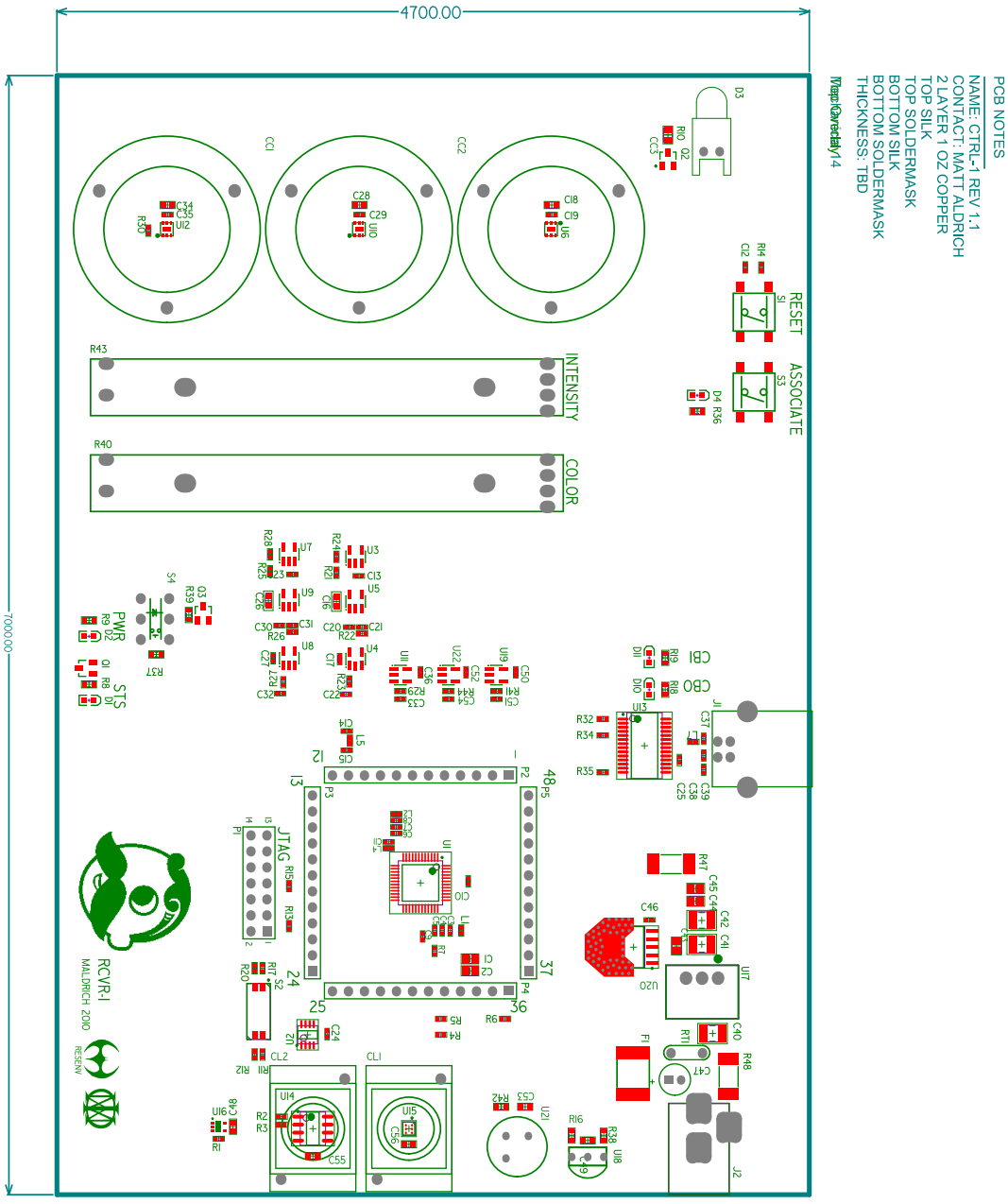
4700.00
7000.00
PCB NOTES
NAME: CTRL-1 REV 1.1
CONTACT: MATT ALDRICH
2 LAYER 1 OZ COPPER
TOP SILK
TOP SOLDERMASK
BOTTOM SILK
BOTTOM SOLDERMASK
THICKNESS: TBD
RESET
ASSOCIATE
INTENSITY
COLOR
PWR
STS
JTAG
RCVR-I
MALDRICH 2010

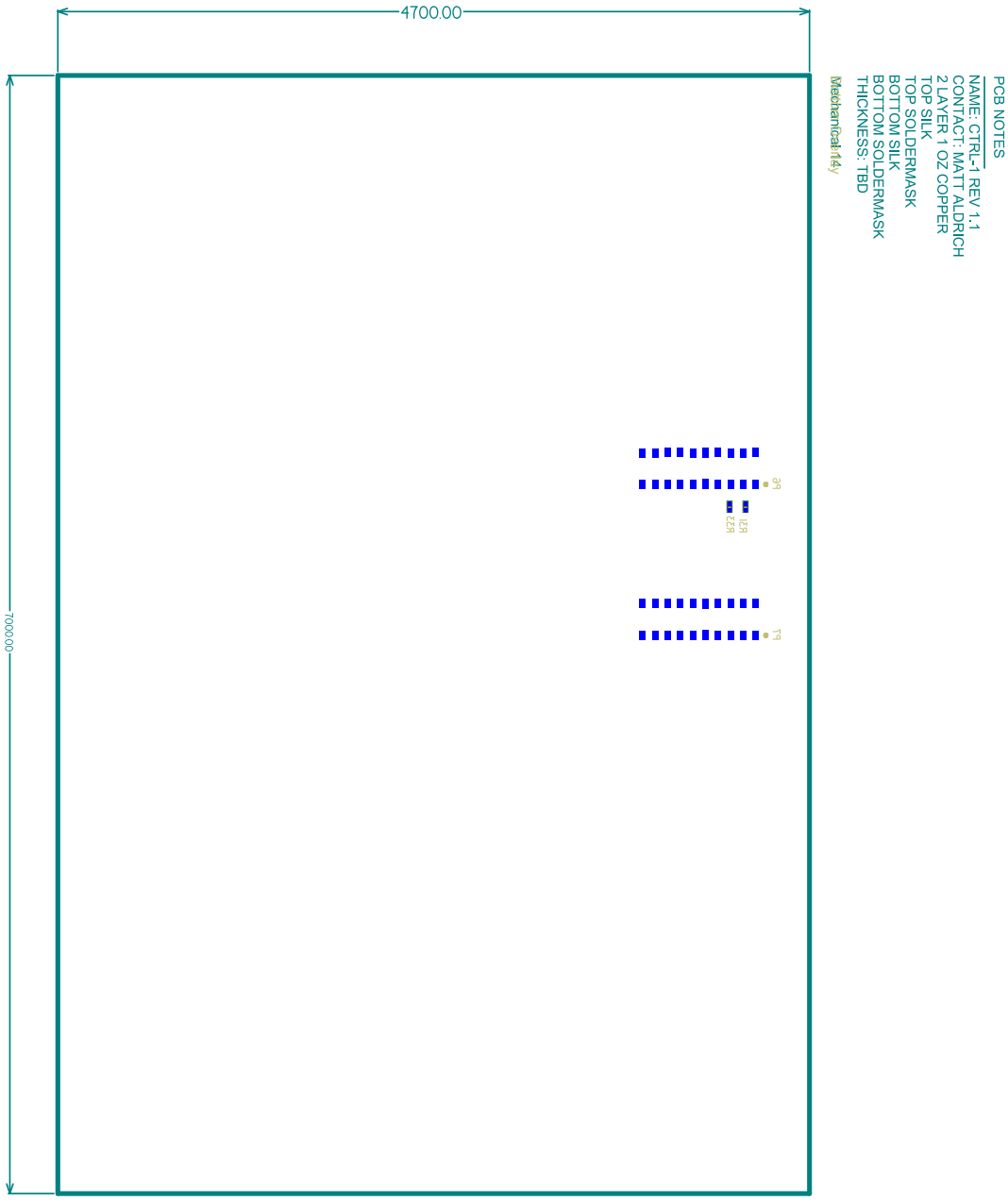
4700.00
7000.00
PCB NOTES
NAME: CTRL-1 REV 1.1
CONTACT: MATT ALDRICH
2 LAYER 1 OZ COPPER
TOP SILK
TOP SOLDERMASK
BOTTOM SILK
BOTTOM SOLDERMASK
THICKNESS: TBD
Mechanical 14
R23
R21
P6
P5

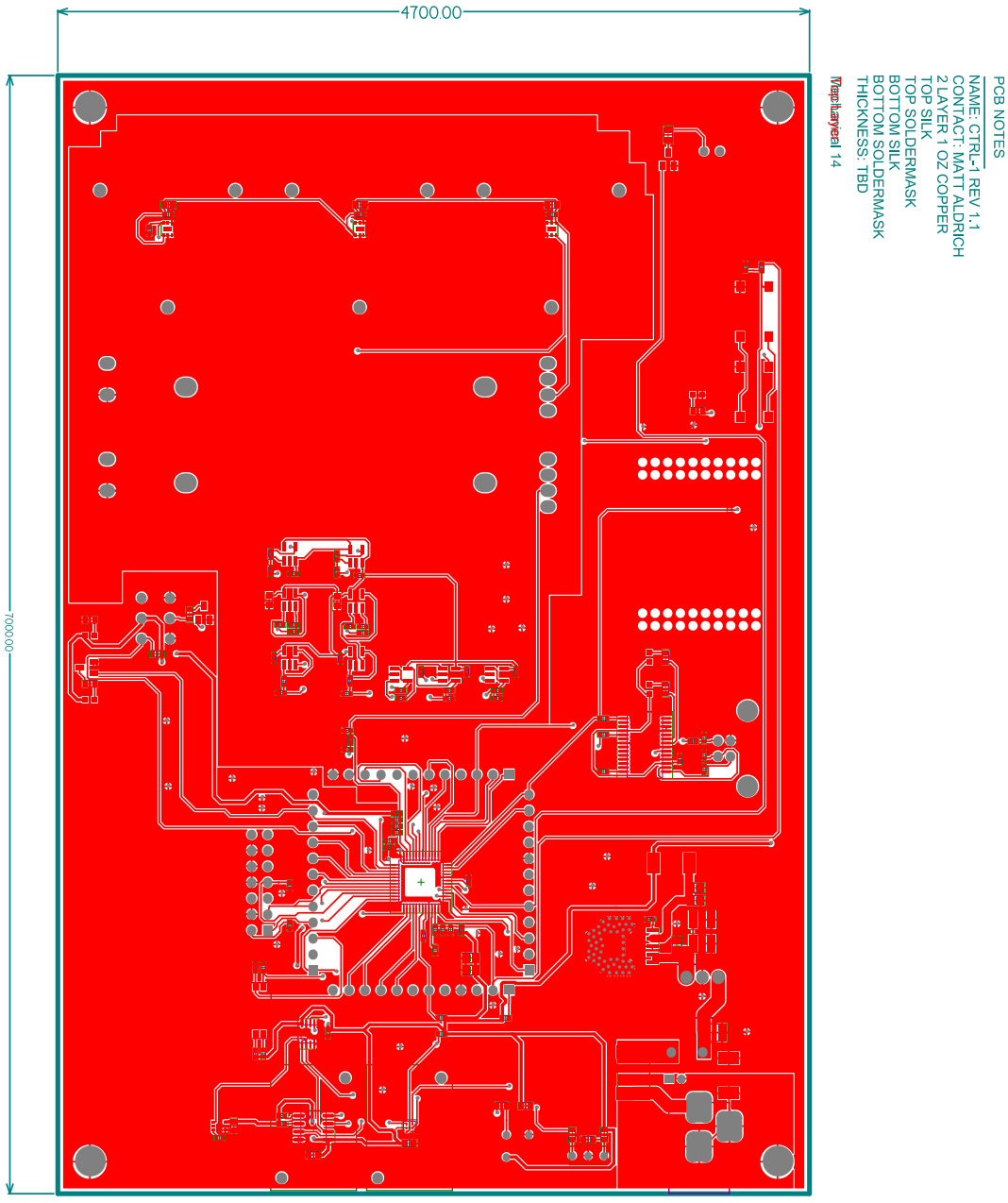
4700.00
7000.00
PCB NOTES
NAME: CTRL-1 REV 1.1
CONTACT: MATT ALDRICH
2 LAYER 1 OZ COPPER
TOP SILK
TOP SOLDERMASK
BOTTOM SILK
BOTTOM SOLDERMASK
THICKNESS: TBD
Top layer1 14

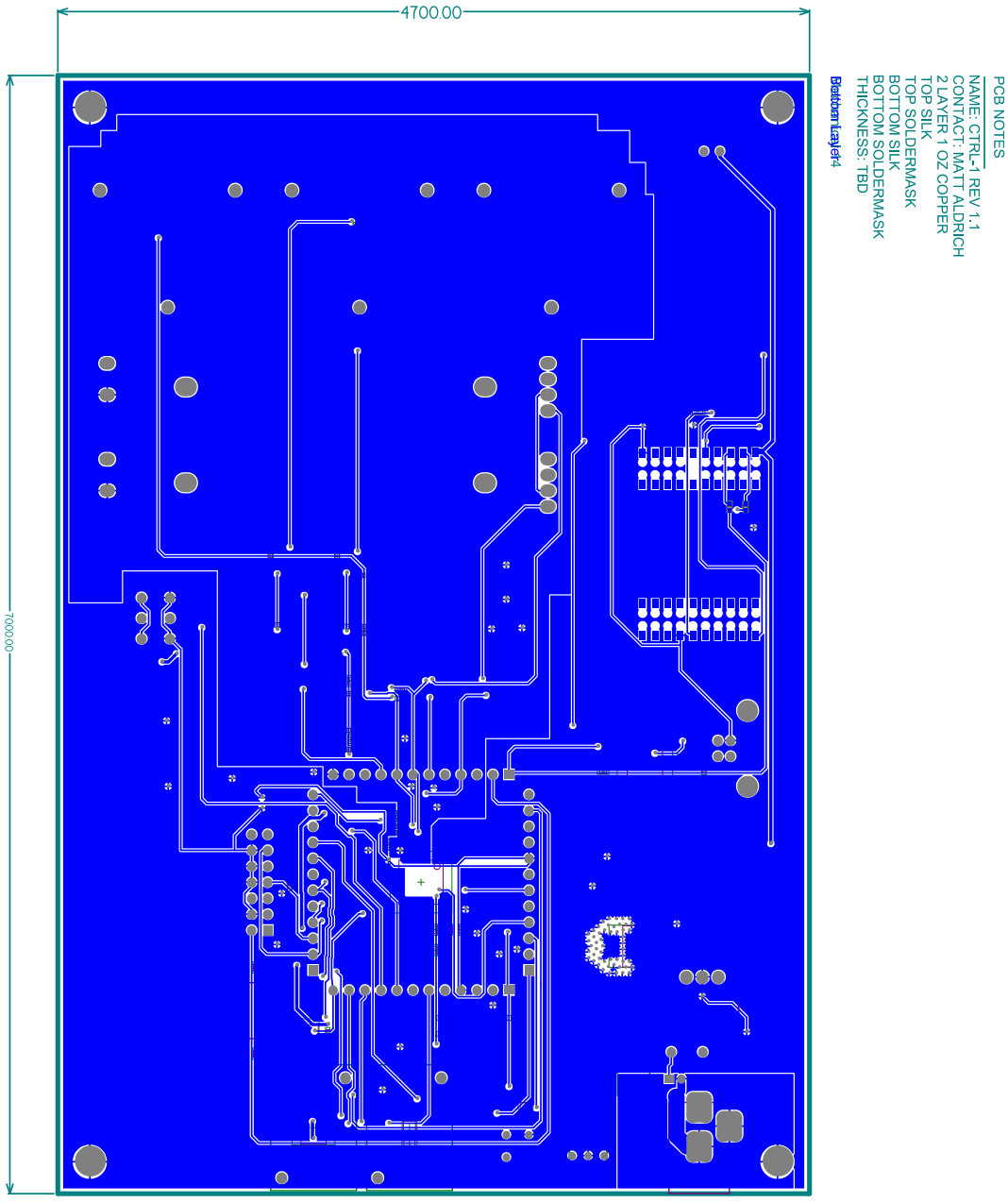
4700.00
7000.00
PCB NOTES
NAME: CTRL-1 REV 1.1
CONTACT: MATT ALDRICH
2 LAYER 1 OZ COPPER
TOP SILK
TOP SOLDERMASK
BOTTOM SILK
BOTTOM SOLDERMASK
THICKNESS: TBD

B.6 Sensor Node Bill of Materials

[follows on next page]

Bill of Materials

Source Data From: Room Sensor, Rev 1
Project: Room Sensor, Rev 1
Design M. Aldrich

Report Date: 1/12/2010 1:01:13 PM
Print Date: 29-Apr-10 6:40:39 PM

#	Designator	Description	Manufacturer 1	Manufacturer Part Number 1	Footprint	Supplier 1	Supplier Part Number 1	Quantity
1	CC1, CC2, CC3	OPAQUE COSINE CORRECTOR	N/A	N/A	N/A	N/A	N/A	3
2	CL1, CL2	F4.63 F2.8 LENS & HOLDER	N/A	N/A	N/A	N/A	N/A	2
3	N/A	Room Sensor, Controls PCB	Advanced Circuits	N/A	N/A	N/A	N/A	1
4	C1, C2	CAP CERAMIC 2.2UF 10V X5R 0805	Kemet	C0805C225K8PACTU	CAPC2012L	Digi-Key	399-3125-1-ND	2
5	C3, C6, C7, C9, C10, C11, C14	CAP CERM 1UF 6.3V X5R 0402	Kemet	C0402C105K9PACTU	CAPC1005L	Digi-Key	399-4873-1-ND	3
6	C4, C8, C37, C46	CAP CER 10000PF 25V 10% X7R 0402	Murata Electronics North America	GRM155R71E103KA01D	CAPC1005L	Digi-Key	490-1312-1-ND	4
7	C5	CAP CER 2.2PF 50V C0G 0402	Murata Electronics North America	GRM1555C1H2R2CZ01D	CAPC1005L	Digi-Key	490-1267-1-ND	1
8	C12	CAP CER 1000PF 50V C0G 0402	Murata Electronics North America	GRM1555C1H102JA01D	CAPC1005L	Digi-Key	490-3244-1-ND	1
9	C20, C30	CAP CER .47UF 6.3V X5R 0402	Murata Electronics North America	GRM155R60J474KE19D	CAPC1005L	Digi-Key	490-3266-1-ND	2
10	C21, C31	CAP CER .22UF 6.3V X5R 0402	Murata Electronics North America	GRM155R60J224KE01D	CAPC1005L	Digi-Key	490-5407-1-ND	2
11	C13, C15, C17, C19, C23, C24, C25, C27, C29, C33, C35, C50, C52	CAP CER .1UF 10V 10% X5R 0402	Murata Electronics North America	GRM155R61A104KA01D	CAPC1005L	Digi-Key	490-1318-1-ND	13
12	C16, C26, C48, C55, C56	CAP CER .1UF 50V 10% X7R 0603	Murata Electronics North America	GRM188R71H104KA93D	CAPC1608N	Digi-Key	490-1519-1-ND	5
13	C18, C28, C34, C49, C53	CAP CER 1.0UF 10V 10% X5R 0603	Murata Electronics North America	GRM188R61A105KA61D	CAPC1608N	Digi-Key	490-1543-1-ND	3
14	C38, C39	CAP CER 30PF 50V 5% C0G 0402	Murata Electronics North America	GRM1555C1H300JZ01D	CAPC1005L	Digi-Key	490-1285-1-ND	2
15	C40, C41, C42	CAP CER 22UF 25V X5R 1210	Taiyo Yuden	TMK325BJ226MM-T	CAPC3225N	Digi-Key	587-2086-1-ND	3
16	C43, C44, C45	CAP CER 2.2UF 6.3V 10% X7R 0805	Murata Electronics North America	GRM21BR70J225KA01L	CAPC2012L	Digi-Key	490-1698-1-ND	3
17	C47	CAP 47UF 35V ELECT NHG RADIAL	Panasonic - ECG	ECA-1VM470	CAPPR2-5x11	Digi-Key	P5164-ND	1
18	C22, C32, C36, C51, C54	CAP CER 3300PF 50V X7R 0402	Murata Electronics North America	GRM155R71H332KA01D	CAPC1005L	Digi-Key	490-3248-1-ND	5
19	D2, D10, D11	LED 570NM GREEN DIFF 0603 SMD	Avago Technologies US Inc.	HSMG-C190	1608	Digi-Key	516-1425-1-ND	3
20	D1, D4	LED 630NM HE RED DIFF 0603 SMD	Avago Technologies US Inc.	HSMS-C190	1608	Digi-Key	516-1422-1-ND	2
21	D3	EMITTER IR 5MM HI EFF 940NM	Vishay/Semiconductors	TSAL6200	HLMP-5029	Digi-Key	751-1204-ND	1
22	(D3)	HOUSING RA FOR 5MM HIGH DOME LED	Avago Technologies US Inc.	HLMP-5029	N/A	Digi-Key	516-1395-ND	1
23	F1	PTC RESET 33V 1.85A SMD 2920	Littelfuse Inc	2920L185DR	TH	Digi-Key	F2871CT-ND	1
24	J1	USB RCPT B-TYPE R/A FULL BACK	FCI	61729-1010BLF	TH	Digi-Key	609-3656-ND	1
25	J2	MALE BARREL CONNECTOR 2.1x5.5	Switchcraft Inc.	RAPC722X	RAPC722X	Mouser	502-RAPC722X	1
26	L1	FERRITE CHIP 60 OHM 1700MA 0402	Murata Electronics North America	BLM15PD600SN1D	1005	Digi-Key	490-5201-1-ND	1
27	L2, L4	FILTER CHIP 220 OHM 700MA 0402	Murata Electronics North America	BLM15EG221SN1D	1005	Digi-Key	490-4005-1-ND	2
28	L5	INDUCTOR MULTILAYER 330NH 0402	TDK Corporation	MLG1005SR33J	1005	Digi-Key	445-3077-1-ND	1
29	(L5)	INDUCTOR MULTILAYER 2.2UH 0402	TDK Corporation	MLF1005A2R2KT	1005	Digi-Key	445-3518-1-ND	1
30	(L5)	FERRITE CHIP 1000 OHM 200MA 0402	Murata Electronics North America	BLM15HG102SN1D	1005	Digi-Key	490-3999-1-ND	1
31	L7	FERRITE CHIP 40 OHM 550MA 0402	TDK Corporation	MMZ1005Y400C	1005	Digi-Key	445-2150-1-ND	1
32	P1	CONN HDR DUAL 14POS .100 SRT AU	Molex Connector Corporation	10-89-7142	TH	Digi-Key	WM26814-ND	1
33	P2, P3, P4, P5	CONN HEADER 12POS .100 VERT TIN	Molex Connector Corporation	22-28-4120	TH	Digi-Key	WM6412-ND	4
34	P6, P7	CONN RECEPT 20POS 2MM STR DL SMD	FCI	91596-120LF	SMT	Digi-Key	609-2730-ND	2
35	Q1, Q2, Q3	MOSFET N-CH 30V 1.7A SSOT3	Fairchild Semiconductor	NDS355AN	SOT-23	Digi-Key	NDS355ANCT-ND	3
36	R24, R28, R30 (0-500 lx)	RES 820K OHM 1/16W 1% 0402 SMD (0-500 lx)	Vishay/Dale	CRCW0402820KFKED	RESC1005L	Digi-Key	541-820KLCT-ND	3
37	(R24, R28, R30) (0-2,000 lx)	RES 402K OHM 1/16W 1% 0402 SMD (0-2,000 lx)	Vishay/Dale	CRCW0402402KFKED	RESC1005L	Digi-Key	541-402KLCT-ND	3
38	(R24, R28, R30) (0-10,000 lx)	RES 182K OHM 1/16W 1% 0402 SMD (0-10,000 lx)	Vishay/Dale	CRCW0402182KFKED	RESC1005L	Digi-Key	541-182KLCT-ND	3
39	(R24, R28, R30) (0-35,000 lx)	RES 100K OHM 1/16W 1% 0402 SMD (0-35,000 lx)	Rohm Semiconductor	MCR01MZPF1003	RESC1005L	Digi-Key	RHM100KLCT-ND	3
40	R13, R15	RES 20.0K OHM 1/16W 1% 0402 SMD	Rohm Semiconductor	MCR01MZPF2002	RESC1005L	Digi-Key	RHM20.0KLCT-ND	2
41	R11, R12	RES 820 OHM 1/16W 1% 0402 SMD	Vishay/Dale	CRCW0402820RFKED	RESC1005L	Digi-Key	541-820LCT-ND	2
42	R17, R20	RES 3.30K OHM 1/16W 1% 0402 SMD	Rohm Semiconductor	MCR01MZPF3301	RESC1005L	Digi-Key	RHM3.30KLCT-ND	2
43	R1, R7, R31, R32, R33, R34, R35	RES 0.0 OHM 1/16W 5% 0402 SMD	Rohm Semiconductor	MCR01MZPJ000	RESC1005L	Digi-Key	RHM0.0JCT-ND	7
44	R2, R3, R4, R5, R6, R21, R22, R25, R26	RES 10.0K OHM 1/16W 1% 0402 SMD	Rohm Semiconductor	MCR01MZPF1002	RESC1005L	Digi-Key	RHM10.0KLCT-ND	9
45	R23, R27, R29, R41, R44	RES 56.0 OHM 1/16W 1% 0402 SMD	Rohm Semiconductor	MCR01MZPF56R0	RESC1005L	Digi-Key	RHM56.0LCT-ND	5

46	R14	RES 2.70K OHM 1/16W 1% 0402 SMD	Rohm Semiconductor	MCR01MZPF2701	RESC1005L	Digi-Key	RHM2.70KLCT-ND	1		
47	R8, R9, R18, R19, R36, R39	RES 560 OHM 1/10W 1% 0603 SMD	Rohm Semiconductor	MCR03EZPF5600	RESC1608N	Digi-Key	RHM560HCT-ND	6		
48	R16, R42	RES 0.0 OHM 1/10W 5% 0603 SMD	Rohm Semiconductor	MCR03EZPJ000	RESC1608N	Digi-Key	RHM0.0GCT-ND	2		
49	R38	RES 100 OHM 1/10W 1% 0603 SMD	Rohm Semiconductor	MCR03EZPFX1000	RESC1608N	Digi-Key	RHM100HCT-ND	1		
50	R37	RES 10.0K OHM 1/10W 1% 0603 SMD	Rohm Semiconductor	MCR03EZPFX1002	RESC1608N	Digi-Key	RHM10.0KHCT-ND	1		
51	R10	RES 16.9 OHM 1/8W 1% 0805 SMD	Rohm Semiconductor	MCR10EZHF16R9	RESC2012L	Digi-Key	RHM16.9CCT-ND	1		
52	(R10)	RES 4.32 OHM 1/8W 1% 0805 SMD	Vishay/Dale	CRCW08054R32FKEA	RESC2012L	Digi-Key	541-4.32CCCT-ND	1		
53	R40, R43	Slide Potentiometers 10K OHM B TAPER	ALPS	RS6011YA6009	TH	Mouser	688-RS6011YA6009	2		
54	R47, R48	RES 0.0 OHM 1W 5% 2512 SMD	Vishay/Dale	CRCW25120000ZOEG	2512	Digi-Key	541-0.0XCT-ND	2		
55	R71	CURRENT LIMITER INRUSH 5.0HM 20%	Cantherm	MF72-005D7	TH	Digi-Key	317-1148-ND	1		
56	S1, S3	SWITCH TACT 6MM 160GF H=4.3MM	Omron Electronics	B3S-1000P	TH	Digi-Key	SW836GCT-ND	2		
57	S2	SWITCH DIP HALF PITCH 2POS	CTS Electrocomponents	218-2LPST	TH	Digi-Key	CT2182LPST-ND	1		
58	S4	TACTILE SWITCHES 260gf RED LED	Mountain Switch	101-TS551LT26002R-EV	TH	Mouser	101-TS551LT26002R-EV	1		
59	(S4)	KEY CAP ROUND BLACK	Mountain Switch	101-TS55KCR-BLK-EV	N/A	Mouser	101-TS55KCR-BLK-EV	1		
60	U1	IC MCU 32-BIT W/FLASH 48-LQFP	Texas Instruments	TM4320F28027PTA	48LQFP	Digi-Key	296-24123-ND	1		
61	U2	IC 2-LINE DATA SELECT/MUX SM8	Texas Instruments	SN74LVC2G157DCTR	TSOP8	Digi-Key	296-13266-1-ND	1		
62	U3, U4, U5, U7, U8, U9, U11, U19, U22	IC OPAMP SNGL R-R I/O LN SOT23-5	Analog Devices	AD8605ART-Z	SOT23-5	Digi-Key	AD8605ARTZREEL7CT-ND	9		
63	U6, U10, U12	IC PHOTO DETECTOR AMBIENT 6-ODFN	Intersil	ISL29009IROZ-T7	6DFN	Digi-Key	ISL29009IROZ-T7CT-ND	3		
64	U13	IC USB TO SERIAL UART 28-SSOP	FTDI	FT232RL-R	28SSOP	Digi-Key	768-1007-1-ND	1		
65	U14	Photodiodes TriColor Sensor LTF Low Power	TAOS	TCS3200D-TR	8SOIC	Mouser	856-TCS3200D-TR	1		
66	U15	Photodiodes TriColor Sensor RGB, Clear Ch	TAOS	TCS3414CS	6BGA	Mouser	856-TCS3414CS	1		
67	U16	IC PWM TEMP SNSR CMOS/TTL SC70-5	Analog Devices Inc	TMP05AKSZ-500RL7	SC-70	Digi-Key	TMP05AKSZ-500RL7CT-ND	1		
68	U17	SWITCHING REGULATOR, 5V, 1.0 A	Recom Power Incorporated	R-7885.0-1.0	TH	Allied	394-0052	1		
69	U18	IC IR RCVR MOD 38KHZ DOME AXIAL	Vishay/Semiconductors	TSOP38338	TH	Digi-Key	751-1388-ND	1		
70	U20	IC LDO REG 3.3V 1A SOT223-6	Texas Instruments	TPS79633DCQR	SOT223-6	Digi-Key	296-13766-1-ND	1		
71	U21	SENSOR MOTION DIG STD WHT PCB	Panasonic Electric Works	AMN11112	TH	Digi-Key	255-1812-ND	1		
								167		
Approved			Notes							
			Line Item (35) Eq. P/N: 3M, 953220-2000-AR-PR; 3M, 956220-2000-AR-PR; Sullins NPPN102GHNP-RC (DIGIKEY)							
			Line Item (66) Eq. P/N: TAOS, TCS3210D-TR (MOUSER)							
			Line Item (71) Alternate Supplier: Mouser, PN: 595-TPS79633DCQ							

B.7 LED Ring Schematic

[follows on next page]

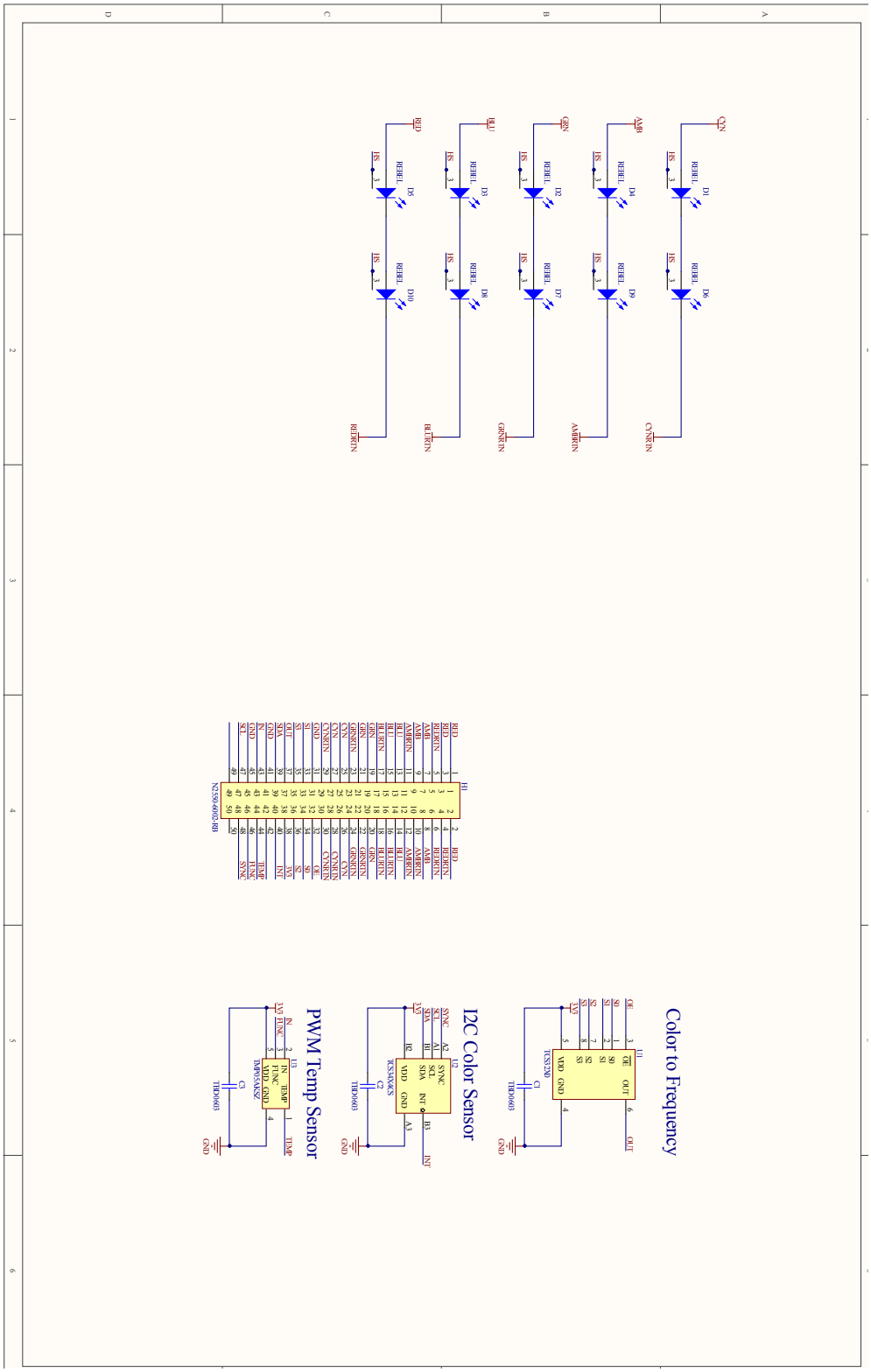
Color to Frequency
I2C Color Sensor
PWM Temp Sensor

B.8 LED Ring PCB

[follows on next page]

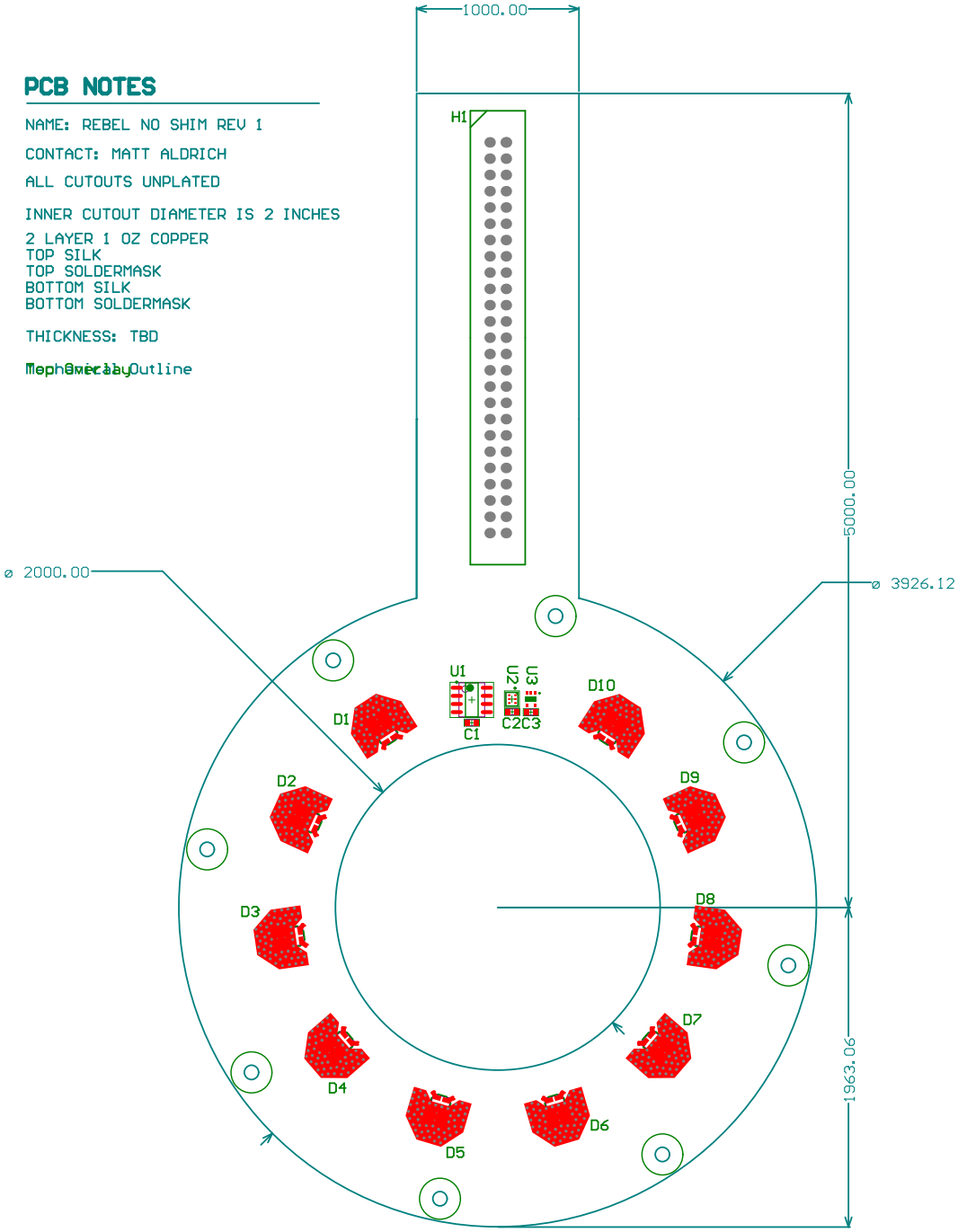
PCB NOTES
NAME: REBEL NO SHIM REV 1
CONTACT: MATT ALDRICH
ALL CUTOUTS UNPLATED
INNER CUTOUT DIAMETER IS 2 INCHES
2 LAYER 1 OZ COPPER
TOP SILK
TOP SOLDERMASK
BOTTOM SILK
BOTTOM SOLDERMASK
THICKNESS: TBD
Mechanical Outline
1000.00
5000.00
ø 2000.00
ø 3926.12
1963.06
H1
U1
U2
U3
C1
C2
C3
D1
D2
D3
D4
D5
D6
D7
D8
D9
D10

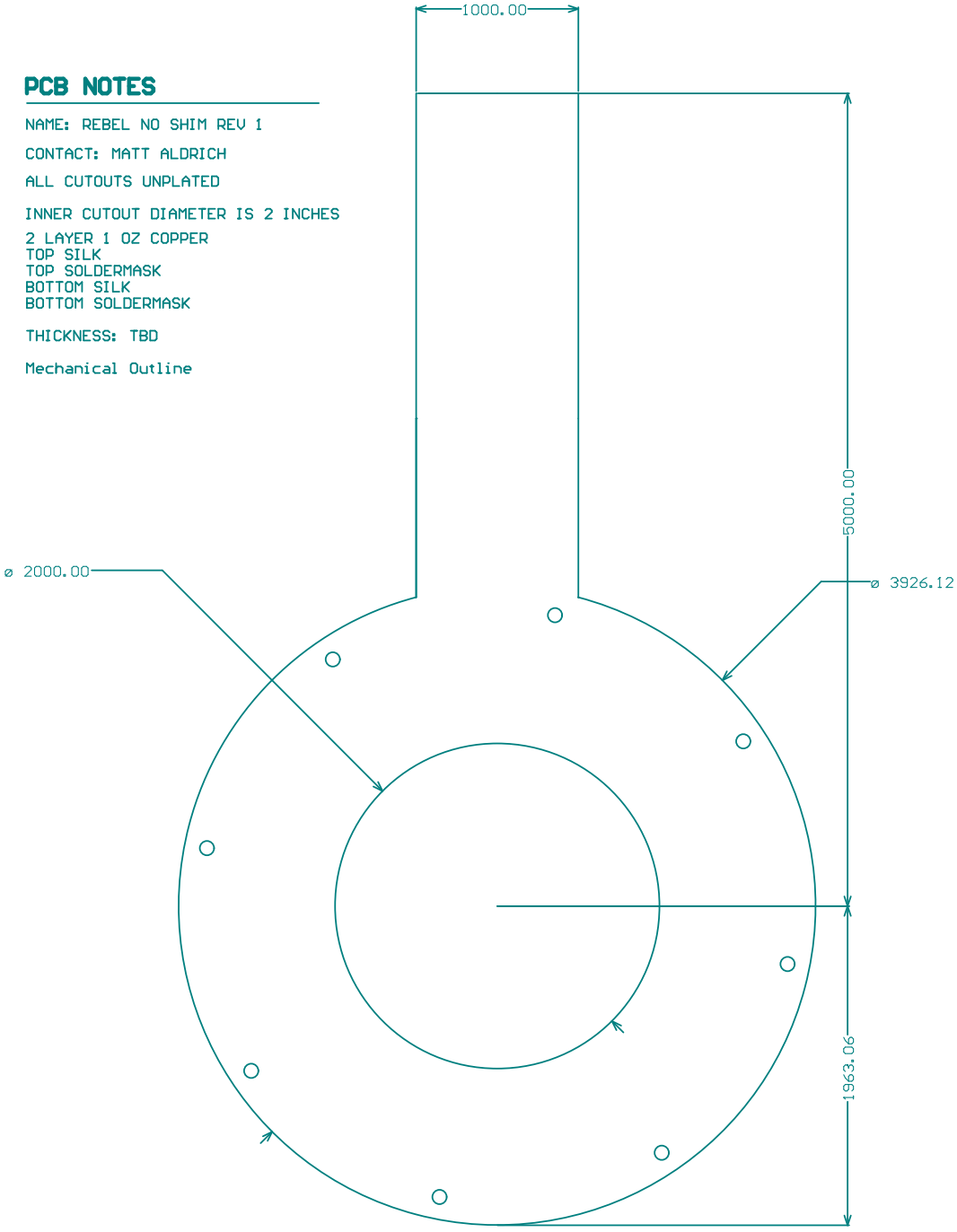
PCB NOTES
NAME: REBEL NO SHIM REV 1
CONTACT: MATT ALDRICH
ALL CUTOUTS UNPLATED
INNER CUTOUT DIAMETER IS 2 INCHES
2 LAYER 1 OZ COPPER
TOP SILK
TOP SOLDERMASK
BOTTOM SILK
BOTTOM SOLDERMASK
THICKNESS: TBD
Mechanical Outline
1000.00
5000.00
ø 2000.00
ø 3926.12
1963.06

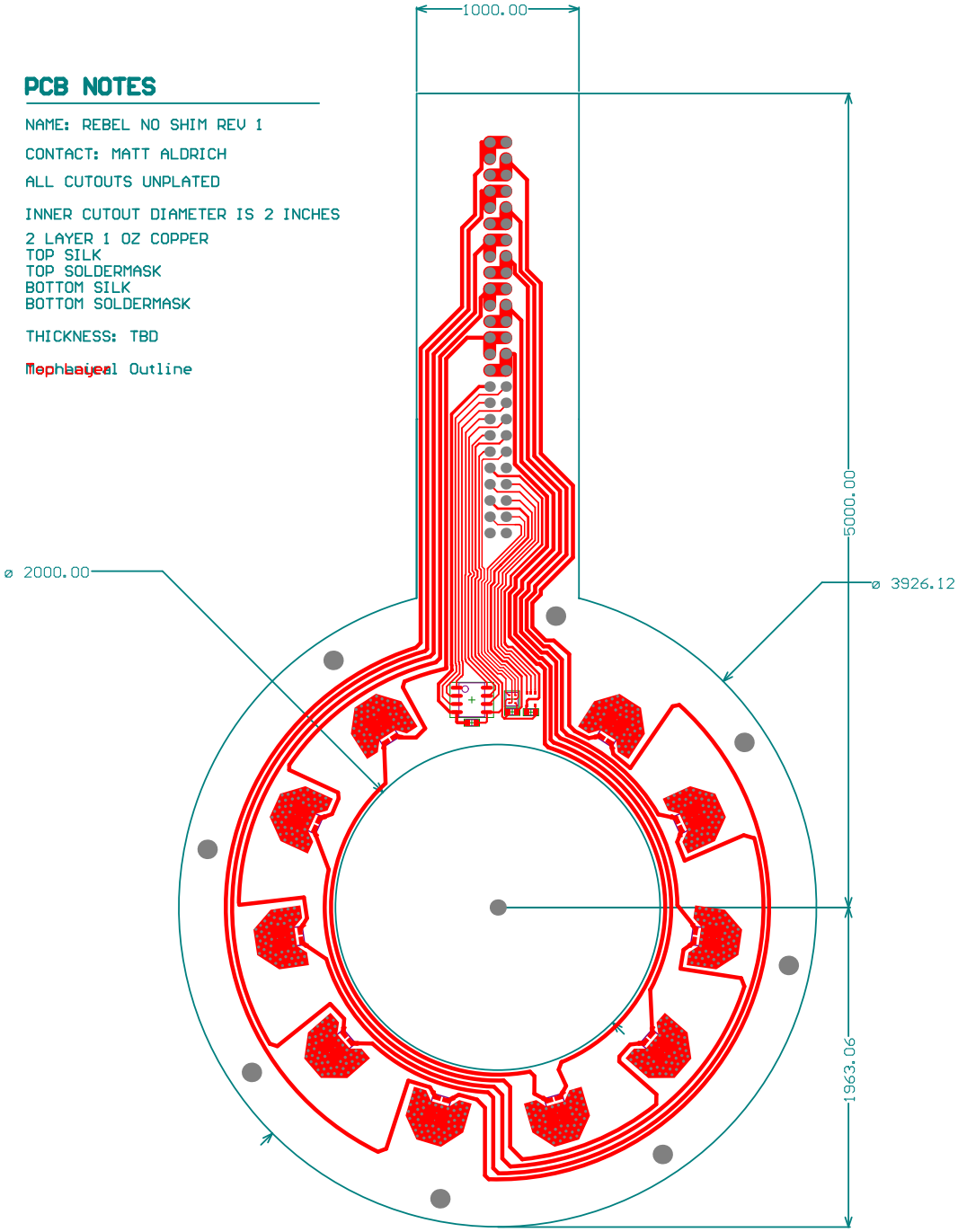
1000.00
PCB NOTES
NAME: REBEL NO SHIM REV 1
CONTACT: MATT ALDRICH
ALL CUTOUTS UNPLATED
INNER CUTOUT DIAMETER IS 2 INCHES
2 LAYER 1 OZ COPPER
TOP SILK
TOP SOLDERMASK
BOTTOM SILK
BOTTOM SOLDERMASK
THICKNESS: TBD
Mephlayeal Outline
5000.00
ø 2000.00
ø 3926.12
1963.06

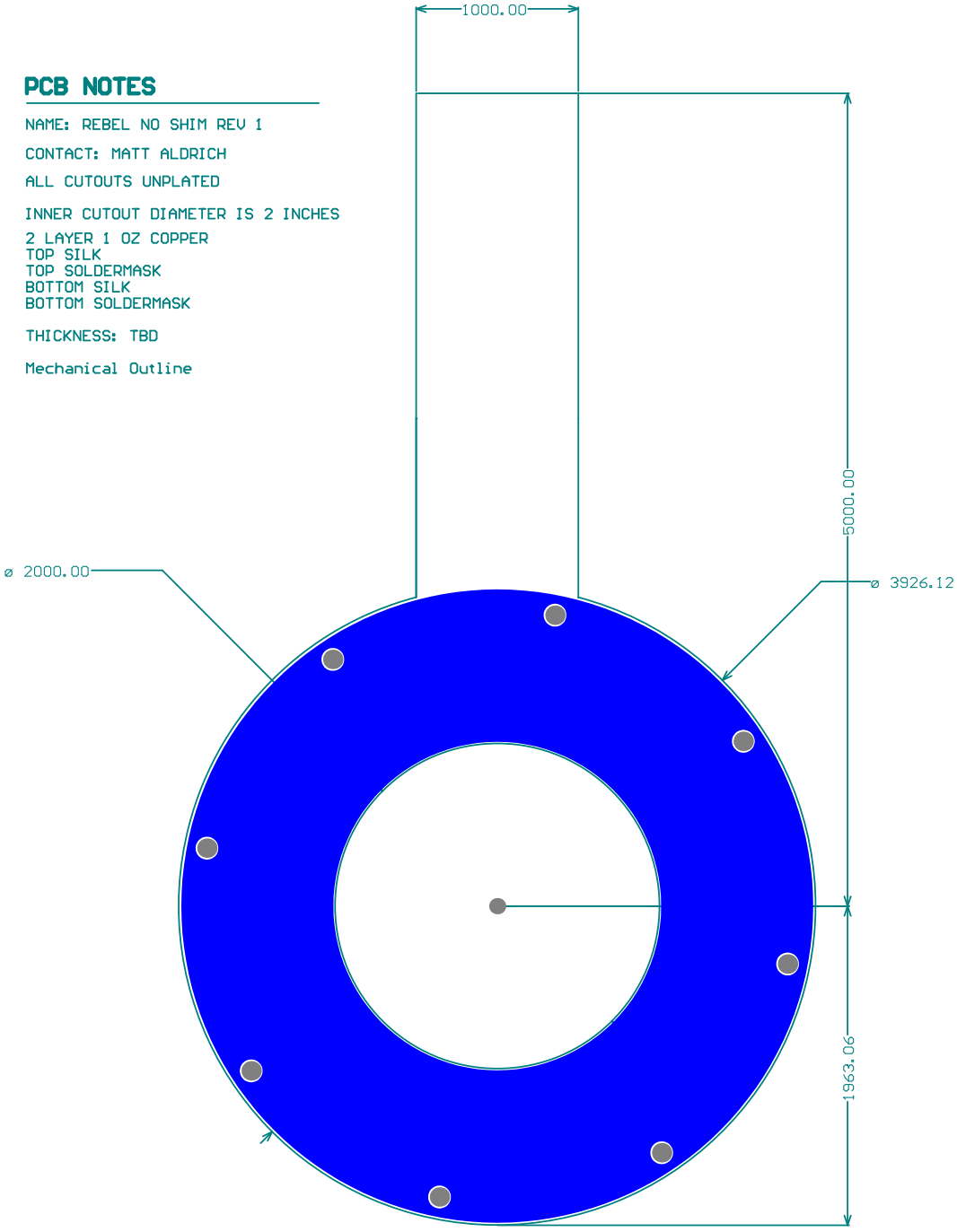
PCB NOTES
NAME: REBEL NO SHIM REV 1
CONTACT: MATT ALDRICH
ALL CUTOUTS UNPLATED
INNER CUTOUT DIAMETER IS 2 INCHES
2 LAYER 1 OZ COPPER
TOP SILK
TOP SOLDERMASK
BOTTOM SILK
BOTTOM SOLDERMASK
THICKNESS: TBD
Mechanical Outline
1000.00
5000.00
ø 2000.00
ø 3926.12
1963.06

Appendix C

Firmware

Due to length, all source code and binaries for the LED controller and sensor node can be found at:

`http://media.mit.edu/~maldrich/lighting/`

Appendix D

Radiometric Traceability

Attached are the traceability documents from Ocean Optics outlining NIST calibration standards and uncertainty that is carried over in the radiometric calibration source used in these experiments.

OceanOptics.com

Traceability of the Ocean Optics Inc. Calibration Laboratory

We are not an ISO certified organization but have established a calibration program for the calibration laboratory that is intended to meet the ISO9000 series requirements. We have the following manuals on file that have been reviewed and approved by our Director of Total Technical Services. We are constantly pursuing every effort to improve, update, and optimize our calibration program.

We currently have a variety of traceability documents and quality manuals. The following have been developed in-house for our program.

1. **Quality Services Quality Survey** - This is our procedure for certifying and auditing our calibration service provider vendors.
2. **Calibration and Control of Measuring and Test Equipment** – defines the establishment and maintenance of our calibration program for the calibration laboratory which includes calibration procedures, calibration software validation, calibration traceability, environment, labels and tags, etc.
3. **Customer Equipment Calibration Program** – defines the establishment of a program for the calibration of all customer owned equipment or equipment being placed in stock for future sales.

Attached are the certifications for our primary standards. We use a Deuterium and Quartz-Tungsten-Halogen (QTH) lamps as primary standards. The Deuterium lamp is calibrated by the National Physical Laboratory in the United Kingdom. Attached is a copy of the calibration certificate as well as their ISO certification. The QTH lamp is calibrated by Eppley Labs. Attached is a copy of the calibration certificate as well as information concerning the traceability of their standards to National Institute of Standards and Technology (NIST).

We also utilize some general purpose test equipment that is calibrated locally by two calibration laboratories. They are: Technical Maintenance Inc. (ISO 17025 certified) and Certified Calibrations Inc. (we do a Quality Survey and physical audit of them).

We currently use a calibration software program, GageInSite®, which allows us to store, track, and provide calibration information for both our company and our customer's equipment.

Any further assistance concerning our calibration program or traceability, please contact our metrologist, Jim Niswender. His email address is: jim.niswender@oceanoptics.com or his direct phone number is: (727) 450-7352.

Dr. Jorge J. Macho
Director
Total Technical Services

830 Douglas Avenue • Dunedin, FL 34698 • 727.733.2447 • Fax 727.733.3962 • Info@OceanOptics.com

CALIBRATION CERTIFICATES

FOR THE PRIMARY

STANDARD LAMPS

CERTIFICATE
OF
CALIBRATION

Operator :	ljl
Date calibrated :	29th September 2004
Lamp type :	Cathodeon R48 Deuterium
Lamp serial no. :	CH6902
Serial # of standard used for calibration:	$65787_{NPL2003}$ 0088
Calibration Record:	29sep04
Order Ack:	7392

Calibrations Carried Out

Spectral Irradiance at a distance of 200mm in units of $mW.m^{-2}.nm^{-1}$ over a wavelength range of 200nm to 400nm at intervals of 5nm.

Measurements

The lamp was mounted vertically and positioned so that a horizontal line through the centre of the area to be irradiated, passed through the centre of the lamp emitting area and was also perpendicular to the lamp window.

The calibration refers to the spectral irradiance over an area, approximately $10mm^2$ of a surface in a vertical plane located at a distance of 200mm from the outside surface of the output window.

The lamp was operated at 300mA from a power supply, in which the lamp starting sequence was controlled automatically.

The relative spectral irradiance of the lamp, operated as described above, was measured by comparison with a Bentham CL3 which had been calibrated by NPL over the wavelength range 200nm to 400nm, at intervals of 5nm. The absolute values of spectral irradiance were established by comparing the output of the lamp at 350nm with that of a Bentham CL2 which had been calibrated by NPL over the range 300nm to 800nm.

The lamp was run for 30 minutes before measurements commenced.

Results

The values for the spectral irradiance in $mW.m^{-2}.nm^{-1}$ at 5nm intervals over the wavelength range 200nm to 400nm are stored on disk.

Uncertainties

The total systematic uncertainty of this calibration is estimated to be not greater than 2.5% relative to the NPL spectral irradiance scale.

Spectral Irradiance ($mW.m^{-2}.nm^{-1}$) of R48 deuterium lamp (# CH6902) at 200mm from the output window operated at 300mA.

200	7.337445
205	6.749286
210	6.234938
215	5.745168
220	5.285789
225	4.819447
230	4.338613
235	3.918048
240	3.542822
245	3.211198
250	2.888547
255	2.632085
260	2.379516
265	2.187343
270	1.999666
275	1.840223
280	1.68755
285	1.56238
290	1.441013
295	1.33564
300	1.229433
305	1.143031
310	1.059486
315	0.984201
320	0.911093
325	0.851411
330	0.794357
335	0.740376
340	0.688099
345	0.650118
350	0.612197
355	0.57834
360	0.547485
365	0.520439
370	0.495402
375	0.487855
380	0.472011
385	0.443718
390	0.419512
395	0.412981
400	0.402733

United Kingdom Accreditation Service

ACCREDITATION CERTIFICATE

UKAS
UNITED KINGDOM ACCREDITATION SERVICE

CALIBRATION LABORATORY
No. 0478

National Physical Laboratory
Hampton Road
Teddington
Middlesex
TW11 0LW

is accredited to BS/EN/ISO/IEC 17025:1999 *General Requirements for the competence of testing and calibration laboratories* to undertake calibrations as detailed in the schedule bearing the above accreditation number.

From time to time the schedule to this certificate may be revised and reissued by the United Kingdom Accreditation Service.

This Accreditation shall remain in force until the expiry date printed below, subject to continuing conformity with United Kingdom Accreditation Service requirements.

Initial Accreditation 27 November 1996

Accreditation Manager, United Kingdom Accreditation Service

This certificate issued on 01 August 2006 **Expiry date 31 May 2007**

The Department of Trade and Industry (DTI) has entered into a memorandum of understanding with the United Kingdom Accreditation Service (UKAS) through which UKAS is recognised as the national body responsible for assessing and accrediting the competence of organisations in the fields of calibration, testing, inspection and certification of systems, products and persons.

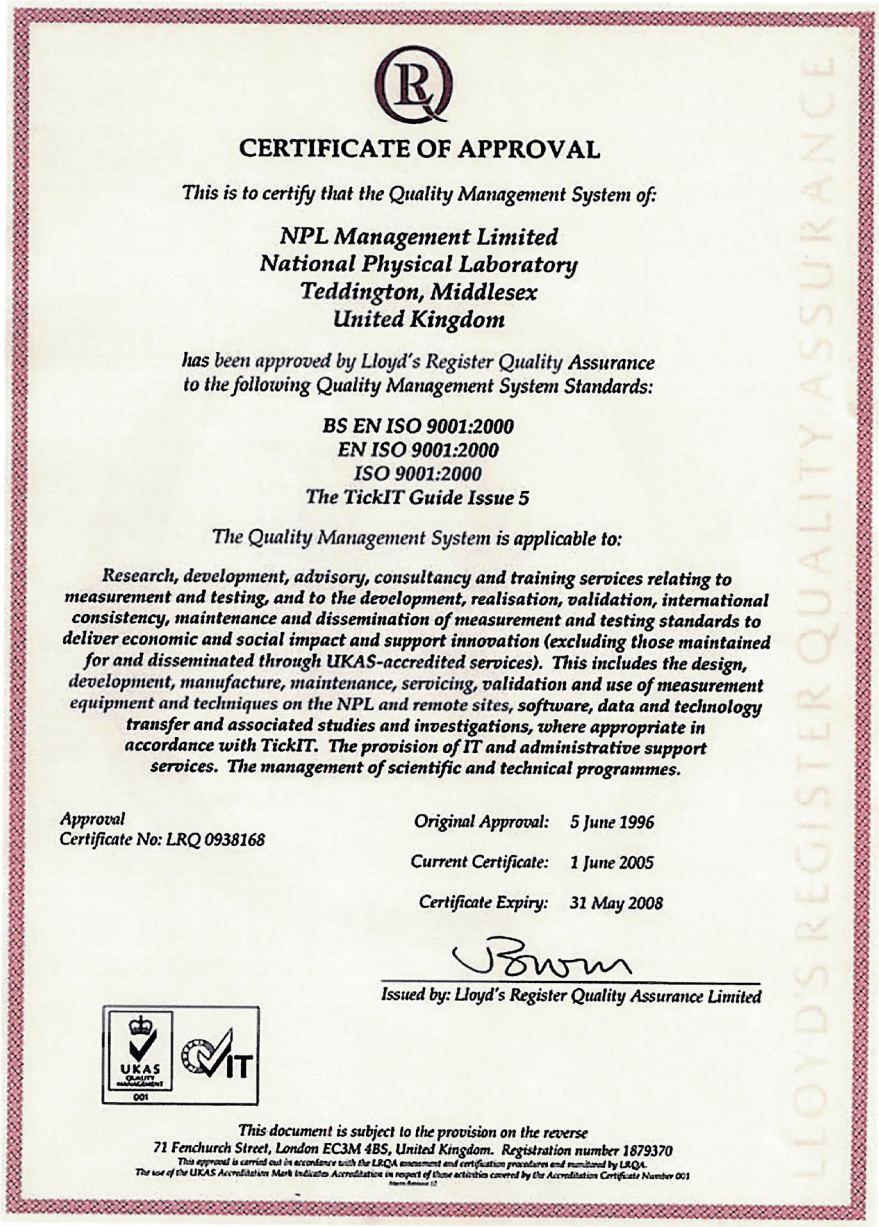

CERTIFICATE OF APPROVAL

This is to certify that the Quality Management System of:

NPL Management Limited
National Physical Laboratory
Teddington, Middlesex
United Kingdom

has been approved by Lloyd's Register Quality Assurance to the following Quality Management System Standards:

BS EN ISO 9001:2000
EN ISO 9001:2000
ISO 9001:2000
The TickIT Guide Issue 5

The Quality Management System is applicable to:

Research, development, advisory, consultancy and training services relating to measurement and testing, and to the development, realisation, validation, international consistency, maintenance and dissemination of measurement and testing standards to deliver economic and social impact and support innovation (excluding those maintained for and disseminated through UKAS-accredited services). This includes the design, development, manufacture, maintenance, servicing, validation and use of measurement equipment and techniques on the NPL and remote sites, software, data and technology transfer and associated studies and investigations, where appropriate in accordance with TickIT. The provision of IT and administrative support services. The management of scientific and technical programmes.

Approval
Certificate No: LRQ 0938168

Original Approval: 5 June 1996

Current Certificate: 1 June 2005

Certificate Expiry: 31 May 2008

Issued by: Lloyd's Register Quality Assurance Limited

UKAS QUALITY MANAGEMENT 001

IT

This document is subject to the provision on the reverse
71 Fenchurch Street, London EC3M 4BS, United Kingdom. Registration number 1879370
This approval is carried out in accordance with the LRQA assessment and certification procedures and monitored by LRQA.
The use of the UKAS Accreditation Mark indicates Accreditation in respect of those activities covered by the Accreditation Certificate Number 001

LLOYD'S REGISTER QUALITY ASSURANCE

THE EPPLEY LABORATORY, INC.
12 Sheffield Ave., P.O. Box 419, Newport, RI 02840 USA
Telephone: 401-847-1020 Fax: 401-847-1031
Email: info@eppleylab.com Internet: www.eppleylab.com

EPLAB
Scientific Instruments
for Precision Measurements
Since 1917

CERTIFICATE OF CALIBRATION
OF A STANDARD OF SPECTRAL IRRADIANCE

FOR: Ocean Optics, Inc.
830 Douglas Ave.
Dunedin, FL

S.O. 60442 Lamp Serial No. EH-165
Lamp Type: Q100/T4/CL

1. Spectral Range of Calibration: 250 nm to 2400 nm

2. Method of Calibration:

See "Instructions for Using the NIST 1000 Watt Quartz Halogen Lamp Standards of Spectral Irradiance". A copy accompanies this Certificate.

3. Standards of Reference:

The Eppley Laboratory Working Standard was: EN-113
It is traceable to NIST Standard: F-211

4. Results:

The Spectral Irradiance Values in Watts per cm^3 are given in the Appended Table for the wavelengths designated for traceability to the NIST Scale. Wavelengths are given in nanometers.

TESTED BY: R. T. Eppley

CHECKED BY: Thomas J. Kirk

DATE: 13-Oct-05

TABLE OF RESULTS

Spectral Irradiance in watts per cm^3 at a distance of 50 cm
Lamp no. EH-165 operated at 6.30 Amperes D.C.

Wavelength (nm)	Spectral Irradiance
250	0.017
260	0.029
270	0.048
280	0.077
290	0.116
300	0.170
310	0.241
320	0.332
330	0.443
340	0.583
350	0.761
400	2.103
450	4.322
500	7.149
555	10.570
600	13.520
654.6	16.820
700	18.990
800	22.220
900	23.500
1050	22.870
1150	21.240
1200	20.260
1300	18.240
1540	13.460
1600	12.330
1700	10.670
2000	7.120
2100	6.320
2300	4.950
2400	4.340

THE EPPLEY LABORATORY, INC.
12 Sheffield Ave., P.O. Box 419, Newport, RI 02840 USA
Telephone: 401-847-1020 Fax: 401-847-1031
Email: info@eppleylab.com Internet: www.eppleylab.com

EPLAB
Scientific Instruments
for Precision Measurements
Since 1917

November 21, 2005

Ocean Optics Inc.
Attention: Jim Niswender
Fax: 727-733-3962

Jim,

Here is a Traceabilty Statement and the Calibration Reposts for Eppley's NIST Standard Lamp F-211 and Working Standard EN-113.

We trust this will satisfy your QA Requirements.

Sincerely,

Thomas D. Kirk,
President

THE EPPLEY LABORATORY, INC.
12 Sheffield Ave., P.O. Box 419, Newport, RI 02840 USA
Telephone: 401-847-1020 Fax: 401-847-1031
Email: info@eppleylab.com Internet: www.eppleylab.com

EPLAB
Scientific Instruments
for Precision Measurements
Since 1917

EPPLEY STANDARD LAMP
TRACEABILITY STATEMENT

Standard Lamps calibration cycles are typically based on hours of usage as opposed to annual cycles. Eppley uses a lamp life of 50 hours which is below typical and accepted usage values. All NIST Reference Standards and EPLAB Working Standards are replaced after 50 hours of usage.

Lineage of Traceability:

NIST Reference Standard, Serial Number F-211
Test No. 534/237124-86 dated March 6, 1987
Hours of Use to Date: 18.5 hours
Hours of Use left until replacement: 31.5 hours

EPLAB Working Standard, Serial Number EN-113
Calibrated on September 17, 2002
Hours of Use to Date: 23 hours
Hours of Use left until replacement: 27 hours

EPLAB and NIST Uncertainties with respect to SI Units are:

Wavelength (nm)	250	350	654.6	900	1300	1600	2000	2400
Uncertainty	2.23	1.35	1.01	1.34	1.42	1.89	3.29	6.51

November 2005

THE EPPLEY LABORATORY, INC.
12 Sheffield Ave., P.O. Box 419, Newport, RI 02840 USA
Telephone: 401-847-1020 Fax: 401-847-1031

EPLAB
Scientific Instruments for Precision Measurements Since 1917

CERTIFICATE OF CALIBRATION
OF A STANDARD OF SPECTRAL IRRADIANCE

FOR: Lab Standard

S.O. Lamp Serial No. EN-113
Lamp Type: FEL

1. Spectral Range of Calibration: 250 nm to 2400 nm

2. Method of Calibration:

See "Instructions for Using the NIST 1000 Watt Quartz Halogen Lamp Standards of Spectral Irradiance". A copy accompanies this Certificate.

3. Standards of Reference:

The Eppley Laboratory Working Standard was:
It is traceable to NIST Standard: F-211

4. Results:

The Spectral Irradiance Values in Watts per cm^3 are given in the Appended Table for the wavelengths designated for traceability to the NIST Scale. Wavelengths are given in nanometers.

TESTED BY: R. T. Essman

CHECKED BY: Thomas D Kirk

DATE: 17-Sep-2002

TABLE OF RESULTS

Spectral Irradiance in watts per cm^3 at a distance of 50 cm
Lamp no. EN-113 operated at 7.90 amps DC.

Wavelength (nm)	Spectral Irradiance
250	0.156
260	0.276
270	0.464
280	0.733
290	1.111
300	1.628
310	2.308
320	3.165
330	4.239
340	5.562
350	7.183
400	19.820
450	40.520
500	67.590
555	101.200
600	128.700
654.6	158.500
700	178.900
800	208.300
900	221.200
1050	211.800
1150	197.100
1200	188.400
1300	170.300
1540	126.100
1600	116.500
1700	101.800
2000	68.700
2100	61.000
2300	47.300
2400	42.000

FORM NBS-443
(REV. 12-68)

U.S. DEPARTMENT OF COMMERCE
NATIONAL BUREAU OF STANDARDS
Gaithersburg, MD 20899

REPORT OF CALIBRATION

of
One Standard of Spectral Irradiance
(250 nm to 2400 nm)
Supplied to:

Eppley Laboratory, Inc.
12 Sheffield Avenue
Newport, RI 02840

(See your Purchase Order Number 5630 dated April 14, 1986)

1. Material

One 1000-watt, quartz-halogen, modified type FEL, tungsten coiled-coil filament lamp has been supplied by the National Bureau of Standards as a standard of spectral irradiance and bears the designation F-211.

2. Calibration

The lamp was calibrated using the equipment and procedures described in NBS Special Publication 250-20, "Spectral Irradiance Calibrations at NBS", Walker, J.H., Saunders, R.D., Jackson, J.K., and McSparron, D.A., (1987), a copy of which is enclosed. The preparation and operation of the modified type FEL lamp supplied for this calibration are described in the enclosure, "Type FEL Lamp Standards of Spectral Irradiance - 1986". Note particularly paragraph IV of this enclosure which describes the orientation of the test lamp.

3. Results

The results of this test are given in the attached Table 1. The uncertainties of the reported values, at the 3σ level, are summarized in Table 2. Details on the estimation of these uncertainties are given in SP 250-20.

Prepared by:
John K. Jackson
Radiometric Physics Division
Center for Radiation Research

Approved by:
Donald A. McSparron
Radiometric Physics Division
Center for Radiation Research

NBS Test No.: 534/237124-86
Date: March 6, 1987

REPORT OF CALIBRATION
Eppley Laboratory, Inc.
Newport, RI 02840

TABLE 1

Spectral irradiance (W/cm^3) at 50.0 cm from lamp F-211 when operated on dc with the polarity as indicated on the identification plate attached to the lamp base.

Wavelength (nm)	Lamp No. F-211 7.900 A
250	0.167
260	0.295
270	0.491
280	0.771
290	1.162
300	1.696
310	2.393
320	3.274
330	4.370
340	5.717
350	7.339
400	20.01
450	40.48
500	67.07
555	99.74
600	126.2
654.6	155.0
700	174.9
800	204.0
900	213.9
1050	204.2
1150	189.8
1200	181.1
1300	163.7
1540	120.9
1600	112.2
1700	97.4
2000	65.7
2100	58.3
2300	44.8
2400	40.0

NBS Test No.: 534/237124-86
Date: March 6, 1987

THE EPPLEY LABORATORY, INC.
12 Sheffield Ave., P.O. Box 419, Newport, RI 02840 USA
Telephone: 401-847-1020 Fax: 401-847-1031
Email: info@eppleylab.com Internet: www.eppleylab.com

EPLAB
Scientific Instruments
for Precision Measurements
Since 1917

November 7, 2005

Ocean Optics
Att: Jim Niswender
Fax No. 727-733-3962

Dear Jim:

NIST reference standards maintained by The Eppley Laboratory are used sparingly to generate working standards which are then utilized to calibrate customer's standard lamps. This procedure minimizes the actual number of hours a NIST standard would be used thus preserving accurate traceability.

Richard T. Eggeman

REPORT OF CALIBRATION
Eppley Laboratory, Inc.
Newport, RI 02840

TABLE 2
1986 SPECTRAL IRRADIANCE SCALE TRANSFER UNCERTAINTY (3σ)
IN PERCENT

	250 nm	350 nm	654.6 nm	900 nm	1300 nm	1600 nm	2000 nm	2400 nm
I. NBS SPECTRAL RADIANCE SCALE								
a. Absolute error (with respect to SI units)	1.41	1.01	0.55	0.49	0.41	0.44	0.70	1.16
b. NBS long term reproducibility	0.58	0.42	0.25	0.34	0.33	0.39	0.69	1.15
II. RADIANCE TO IRRADIANCE TRANSFER								
a. Systematic errors	0.36	0.31	0.27	0.26	0.26	0.25	0.25	0.25
b. Random errors (3σ precision)	0.43	0.11	0.08	0.84	0.86	1.46	2.60	5.73
c. Model error	1.38	0.80	0.78	0.77	0.77	0.82	1.00	1.20
III. TEST LAMP IRRADIANCE TRANSFER								
a. Systematic errors	0.01	0.01	0.01	0.01	0.01	0.01	0.01	0.01
b. Random errors (3σ precision)	0.88	0.22	0.16	0.42	0.68	0.72	1.59	2.60
IV. UNCERTAINTY OF REPORTED VALUES (Quadrature Sum)								
a. With respect to SI units	2.23	1.35	1.01	1.34	1.42	1.89	3.29	6.51
b. NBS long term reproducibility	1.83	0.99	0.88	1.29	1.40	1.88	3.29	6.51

NBS Test No.: 534/237124-86
Date: March 6, 1987

Measurement of two NIST standards falling within the uncertainties listed above demonstrates the transfer capability of the Eppley Laboratory to NIST issued standards.

Bibliography

[1] Abramson, M. A., 2003. Pattern search algorithms for mixed variable general constrained optimization problems. Ph.D. thesis, Rice University.

[2] Abramson, M. A., Audet, C., Dennis, J. E., Le Digabel, S., 2009. Orthomads: A deterministic MADS instance with orthogonal directions. SIAM J.Optim. 20 (2), 948–966.

[3] Ackermann, B., Schulz, V., Martiny, C., Hilgers, A., Zhu, X., 2006. Control of LEDs. In: Industry Applications Conference, 2006. 41st IAS Annual Meeting. Conference Record of the 2006 IEEE. Vol. 5. pp. 2608–2615.

[4] Akashi, Y., Leslie, R., Novello, M., Nakamura, Y., 2001. Comparing lighting energy conservation measures in the United States and Japan 285, 127.

[5] Aldrich, M., Garbus, M., 2008. Calibration method and apparatus for lighting fixtures using multiple spectrum light sources and light mixing. U.S. Patent Application, 20080103714.

[6] Ashdown, I. E., 2004. Neural networks for LED color control. Vol. 5187. SPIE, pp. 215–226.

[7] Audet, C., Béchard, V., Chaouki, J., Jun. 2008. Spent potliner treatment process optimization using a MADS algorithm. Optimization and Engineering 9 (2), 143–160.

[8] Audet, C., Béchard, V., Digabel, S., 2008. Nonsmooth optimization through mesh adaptive direct search and variable neighborhood search. J.Global Optimiz. 41 (2), 299–318.

[9] Audet, C., Custódio, A. L., Dennis, Jr, J., 2007. Erratum: Mesh adaptive direct search algorithms for constrained optimization. SIAM J.on Optimization 18 (4), 1501–1503.

[10] Audet, C., Dennis, Jr, J., 2006. Mesh adaptive direct search algorithms for constrained optimization. SIAM J.on Optimization 17 (1), 188–217.

[11] Azevedo, I. L., Morgan, M. G., Morgan, F., 2009. The transition to solid-state lighting. Proceedings of the IEEE 97 (3), 481–510.

[12] Bergh, A., Craford, G., Duggal, A., Haitz, R., 2001. The promise and challenge of solid-state lighting. Phys Today 54 (12), 42–47.

[13] Bolt, R. A., 1980. "Put that there": Voice and gesture at the graphics interface. In: SIGGRAPH '80: Proceedings of the 7th annual conference on Computer graphics and interactive techniques. Vol. Seattle, Washington, United States. ACM, New York, NY, USA, pp. 262–270.

[14] Boynton, R. M., 1996. History and current status of a physiologically based system of photometry and colorimetry. J.Opt.Soc.Am.A 13 (8), 1609–1621.

[15] Burmen, M., Pernus, F., Likar, B., 2008. LED light sources: a survey of quality-affecting factors and methods for their assessment. Measurement Science and Technology (12), 122002–.

[16] Crisp, V. H. C., 1977. Preliminary study of automatic daylight control of artificial lighting. Lighting Research and Technology 9 (1), 31–41.

[17] Crisp, V. H. C., 1978. The light switch in buildings. Lighting Research and Technology 10 (2), 69–82.

[18] Crisp, V. H. C., Henderson, G., 1982. The energy management of artificial lighting use. Lighting Research and Technology 14 (4), 193–206.

[19] Dantzig, G., 1974. Linear programming and extensions. Princeton University Press.

[20] Davis, W., Ohno, Y., 2005. Toward an improved color rendering metric. Vol. 5941. SPIE, pp. 59411G–.

[21] Esch, J., 2009. Prolog to the transition to solid-state lighting. Proceedings of the IEEE 97; 97 (3), 478–480.

[22] Feldmeier, M., 2009. Personalized building comfort control. Ph.D. thesis, Massachusetts Institute of Technology.

[23] Garcia, J., Dalla-Costa, M. A., Cardesin, J., Alonso, J. M., Rico-Secades, M., 2009. Dimming of high-brightness LEDs by means of luminous flux thermal estimation. Power Electronics, IEEE Transactions on 24; 24 (4), 1107–1114.

[24] Graves, H., 2006. Developing the domestic luminaire market for LED technology - how can policy help drive synchronous development? In: EEDAL 06 - Energy Efficiency in Domestic Appliances and Lighting, 4th Int'l Conference on.

[25] Guo, X., Houser, K., 2004. A review of colour rendering indices and their application to commercial light sources. Lighting Research and Technology 36 (3), 183–197.

[26] Harris, J. B., 1993. Electric lamps, past and present. Engineering Science and Education Journal 2; 2 (4), 161–170.

[27] Hooke, R., Jeeves, T. A., 1961. "Direct search" solution of numerical and statistical problems. J.ACM 8 (2), 212–229.

[28] Hunt, D. R. G., 1977. Simple expressions for predicting energy savings from photoelectric control of lighting. Lighting Research and Technology 9 (2), 93–102.

[29] Hunt, D. R. G., 1979. Improved daylight data for predicting energy savings from photoelectric controls. Lighting Research and Technology 11 (1), 9–23.

[30] Hwang, J., Lee, D.-H., Park, S., Kim, Y.-W., Park, S.-N., 2009. Measurement uncertainty evaluation for emission color and luminance of displays. Appl. Opt. 48 (1), 99–105.

[31] Jones, D. R., Perttunen, C. D., Stuckman, B. E., 1993. Lipschitzian optimization without the lipschitz constant. J.Optimiz.Theory Appl. 79 (1), 157–181.

[32] Kolda, T. G., Lewis, R. M., Torczon, V., 2004. Optimization by direct search: New perspectives on some classical and modern methods. SIAM Rev 45 (3), 385–482.

[33] Krames, M. R., Shchekin, O. B., Mueller-Mach, R., Mueller, G. O., Zhou, L., Harbers, G., Craford, M. G., 2007. Status and future of high-power light-emitting diodes for solid-state lighting. Display Technology, Journal of 3 (2), 160–175.

[34] Lee, E., 2008. Cyber physical systems: Design challenges. In: Object Oriented Real-Time Distributed Computing (ISORC), 2008 11th IEEE International Symposium on. pp. 363–369.

[35] Lei, Z., Xia, G., Ting, L., Xiaoling, G., Qiao Ming, L., Guangdi, S., 2007. Color rendering and luminous efficacy of trichromatic and tetrachromatic LED-based white LEDs. Microelectron.J. 38 (1), 1–6.

[36] Lewis, R. M., Torczon, V., 2000. Pattern search methods for linearly constrained minimization. SIAM Journal on Optimization 10 (3), 917–941.

[37] Lewis, R. M., Torczon, V., Trosset, M. W., 2000. Direct search methods: then and now. J.Comput.Appl.Math. 124 (1-2), 191–207.

[38] Machado, C., Mendes, J. A., August, 2008. Automatic light control in domotics using artificial neural networks. In: World Academy of Science, Engineering and Technology. Vol. 44. pp. 813–.

[39] Mistry, P., Maes, P., 2009. Sixthsense: a wearable gestural interface. In: SIGGRAPH ASIA '09: ACM SIGGRAPH ASIA 2009 Sketches. Vol. Yokohama, Japan. ACM, New York, NY, USA, pp. 1–1.

[40] Mozer, M., 1998. The neural network house: An environment that adapts to its inhabitants. In: Proc. AAAI Spring Symp. Intelligent Environments.

[41] Muthu, S., Gaines, J., 2003. Red, green and blue LED-based white light source: implementation challenges and control design. In: Industry Applications Conference, 2003. 38th IAS Annual Meeting. Conference Record of the. Vol. 1; 1. pp. 515–522 vol.1.

[42] Muthu, S., Schuurmans, F. J., Pashley, M. D., 2002. Red, green, and blue LED based white light generation: issues and control. In: Industry Applications Conference, 2002. 37th IAS Annual Meeting. Conference Record of the. Vol. 1; 1. pp. 327–333 vol.1.

[43] Narendran, N., Deng, L., Pysar, R. M., Gu, Y., Yu, H., 2004. Performance characteristics of high-power light-emitting diodes. Vol. San Diego, CA, United States. SPIE, pp. 267–275.

[44] Narendran, N., Gu, Y., 2005. Life of LED-based white light sources. Display Technology, Journal of 1 (1), 167–171.

[45] Navigent Consulting, Inc., 2009. Solid-state lighting research and development portfolio: Multi-year program plan fy'09-fy'15. Tech. rep., Lighting Research and Development Building Technologies Program, Office of Energy Efficiency and Renewable Energy, U.S. Dept. of Energy, Chicago.

[46] Nelder, J. A., Mead, R., 1965. A simplex method for function minimization. The Computer Journal 7 (4), 308–313.

[47] Ohno, Y., 2005. Spectral design considerations for white LED color rendering. Opt.Eng. 44 (11), 111302–.

[48] Pacific Northwest National Laboratory, 2009. Summary of results: Round 9 of product testing. Tech. Rep. 9, Department of Energy.

[49] Park, H., Burke, J., Srivastava, M. B., 2007. Design and implementation of a wireless sensor network for intelligent light control. In: IPSN '07: Proceedings of the 6th international conference on Information processing in sensor networks. Vol. Cambridge, Massachusetts, USA. ACM, New York, NY, USA, pp. 370–379.

[50] Park, S., Lee, D.-H., Kim, Y.-W., Park, S.-N., 2007. Uncertainty evaluation for the spectroradiometric measurement of the averaged light-emitting diode intensity. Appl. Opt. 46 (15), 2851–2858.

[51] Philips Lighting Research, 2010. Dynamic lighting. www.dynamiclighting.philips.com/, Accessed March 2010.

[52] Phillips, J., Coltrin, M., Crawford, M., Fischer, A., Krames, M., Mueller-Mach, R., Mueller, G., Ohno, Y., Rohwer, L., Simmons, J., J.Y.Tsao, 2007. Research challenges to ultra-efficient inorganic solid-state lighting. Laser & Photonics Review 1 (4), 307–333.

[53] Powell, M. J. D., 1998. Direct search algorithms for optimization calculations. Acta Numerica 7 (-1), 287–.

[54] Rains, J., May, D., Ramer, D., February 2006. Optical integrating chamber lighting using multiple color sources. U.S. Patent Number, 6,995,355.

[55] Ramer, D., Rains, J., Bagwell, R. S., January 2002. Direct view lighting system with constructive occlusion. U.S. Patent Number, 6,334,700.

[56] Rosenbrock, H. H., 1960. An automatic method for finding the greatest or least value of a function. The Computer Journal 3 (3), 175–184.

[57] Ryer, A., 1997. The Light Measurement Handbook, 2nd Edition. International Light, Inc., Newburyport, MA 01950-4092.

[58] Sandahl, L., Gilbride, T., Ledbetter, M., Steward, H., Calwell, C., 2006. Compact fluorescent lighting in America: lessons learned on the way to market. Richland WA: Pacific Northwest National Laboratory.

[59] Schubert, E. F., 2006. Innovations in light-emitting diodes. In: Lasers and Electro-Optics and 2006 Quantum Electronics and Laser Science Conference. CLEO/QELS 2006. Conference on. pp. 1–2.

[60] Schubert, E. F., Kim, J. K., 2005. Solid-state light sources getting smart. Science 308 (5726), 1274–1278.

[61] Schubert, E. F., Kim, J. K., Luo, H., Xi, J.-Q., 2006. Solid-state lighting - a benevolent technology. Reports on Progress in Physics 69 (12), 3069–3099.

[62] Sciacchitano, M., September 2009. Test fixture dome assembly. Solidworks 2008 SP0.0.

[63] Sha, L., Gopalakrishnan, S., Liu, X., Wang, Q., 2009. Cyber-physical systems: A new frontier. pp. 3–13.

[64] Singhvi, V., Krause, A., Guestrin, C., Garrett, Jr, J. H., Matthews, H. S., 2005. Intelligent light control using sensor networks. In: SenSys '05: Proceedings of the 3rd international conference on Embedded networked sensor systems. Vol. San Diego, California, USA. ACM, New York, NY, USA, pp. 218–229.

[65] Slocum, A., 2005. Policy options to enhance technology diffusion: modeling the greenhouse gas reduction potential of solid-state lighting. Ph.D. thesis, Rochester Institute of Technology.

[66] Sluis, V., Cortenraad, H. M. R., Diederiks, E. M. A., Hoonhout, H. C. M., Yalvac, M. A., 06 2007. Color matching for display system for shops. WO 2007/072376.

[67] Stanikunas, R., Vaitkevicius, H., Svegzda, A., Viliunas, V., Bliznikas, Z., Breive, K., Vaicekauskas, R., Novickovas, A., Kurilcik, G., Zukauskas, A., Gaska, R., Shur, M. S., 2005. Polychromatic solid-state lamps versus tungsten radiator: hue changes of munsell samples. J.Phys.D 38 (17), 3202–3207.

[68] Stevenson, R., 2009. The LED's dark secret. IEEE Spectrum 46 (8), 26–31.

[69] Teixeira, T., Jung, D., Dublon, G., Savvides, A., 2009. Identifying people in camera networks using wearable accelerometers. In: PETRA '09: Proceedings of the 2nd International Conference on PErvsive Technologies Related to Assistive Environments. Vol. Corfu, Greece. ACM, New York, NY, USA, pp. 1–8.

[70] Teixeira, T., Jung, D., Dublon, G., Savvides, A., 2009. Pem-id: Identifying people by gait-matching using cameras and wearable accelerometers. Vol. Como, Italy. ACM/IEEE, pp. 1–8.

[71] The MathWorks, Inc., March 2010. Global Optimization Toolbox 3. The Mathworks, Inc., 3 Apple Hill Drive Natick, MA 01760-2098, 14th Edition.

[72] Thompson, M. d. R., 2007. Psychophysical evaluations of modulated color rendering for energy performance of LED-based architectural lighting. Ph.D. thesis, Massachusetts Institute of Technology.

[73] Tor, J., December 2009. Test fixture heatsink. Solidworks 2008 SP0.0.

[74] Torczon, V., 1997. On the convergence of pattern search algorithms. SIAM J.on Optimization 7 (1), 1–25.

[75] Trevisanello, L. R., Meneghini, M., Mura, G., Sanna, C., Buso, S., Spiazzi, G., Vanzi, M., Meneghesso, G., Zanoni, E., 2007. Thermal stability analysis of high brightness LED during high temperature and electrical aging. Vol. 6669. SPIE, pp. 666913–.

[76] van der Broeck, H., Sauerlander, G., Wendt, M., 2007. Power driver topologies and control schemes for LEDs. In: Applied Power Electronics Conference, APEC 2007 - Twenty Second Annual IEEE. pp. 1319–1325.

[77] Webb, A. R., 2006. Considerations for lighting in the built environment: Non-visual effects of light. Energy Build. 38 (7), 721–727.

[78] Wen, Y.-J., Granderson, J., Agogino, A. M., 2006. Towards embedded wireless-networked intelligent daylighting systems for commercial buildings. In: SUTC '06: Proceedings of the IEEE International Conference on Sensor Networks, Ubiquitous, and Trustworthy Computing -Vol 1 (SUTC'06). IEEE Computer Society, Washington, DC, USA, pp. 326–331.

[79] Wyszecki, G., Stiles, W. S., 1982. Color Science : Concepts and Methods, Quantitative Data and Formulae. Vol. 2. Wiley, New York.

[80] Zachau, M., Becker, D., Berben, D., Fiedler, T., Jermann, F., Zwaschka, F., 2008. Phosphors for solid state lighting. Vol. 6910. SPIE, pp. 691010–.

[81] Zukauskas, A., Vaicekauskas, R., Ivanauskas, F., Gaska, R., Shur, M. S., 2002. Optimization of white polychromatic semiconductor lamps. Appl.Phys.Lett. 80 (2), 234–236.

[82] Zukauskas, A., Vaicekauskas, R., Ivanauskas, F., VaitkeviCius, H., Shur, M. S., 2008. Rendering a color palette by light-emitting diodes. Appl.Phys.Lett. 93 (2), 021109–.